NREL/TP-411-5456 • UC Category: 271 • DE93010009

Optimization of Transparent and Reflecting Electrodes for Amorphous Silicon Solar Cells

Annual Subcontract Report 1 May 1991 – 30 April 1992

R. G. Gordon
Harvard University
Cambridge, Massachusetts

NREL technical monitor: B. Stafford

National Renewable Energy Laboratory
1617 Cole Boulevard
Golden, Colorado 80401-3393
Operated by Midwest Research Institute
for the U.S. Department of Energy
under Contract No. DE-AC02-83CH10093

Prepared under Subcontract No. XH-1-11032-1

April 1993

NOTICE

Printed in the United States of America
Available from:
National Technical Information Service
U.S. Department of Commerce
5285 Port Royal Road
Springfield, VA 22161

Price: Microfiche A01
Printed Copy A06

Codes are used for pricing all publications. The code is determined by the number of pages in the publication. Information pertaining to the pricing codes can be found in the current issue of the following publications which are generally available in most libraries: *Energy Research Abstracts (ERA)*; *Government Reports Announcements* and Index (*GRA* and I); *Scientific and Technical Abstract Reports (STAR)*; and publication NTIS-PR-360 available from NTIS at the above address.

SUMMARY

1.0 BACKGROUND

Transparent conducting materials are essential components of many kinds of solar cells, in which they serve as front-surface electrodes. In tandem cells, back surface electrodes also need to be transparent. Finally, some designs for highly reflective back contacts also call for a transparent conducting layer. The compositions of these transparent conducting layers are usually based on oxides of tin, indium and/or zinc, and are hence referred to as transparent conducting oxides (TCO). In addition to having low electrical sheet resistance and contact resistance, and low optical absorption, the structure of a TCO must minimize reflection losses. The TCO must also resist degradation during cell fabrication and use. Finally, the method for making the TCO must be inexpensive and safe.

Our general objectives are to improve the performance of TCO materials and the methods for their production. We aim to reduce their electrical resistance, optical absorption and reflection losses, and to avoid degradation of the materials. For the production method, the prime consideration is to deposit the TCO layers at a high rate with relatively simple apparatus. The method chosen is chemical vapor deposition at atmospheric pressure (APCVD), since it has been demonstrated, in the glass-coating industry, to be the most cost-effective method for making large areas of TCO coatings.

In the previous contract period, we discovered a new material, fluorine-doped zinc oxide (ZnO:F) which displays the best properties known for any TCO. ZnO:F has the lowest sheet resistance (5 ohms per square) for a film having only 3% optical absorption averaged over the solar spectrum and a typical amorphous silicon cell's efficiency. We also found an APCVD method to make ZnO:F with a roughness suitable for efficient light-trapping in solar cells. Amorphous silicon solar cells based on ZnO:F showed the high quantum efficiency expected from these properties. However, the fill factors and open-circuit voltages of these cells were not as high as desired. It is possible that these problems arise from poor electrical contact between the ZnO:F and the subsequently deposited p-type amorphous silicon layer.

2.0 OBJECTIVES

The general objective of this work is to improve the performance of solar cells by improving the electrical and optical properties of their TCO layers. Improved electrical contact between the TCO and the amorphous silicon should be achieved by increasing the concentration of free (conduction) electrons in the TCO, particularly in the surface layer of the TCO that contacts the silicon.

3.0 RESULTS

Variation of the deposition conditions for ZnO:F did not, however, succeed in increasing the electron concentration above about 5×10^{20} cm^{-3}. Therefore, the dopants boron, aluminum and gallium were investigated, to see if they could induce higher electron concentrations in zinc oxide. Boron did not produce any more free electrons than fluorine did. Aluminum and gallium were successful in raising the free electron concentration, with gallium more than doubling the electron concentration. Three preprints describing these studies form the body of this report.

The electron mobilities found for boron-, aluminum- or gallium-doped zinc oxide are however, lower than those of fluorine-doped zinc oxide. Since the highest mobility is desired for a TCO material, ZnO:F is preferred for the bulk of an optimized TCO layer. A thin surface layer of ZnO:Ga may be used to increase the electron concentration of the surface of the TCO, in order to decrease the contact resistance.

1. DEPOSITION OF BORON DOPED ZINC OXIDE FILMS AND THEIR ELECTRICAL AND OPTICAL PROPERTIES

ABSTRACT

Boron doped zinc oxide films were deposited by atmospheric pressure chemical vapor deposition in a laminar flow reactor from diethyl zinc, tert-butanol and diborane in the temperature range between 300°C and 420°C. When the deposition temperature was above 320°C, both doped and undoped films have highly oriented crystallites with their c-axes perpendicular to the substrate plane. Films deposited from 0.07% diethyl zinc and 2.4% tert-butanol have electron densities between $3.5x10^{20}$ cm^{-3} and $5.5x10^{20}$ cm^{-3}, conductivities between 250 $\Omega^{-1}cm^{-1}$ and 2500 $\Omega^{-1}cm^{-1}$ and mobilities between 2.5 $cm^2/V\text{-}s$ and 35.0 $cm^2/V\text{-}s$, depending on dopant concentration, film thickness and deposition temperature. Optical measurements shows that the maximum infrared reflectance of the doped films is close to 90%, compared to about 20% for undoped films. Film visible absorption and film conductivity were found to increase with film thickness. The ratio of conductivity to visible absorption coefficient for doped films was between 0.1 Ω^{-1} and 1.1 Ω^{-1}. The band gap of the film changes from 3.3 eV to 3.7 eV when the film is doped with 0.012% diborane.

I. INTRODUCTION

Zinc oxide films have attracted considerable interest in recent years because they can be made to have high electrical conductivity, high infrared reflectance and high visible transmittance. These films have potential applications in energy efficient windows, solar cells, liquid crystal displays and other optoelectronic devices [1-7]. Although indium or tin based oxide films are presently used as transparent electrodes for such devices, indium and tin are in rather limited supplies and are more expensive than zinc [8]. The fabrication process for amorphous silicon solar cells uses plasma-enhanced chemical vapor deposition to deposit a thin layer of *a*-Si:H. The oxide films must be exposed to a hydrogen plasma, which reduces the oxides to metals, resulting in a loss of transparency, especially in the blue region of the spectrum. This degradation process occurs even at low temperature and low plasma power density [9,10]. Therefore, it may be impractical to use indium or tin based oxide films in the mass production of low cost optoelectronic devices such as photovoltaic cells. Zinc oxide films are more stable than indium or tin based oxide films in the presence of a hydrogen plasma [10]. Zinc is a cheap, abundant, and nontoxic element. If highly conductive zinc oxide films with high optical transmission can be made with an inexpensive thin film deposition technique, they will cost less than indium or tin based oxide films.

Zinc oxide is an n-type semiconductor with a hexagonal wurtzite structure and a band gap of about 3.3 eV [8]. Pure zinc oxide is highly transparent in the visible region, but it has low conductivity and low infrared reflectance. Although non-stoichiometric zinc oxide films with excellent electrical and optical properties have been successfully deposited, these films are not very stable at high temperatures. After heat treatment under vacuum or in an inert gas ambient at 400°C, film sheet resistance increased by one to three orders of magnitude [2]. For practical applications, non-stoichiometric zinc oxide films with unstable electrical properties have a disadvantage compared to indium or tin based oxide films. On the other hand, doped zinc oxide films can be

made to have very stable electrical and optical properties. Zinc oxide films doped with atoms such as fluorine [11,12], boron [7], aluminum [2,4,5,10,13], gallium [14] and indium [15,16] have high electrical conductivity, high infrared reflectance, and high visible transmittance.

Zinc oxide films have been deposited on various substrates by different techniques such as metalorganic chemical vapor deposition (MOCVD) [1,3,7,11,12], rf magnetron sputtering [2,9,14,16], reactive sputtering [4,5], ion beam sputtering [13], and spray pyrolysis [10,15]. Aluminum, gallium and indium doped zinc oxide films have been prepared by rf magnetron sputtering of zinc oxide target containing dopant atoms in the form of oxide, or by rf magnetron sputtering of pure zinc oxide together with dc magnetron sputtering of dopant atoms in the presence of oxygen. Fluorine and boron doped zinc oxide films have only been prepared by metalorganic chemical vapor deposition, which is especially useful for large scale coatings at high growth rates. The commonly used zinc precursors are diethyl zinc (DEZ) and dimethyl zinc (DMZ). The oxidant can be pure oxygen, water, alcohol or even some heterocyclic oxygen-containing compounds such as furan (C_4H_4O), tetrahydrofuran (C_4H_8O) or tetrahydrophyran ($C_5H_{10}O$) [17,18]. Even carbon dioxide has been used to react with DEZ to deposit zinc oxide film by plasma-enhanced MOCVD [19]. Diethyl zinc is cheaper than dimethyl zinc and reacts less violently with water or alcohol. It has been widely used to deposit both doped and undoped zinc oxide films at various temperatures by both atmospheric pressure and low pressure chemical vapor deposition techniques.

In this chapter we report the deposition of boron doped zinc oxide films from diethyl zinc, tert-butanol, and diborane by atmospheric pressure chemical vapor deposition at various deposition temperatures. The electrical and optical properties of doped films are characterized by Hall coefficient, resistance, transmittance and reflectance measurements.

II. EXPERIMENTAL PROCEDURES

Zinc oxide films were fabricated on soda lime glass substrates and quartz substrates by atmospheric pressure chemical vapor deposition in an laminar flow rectangular nickel reactor which has been described previously [11]. High purity helium (99.995%, from Matheson Gas Products) was used as the carrier gas for diethyl zinc (from Ethyl Corporation) and tert-butanol (from Aldrich Chemical Company, Inc.). Small amounts of water in the tert-butanol were removed by mixing with 4 Å molecular sieves. The diethyl zinc bubbler was kept at 25°C and its vapor pressure at this temperature was 16.1 Torr. Diborane (2.2% in high purity helium, from Matheson Gas Products) was mixed with diethyl zinc and then diluted further by high purity helium before flowing into the reactor. The tert-butanol bubbler was kept in an oven at 50°C to achieve a high vapor pressure of 163 Torr. Since diethyl zinc and diborane react quickly with tert-butanol, they were introduced into the reactor separately through slit-shaped nozzles, separated from each other by a buffer flow of helium. The gas flow in each line was 3.0 l/min and so the total gas flow was 9.0 l/min through a cross section of 0.6 cm x 12.0 cm. The reactor was heated from the bottom by a hot plate, and its top and bottom temperatures were determined by thermocouples inserted in holes in the side of the reactor. The temperature of the substrate was taken to be the bottom temperature of the reactor. The temperature difference between the top side of the reactor and the substrate depends on the substrate temperature and varies from 60°C to 90°C when the substrate temperatures are between 300°C and 420°C. This temperature gradient drives the powder produced during the deposition to the upper side of the reactor, leaving the film free of powder. The deposition temperature was stabilized to ±1°C. The reactor nozzle was insulated from the heated block by a thin-walled zone of width 3.5 cm and its temperature was usually about 150°C lower than that of the central part of the reactor. This low temperature zone ensures the establishment of laminar flow before the gas mixture reaches the substrate. The soda lime glass substrates were first cleaned with a 5% sodium-free detergent solution (Detergent 8, from Alconox, Inc.) and then rinsed with deionized water. The quartz substrates were cleaned with 1:1 H_2O_2 and sulfuric acid solution and then rinsed with deionized water.

Film thickness and refractive index were determined by a Rudolph Research AutoEl-II ellipsometer and a Metricon PC-2000 prism coupler. Ellipsometer measurements are most accurate for films with thicknesses above 50 nm and below the full cycle thickness. The full cycle thickness depends on the incident angle of the light beam and the film refractive index. For an incident angle of 70°, the full cycle thickness is about 200 nm for zinc oxide films with refractive indices of about 1.9. The thicknesses and refractive indices of thicker films (thickness above 500 nm) were accurately determined with the prism coupler.

X-ray diffraction measurements were made on a Philips powder crystallography instrument by using copper K_α radiation. The voltage and current used were 46 kV and 16 mA. A JEOL JSM-6400 scanning electron microscope (SEM) was used to obtain the crystallite orientation and size. The surface composition and depth profile were obtained by an SSX-100 ESCA X-ray photoelectron spectrometer (XPS). Boron concentration in the film could not be determined by XPS.

The sheet resistance R was measured by using a Veeco FPP-100 Four Point Probe. Assuming that the film is homogeneous in the direction perpendicular to the substrate plane, the film bulk resistivity ρ is obtained from $\rho = Rt$, where t is the film thickness. In order to measure the Hall coefficient, the film on the substrate was covered by a strip of Scotch tape 0.5 inch wide. The rest of the film on the substrate was etched away by immersing the sample in 4M hydrochloric acid. The transverse voltage in the presence of a dc current was measured in a constant perpendicular magnetic field by using a Varian V-2300-A electromagnet, which was calibrated by a Gaussmeter and was found to have a strength of 10.0 kG. Before turning on the magnetic field, the voltage meter was zeroed by a potentiometer to reduce experimental errors. The measurement was repeated by reversing the direction of the magnetic field. The magnitudes of the two measured voltages were approximately equal with opposite sign, indicating that the hysteresis effect is negligible. The Hall coefficient R_H was then calculated from the averaged transverse voltage V (in mV), dc current I (in mA), the magnetic field B (in kG), and the thickness of the film t (in μm) according to the formula $R_H = (10.0Vt)/(IB)$.

The infrared spectra were taken on a Nicolet Model 800 Fourier Transform spectrometer with a relative reflection attachment, which could measure near normal reflectance (incident angle less than 5°). A gold mirror with a known reflectance was used as the reflectance standard in the wavelength range from 2.0 μm to 20 μm [20]. The near ultraviolet, visible and near infrared spectra were obtained with a Varian 2390 spectrophotometer using an integrating sphere detector to measure total reflectance and transmittance. The reflectance standard is a barium sulphate plate and its reflectance is taken to be 100.0% between 0.2 and 2.2 μm. The absorption of the light within the film was then obtained by subtraction of the total reflectance and total transmittance from 100.0%. Corrections for absorption in the glass substrate were usually less than 1.0% in the wavelength range between 0.4 μm and 2.0 μm.

III. RESULTS AND DISCUSSION

A. Film growth

Undoped zinc oxide films were deposited from diethyl zinc and tert-butanol. Doped films with different electrical and optical properties were made by introducing different amounts of diborane into the reactant gas mixture. Film growth rates were calculated from the measured film thickness and the deposition time. The refractive index of the undoped film is around 1.95 and that of the doped films is between 1.8 and 1.9. The temperature strongly influences the film growth rate. Figure 1 shows the growth rate profile for different deposition temperatures. Diethyl zinc, tert-butanol and diborane concentrations in the gas phase were 0.07%, 2.4% and 0.012%, respectively. At 300°C there is some film deposited at the beginning and end of the substrate,

separated by an area without any film. The no-film area and the film at the beginning of the substrate were covered by some black powder. Since the black powder is found on the substrate only when there is diborane in the gas mixture, the black powder is thought to be boron produced from the decomposition of diborane at high temperatures. At higher deposition temperatures, the growth rate profiles are still divided into two areas with much film growth, separated by an area with less growth. The peak position of the first area with film growth was difficult to determine because of the extreme nonuniformity of the film in this area and the closeness of the film to the cold zone of the reactor. Some black powder was observed to stick on this first part of the film. This part of the film is thought to be produced from the reaction of diethyl zinc with water in the tert-butanol, because the film growth pattern in this area is similar to that produced from pure water and diethyl zinc at the same temperature. Although tert-butanol has been carefully purified to remove residual water, its brass bubbler has been heated to a high temperature (50°C) and the stainless steel tubing to transport tert-butanol was kept at a still higher temperature (around 90°C) by using heating tapes. The temperature of the nickel reactor nozzle was maintained above 150°C. Some tert-butanol will be dehydrated to produce water and hydrocarbon compounds at high temperatures in the presence of metals. The water produced *in situ* in the tert-butanol gas line will be transported into the reactor to react with diethyl zinc to form zinc oxide film on the first part of the substrate. The peak position of the second area with much film growth is easily found. This part of the film is produced from the reaction of tert-butanol and diethyl zinc. The appearance of the peak position further down the substrate indicates that the film is produced from intermediate film precursors formed in the gas phase from diethyl zinc and tert-butanol. The net buildup of the film precursors in the gas phase makes the film exhibit an initially rising growth rate. The decline of the growth rate after the peak position corresponds to the depletion of the film precursors in the gas phase. The peak position moves towards the reactor nozzle as the temperature increases. At low temperatures, the reactions to form film precursors are slow and it takes a long time to build maximum film precursor concentrations in the gas phase. Thus the deposition is slow and the peak position is far downstream. At high temperatures, gas phase reactions are fast enough to produce maximum film precursor concentrations in a short time. Film growth rate is high and the peak position appears earlier along the gas flow direction. The dependence of the peak growth rate on deposition temperature is given in Figure 2. The reactant concentrations are the same as those in Figure 1. The peak growth rate increases steadily with deposition temperature.

The tert-butanol concentration does not influence film peak growth rate when it is above 0.7%. Figure 3 shows the peak growth rate dependence on the tert-butanol concentration for films deposited at 360°C with a diethyl zinc concentration of 0.07% and diborane concentration of 0.012%. The growth rate is almost a constant in the tert-butanol concentration range between 0.75% and 2.5%. The same growth rate behavior has been observed in the deposition of zinc oxide films from diethyl zinc and ethanol [11]. At constant diethyl zinc concentration, the growth rate usually increases with oxidant (alcohol) concentration in the low concentration range. When the oxidant concentration exceeds that needed by the diethyl zinc in the gas mixture, all the diethyl zinc reacts completely with tert-butanol and the growth rate does not increase at higher oxidant concentrations.

The dopant diborane also influences the film growth rate. Figure 4 shows that the peak growth rate decreases with dopant concentration for films deposited at 360°C from 0.07% diethyl zinc and 2.4% tert-butanol. Diborane is not very stable at high temperatures. It decomposes to boron and hydrogen. The boron will stick at the beginning of the substrate, and appear as black powder. The diborane reacts not only with tert-butanol but also with reaction intermediates, and so it interferes with film precursor formation steps, slowing down the deposition, and moving the growth rate peak position downstream. Some boron atoms are incorporated into the film precursors. The doped zinc oxide films will be produced from these film precursors as they diffuse onto the substrate.

B. Film structure

X-ray diffraction measurement showed that both undoped and doped zinc oxide films deposited at all temperatures from 0.07% diethyl zinc, 2.4% tert-butanol and 0.012% diborane between 300°C and 420°C were crystalline. The strongest diffraction peak at all temperatures is the (002) peak with 2θ about 34.5°. The (100) peak at 31.8° and (101) peak at 36.3° are observed with relatively strong intensity for films deposited at 300°C. At temperatures above 320°C, the (002) peak has a very high intensity, and all other peaks are extremely weak or disappear completely. Therefore, all the films deposited above 320°C are highly oriented with their c-axes perpendicular to the substrate plane. The dopant diborane does not have significant influence on the x-ray diffraction patterns. The doped films give the same diffraction patterns as the undoped films. The film orientation was not modified by boron doping. Figure 5 gives the x-ray diffraction spectra of two boron doped films deposited at 300°C and 400°C, respectively.

The crystallite dimension along c-axis was determined by measuring the (002) x-ray diffraction peak width. Since the Cu K_α radiation contains two lines of wavelength 1.54056 Å and 1.54439 Å with intensity ratio 2:1 [8], single crystalline zinc oxide with spacing 2.603 Å along (002) direction will give two diffraction peaks separated by $\Delta(2\theta) = 0.088°$ with intensity ration 2:1. Only one peak can be observed in the spectra because of the peak broadening from the small crystallite size. The true peak width B_s corresponding to monochromatic x-ray is found by modelling the observed diffraction peak with two Gaussian curves of height ratio 2:1, width ratio 1:1 and separated by 0.088. The instrument broadening B_0, obtained by measuring the single crystalline Si (111) diffraction peak width with 2θ around 28.5°, was found to be 0.052°. The corrected peak with B can be calculated from the formula $B^2 = B_s^2 - B_0^2$, and the crystallite size t is then estimated according to $t = 0.9\lambda/B\cos\theta$, where λ is the x-ray wavelength and θ is the Bragg diffraction angle [21]. The crystallite sizes along c-axis were found to lie between 35 nm and 45 nm, and varied with the deposition temperature, the dopant concentration, and the sample position on the substrate.

The film morphology and crystallite size in the direction parallel to the substrate plane were determined by scanning electron microscopy (SEM). The undoped film crystallites have disklike structures with disk diameters between 200 nm and 500 nm for films deposited between 300°C and 420°C. Figure 6 (a) shows the electron micrograph of an undoped film deposited at 400°C from 0.07% diethyl zinc and 2.4% tert-butanol. The film thickness is 710 nm. The electron micrograph of a corresponding doped film deposited at 400°C with 0.012% diborane in the gas phase is given in Figure 6 (b). Sample (b) has a thickness of about 1075 nm. The shape and size of the doped film crystallites are quite different from those of the undoped film deposited at the same temperature. The crystallite diameter is always reduced by the introduction of the dopant. It seems that the temperature does not have an influence on the crystallite diameter of doped zinc oxide films. Doped films deposited at all temperatures with thickness above 650 nm were found to have approximately the same crystallite diameter in the direction parallel to the substrate plane. However, the doped films deposited at higher temperatures tend to have more porous structures than those deposited at lower temperatures. Figure 6 (c) and (d) show the electron micrographs of two doped films deposited at 360°C with the same reactant concentrations as sample (b). Sample (c) and (d) have thicknesses of 800 nm and 170 nm, respectively. When the film thickness is below 650 nm, the film crystallite diameter increases with film thickness. The film with a thickness of 170 nm has a crystallite diameter of only about 80 nm; the film with a thickness of 800 nm has a diameter above 200 nm.

C. Film composition

X-ray photoelectron spectroscopy (XPS) detects carbon, oxygen and zinc on the film surface. Boron was not detected on the surface due to its low concentration and the interference from carbon. Even after the surface layer is sputtered away and the carbon concentration decreased to less than 1.0 at.%, boron still could not be detected. This may result from the easy migration of boron atoms out of the film in a vacuum. In order to obtain the film's bulk composition, the surface layer must be sputtered away. Preferential sputtering makes quantitative analysis unreliable. Figure 7 gives a depth profile for films deposited at 360°C from 0.07% diethyl zinc, 2.4% tert-butanol and 0.012% diborane. The sputtering rate is about 1 Å/second. A large amount of carbon exists on the film surface. However, the bulk film contains only a negligible amount of carbon (less than 1.0 at.%).

D. Electrical properties

Boron has a much smaller ionic radius than zinc (B^{3+}, 0.23 Å; Zn^{2+}, 0.74 Å). A boron atom replaces a zinc atom in the crystallite or occupies an interstitial position. Boron is an n-type dopant for zinc oxide. The electron density N_e is calculated from the measured Hall coefficient R_H according to the formula $N_e = 1/(R_H e)$, where e is the electron charge. The electron density dependence on dopant concentration for films deposited at 360°C is shown in Figure 8. In the low dopant concentration range, free electron density increases with diborane concentration. As the diborane concentration becomes high, extra boron atoms in the film will form some insulating boron oxide between zinc oxide crystallites and increase the number of impurity scattering centers, rather than increasing electron density. The electron density will therefore become constant.

Figure 9 shows the electron density dependence on the deposition temperature. The variation of electron density with temperature is small. The films deposited from 0.07% diethyl zinc, 2.4% tert-butanol and 0.012% diborane have electron densities between 4.2×10^{20} cm^{-3} and 5.5×10^{20} cm^{-3}. With the diethyl zinc and diborane concentration kept at 0.07% and 0.012% and the deposition temperature at 360°C, the tert-butanol concentration was varied between 0.75% to 2.5% to deposit doped zinc oxide films. These films were found to have electron densities of about 5.0×10^{20} cm^{-3}, independent of tert-butanol concentration. The film thickness has a very small influence on electron density. An electron density of about 5.0×10^{20} cm^{-3} was found for films deposited at 360°C from 0.07% diethyl zinc, 2.4% tert-butanol and 0.012% diborane, with thickness between 170 nm and 1350 nm.

Film conductivity was determined from the measured sheet resistance and film thickness. Figure 10 shows the conductivity profile for different deposition temperatures. These films are the same as in Figure 1. As mentioned in the discussion of film growth section, the films on the substrate are divided into two parts. The first part, which comes from the reaction of diethyl zinc with water, is non-conductive. Its resistance is above 100 kΩ/square which is the maximum resistance that our four point probe can measure.

We examined the deposition of boron doped zinc oxide film at temperatures between 200°C and 300°C with pure water. It was found that at a given deposition temperature, the higher the dopant flow, the lower the film refractive index. Although the incorporation of boron is not verified directly, the low film refractive index indicates that there is boron in the film. All these boron doped films deposited from diethyl zinc and water are non-conductive (resistance above 100 kΩ/square). This result is different from that in the literature [7], which reports the deposition of boron doped zinc oxide film by low pressure MOCVD from diethyl zinc, water and diborane. They found that a boron doped zinc oxide film with a sheet resistance of 10 Ω/square and a thickness of 3 μm, has an electron density 1.1×10^{20} cm^{-3}, and electron mobility 18.1 $cm^2/V\text{-}s$. In our experiments, the conductive film always comes from the second part on the substrate, which is

produced from the reaction of diethyl zinc and tert-butanol. The conductivity is nonuniform along the gas flow direction. There is a peak conductivity at each temperature. The location of peak conductivity moves towards the reactor nozzle as the temperature increases. This conductivity nonuniformity may be due to the distribution of boron atoms, the thickness difference along the gas flow direction, and the water influence on the deposition.

The thickness dependence of film peak conductivity for films deposited at 360°C is given in Figure 11. The conductivity increases rapidly with film thickness. According to Drude theory [22], conductivity σ is inversely proportional to the free electron scattering frequency γ following the relation

$$\sigma = \frac{N_e e^2}{m_e^* \gamma}, \qquad (1)$$

where N_e is the free electron density, e is the electron charge, m_e^* is the effective mass of conduction electrons. For films deposited under the same conditions with different deposition time, the electron density N_e and ionized impurity scattering frequency are about the same. When the film is very thin, the crystallite size is small and the grain boundary scattering is dominant, which limits the film conductivity. As the film becomes thicker, the influence from grain boundary scattering decreases and the ionized impurity scattering is the main factor limiting film conductivity. Therefore, the film conductivity should approach a constant value as the film becomes very thick. Figure 11 shows that a constant conductivity appears when the film thickness is above 0.7 μm.

The influence of dopant concentration on film conductivity is shown in Figure 12. All the films were deposited at 360°C from 0.07% diethyl zinc and 2.4% tert-butanol with different diborane concentrations. The film thicknesses are all above 0.7 μm. Although the undoped film has a small ionized impurity scattering frequency, its low free electron density makes the conductivity close to zero. As the dopant concentration increases, the conductivity increases rapidly because of the increase in free electron density. However, the impurity scattering frequency also increases with dopant concentration; any further increase in dopant concentration makes the conductivity first level off and then decrease.

The Hall mobility μ_H is obtained from the measured Hall coefficient and the film conductivity σ by the formula $\mu_H = R_H\sigma = e/(m_e^*\gamma)$. The single crystal zinc oxide mobility is around 180 $cm^2/V\text{-}s$ [8]. The boron doped zinc oxide films were found to have mobilities varying from 2.5 $cm^2/V\text{-}s$ to 35 $cm^2/V\text{-}s$. The dependence of film mobility on dopant concentration is given in Figure 13. The films are the same as those in Figure 12. The films have higher mobilities at lower dopant concentrations. High dopant concentration (above 0.013%) leads to a decrease in film mobility because of the high impurity scattering frequency. When dopant concentration increases to 0.02%, the film mobility decreases to about 4.5 $cm^2/V\text{-}s$.

The tert-butanol concentration did not have a significant influence on film mobility when it was varied from 0.75% to 2.5%. The films deposited at 360°C from 0.07% diethyl zinc and 0.012% diborane were found to have mobilities of about 24 $cm^2/V\text{-}s$. Film thickness strongly influences film mobility. Figure 14 shows the mobility dependence on thickness. The films are the same as those in Figure 11. When the film is very thin, crystallite size is small and the grain boundary scattering limits film mobility. As the film becomes thicker, grain boundary scattering plays a less important role than impurity scattering, which is a constant for films deposited at the same conditions. The film mobility is expected to increase rapidly with film thickness and then become constant. Figure 14 shows that a constant mobility of about 25 $cm^2/V\text{-}s$ is obtained for films with thicknesses above 0.7 μm.

The mobility dependence on deposition temperature is given in Figure 15. The films were deposited from 0.07% diethyl zinc, 2.4% tert-butanol and 0.012% diborane. All of the films were deposited with thicknesses above 0.7 μm to reduce the mobility dependence on film thickness. The film mobility is almost a constant in the temperature range between 340°C and 380°C. For temperatures above 380°C, the mobility decreases with deposition temperature. Lower film mobility indicates that the films deposited at higher temperatures have higher electron scattering frequeency.

Figure 16 shows that the film conductivity strongly depends on the deposition temperature. The conductivity first increases slightly and then decreases with deposition temperature. There is a conductivity maximum around 380°C. Since the electron density is about the same for all samples, the temperature variation of the conductivity follows that of the mobility discussed above.

E. Optical properties

Boron doping changes the optical properties of zinc oxide film. The doped films behave like metals in the infrared, having high reflectance. In the visible region, the doped films behave like dielectrics and are highly transparent. The transition between these two behaviors is at the plasma wavelength, which moves to shorter wavelength as the free electron density in the film increases. Many applications of highly transparent and conductive zinc oxide films in optoelectronic devices are based on this peculiar optical property. Figure 17 shows reflectance, transmittance and absorbance of three films with different diborane concentrations deposited at 360°C from 0.07% diethyl zinc and 2.4% tert-butanol. Sample A is undoped and its thickness is 588 nm. Although it is highly transparent in the visible, it has very low infrared reflectance (about 20%) and very high resistance (above 100 kΩ/square). Samples B and C were deposited with 0.012% and 0.02% diborane in the gas phase, respectively. The thicknesses of sample B and C are 483 nm and 583 nm and the sheet resistances are 12.8 Ω/square and 54.4 Ω/square. Both sample B and C are highly transparent in the visible region and begin to absorb light in the near infrared. The plasma wavelengths of sample B and C are at 1.4 μm and 1.5 μm, indicating that sample B has a slightly higher electron density than sample C. The electron densities and mobilities determined by Hall coefficient measurements are 5.4×10^{20} cm^{-3} and 19 $cm^2/V\text{-}s$ for sample B and 4.4×10^{20} cm^{-3} and 4.5 $cm^2/V\text{-}s$ for sample C. There is a much more important difference in the infrared reflectance between sample B and C. Sample C, doped with higher diborane concentration, has a maximum infrared reflectance of only about 65% while sample B has a maximum infrared reflectance of about 90%. A higher infrared reflectance usually indicates a higher electron mobility. This is in agreement with the result obtained from Hall coefficient measurements.

The absorption $A(\lambda)$ obtained from the reflectance and transmittance measurements varies with the wavelength. The undoped films are transparent to near infrared light, whereas the doped films begin to absorb in the near infrared and become opaque in the infrared region. In solar cell applications, the appropriate average absorption A is calculated from

$$A = \frac{\int d\lambda \Psi(\lambda) A(\lambda)}{\int d\lambda \Psi(\lambda)}, \qquad (2)$$

where $\Psi(\lambda)$ is the solar irradiance spectrum for 1.5 air mass. Samples A, B and C shown in Figure 17 have average visible absorptions of 5%, 6% and 10%, respectively. The average absorption increases with dopant concentration. The absorption dependence on film thickness is shown in Figure 18. The samples were deposited at 360°C from 0.07% diethyl zinc, 2.4% tert-butanol and 0.012% diborane. The average absorption increases with film thickness.

Most optoelectronic applications require the films to have low absorption in the visible region and high dc conductivity. The performance of transparent conducting films can be ranked according to a quantity called the Figure of Merit, which is defined as

$$\frac{\sigma}{\alpha} = -\frac{1}{R \ln T}, \tag{3}$$

where σ is the bulk conductivity, α is the average visible absorption coefficient, R is the sheet resistance in Ω/square and T is the average fractional transmittance between 400 nm and 800 nm. Figure 19 shows the Figure of Merit dependence on film thickness. A thinner film with a lower conductivity will have a lower Figure of Merit. As the film becomes thicker, its conductivity increases and finally becomes constant, as does the Figure of Merit. The dopant influence on Figure of Merit is shown in Figure 20. There is a maximum Figure of Merit at a dopant concentration of about 0.005%. The dopant influences both film absorption and conductivity. The undoped film has the highest transmission and the highest sheet resistance. Its Figure of Merit is close to zero. Small amounts of dopant makes the film have some conductivity and the transmission decreases only slightly, so that the Figure of Merit first increases with dopant concentration in the low dopant concentration range. As the dopant concentration becomes high, film conductivity decreases and film absorption increases. The Figure of Merit will therefore decrease with dopant concentration in the high dopant concentration range. Figure 21 shows that the Figure of Merit first increases slightly with temperature and then decreases rapidly after reaching a peak value, which follows that of the film conductivity.

The optical absorption coefficient of a direct band gap semiconductor near the absorption edge, for a photon energy $h\nu$ greater than band gap energy E_g of the material, is given by

$$\alpha = A(h\nu - E_g)^{1/2}, \tag{4}$$

where A is a proportional constant. Since soda lime glass begins to absorb around $\lambda = 320$ nm (corresponding to 3.8 eV), the film band gap was measured only for those samples deposited on quartz substrates. Film transmission was first measured, and then $(\ln T)^2$ (which is proportional to α^2) was plotted as a function of photon energy and a tangential line was drawn near the absorption edge. Figure 22 shows the absorption edge for two samples deposited on quartz substrate at 360°C from 0.07% diethly zinc and 2.4% tert-butanol. The doped sample was deposited by introducing 0.012% diborane into the gas phase. The band gaps determined from Figure 22 are 3.3 eV for the undoped sample and 3.7 eV for the boron doped sample. There is a band gap widening of about 0.4 eV between the doped and undoped samples. In very low electron density materials such as in aluminum doped zinc oxide powder, band gap widening is not detected experimentally because of its low value [23]. However, it has been observed that in aluminum doped zinc oxide films, the band gap increased from 3.4 to 3.9 eV when the aluminum doping was increased from 0 to 2 at.% [4]. Similar band gap widening has been observed in other transparent semiconductors such as tin doped indium oxide films [22]. In heavily doped semiconductors, the lowest states in the conduction band have been filled and the valence electrons must gain extra energy to be excited to higher energy states in the conduction band. This simple mechanism predicts that the band gap widening ΔE_g is proportional to $N_e^{2/3}$. The energy band gap therefore widens as the electron density increases.

IV. CONCLUSIONS

Boron doped zinc oxide films have been deposited from diethyl zinc, tert-butanol and diborane in the temperature range between 300°C and 420°C on soda lime glass and quartz substrates. There were two areas of film growth on the substrate. The film in the first area was produced mainly from the reaction of diethyl zinc and water, while the film in the second area was produced with tert-butanol as oxidant. Only the film in the second area of the substrate was highly conductive. Film growth rates increased with deposition temperature and decreased with diborane concentration. X-ray diffraction revealed that all the films were polycrystalline and those deposited above 320°C were highly oriented with the c-axes perpendicular to the substrate plane. The undoped films had disklike structures with disk diameters between 250 nm and 500 nm. The crystallite dimension of doped films in the direction perpendicular to the substrate plane was between 35 nm and 45 nm and in parallel direction it was above 80 nm, with thicker films having larger crystallite sizes. XPS detected carbon only on the film surface while the film beneath the surface layer was free of carbon contamination. The electron density determined from Hall coefficient measurements was between 3.5×10^{20} cm^{-3} and 5.5×10^{20} cm^{-3} for films deposited with various diborane concentrations from 0.07% diethyl zinc and 2.4% tert-butanol in the temperature rangebetween 340°C and 420°C. The conductivity was not uniform along the gas flow direction and the peak conductivity was between 250 Ω^{-1} cm^{-1} and 2500 Ω^{-1} cm^{-1}. At both very low and very high dopant concentrations the conductivity was low. When the dopant concentration was between 0.005% and 0.015%, the film conductivity was constant and was about 2250 Ω^{-1} cm^{-1}. The Hall mobility obtained from the conductivity and the Hall coefficient was between 2.5 $cm^2/V\text{-}s$ and 35 $cm^2/V\text{-}s$. Very high dopant concentration led to low film conductivity and low mobility. The electron density was almost a constant when the films were deposited in the temperature range between 340°C and 420°C. Film conductivity and mobility first slightly increased with temperature. For temperatues above 380°C, film conductivity and mobility both decreased rapidly with temperature. Film conductivity and mobility also increased as the films became thick because of the low grain boundary scattering frequency of thick films. All of the boron doped films were smooth. The absorption increased with film thickness. Film deposited at 360°C from 0.07% diethyl zinc, 2.4% tert-butanol and 0.012% diborane with a thickness 483 nm had a sheet resistance of 12.8 Ω/square, infrared reflectance close to 90%, and visible absorption of about 6%. The Figure of Merit of the films was between 0.1 Ω^{-1} and 1.1 Ω^{-1}. The band gap determined from the optical absorption coefficient was 3.3 eV for undoped film and 3.7 for film doped with 0.012% diborane.

References

[1]C. K. Lau, S. K. Tiku, and K. M. Lakin, J. Electrochem. Soc. **127**, 1843 (1980).

[2]T. Minami, H. Nanto, and S. Takata, Jpn. J. Appl. Phys. **23**, L280 (1984).

[3]S. Oda, H. Tokunaga, N. Kitajima, J. Hanna, I. Shimizu, and H. Kokado, Jpn. J. Appl. Phys. **24**, 1607 (1985).

[4]Z. C. Jin, I. Hamberg, and C. G. Granqvist, J. Appl. Phys. **64**, 5117 (1988).

[5]Z. C. Jin, I. Hamberg, and C. G. Granqvist, Appl. Phys. Lett. **51**, 149 (1987).

[6]J. B. Yoo, A. L. Fahrenbruch, and R. H. Bube, J. Appl. Phys. **68**, 4694 (1990).

[7]W. W. Wenas, A. Yamada, M. Konagai, and K. Takahashi, Jpn. J. Appl. Phys. **30**, L441 (1991).

[8]D. R. Lide, *Handbook of Chemistry and Physics*, 71st ed. (CRC Press, Boca Raton, Florida, 1991).

[9]T. Minami, H. Sato, H. Nanto, and S. Takata, Thin Solid Films **176**, 277 (1989).

[10]A. F. Aktaruzzaman, G. L. Sharma, and L. K. Malhotra, Thin Solid Films **198**, 67 (1991).

[11]J. Hu and R. G. Gordon, Solar Cells **30**, 437 (1991).

[12]J. Hu and R. G. Gordon, Mater. Res. Soc. Symp. Proc. **202**, 457 (1991).

[13]M. Ruth, J. Tuttle, J. Goral, and R. Noufi, J. Cryst. Growth **96**, 363 (1989).

[14]B. H. Choi, H. B. Im, J. S. Song, and K. H. Yoon, Thin Solid Films **194**, 712 (1990).

[15]S. Major, A. Banerjee, and K. L. Chopra, Thin Solid Films **122**, 31 (1984).

[16]S. N. Qiu, C. X. Qiu, and I. Shih, Solar. Energy Mater. **15**, 261 (1987).

[17]P. J. Wright, R. J. M. Griffiths, and B. Cockayne, J. Cryst. Growth **66**, 262 (1984).

[18]P. Souletie, S. Bethke, B.W. Wessels, and H. Pan, J. Cryst. Growth **86**, 248 (1988).

[19]M. Shimizu, T. Horii, T. Shiosaki, and A. Kawabata, Thin Solid Films **96**, 149 (1982).

[20]D. A. Strickler, Ph. D. thesis, Harvard University, 1989.

[21]B. D. Cullity, *Elements of X-ray Diffraction*, 2nd ed. (Addison-Wesley, Reading, Massachusetts, 1978).

[22]I. Hamberg and C. G. Granqvist, J. Appl. Phys. **60**, R123 (1986).

[23]H. T. Yuan and J. F. Cordaro, J. Appl. Phys. **69**, 959 (1991).

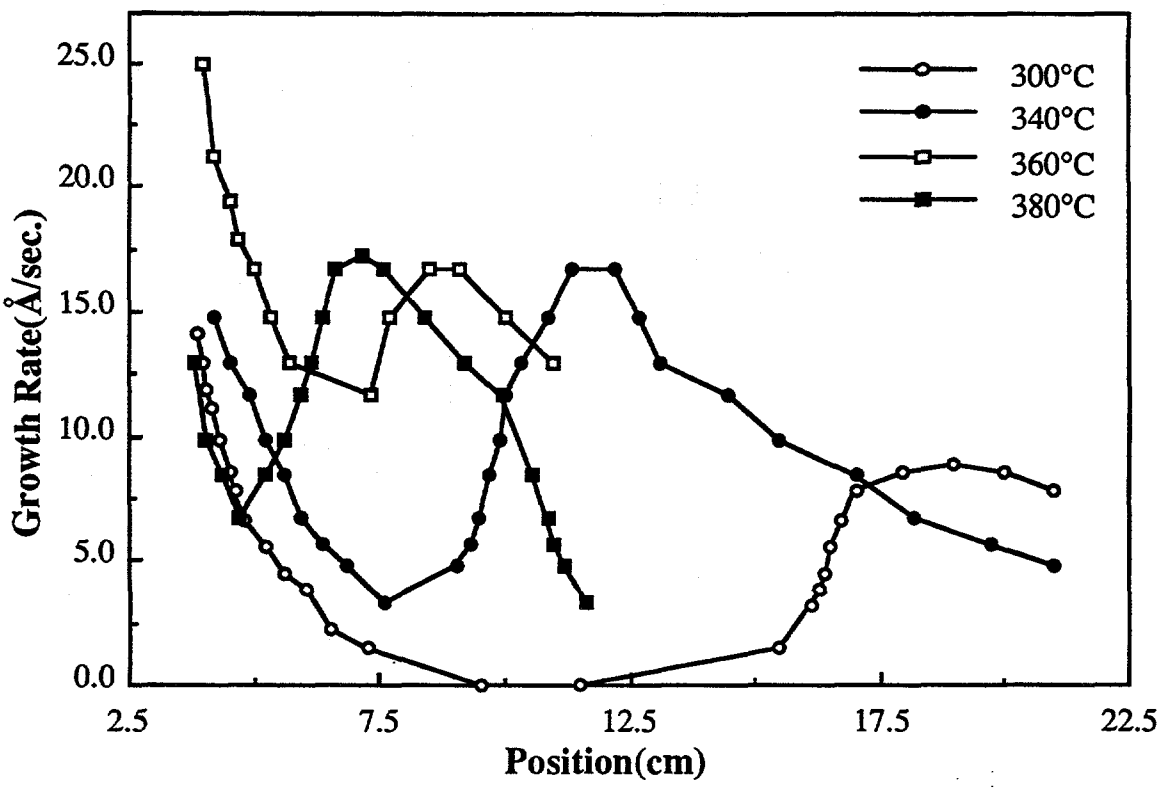

FIG. 1. Growth rate profile for films deposited at different temperatures. The films were deposited from 0.07% diethyl zinc, 2.4% tert-butanol and 0.012% diborane.

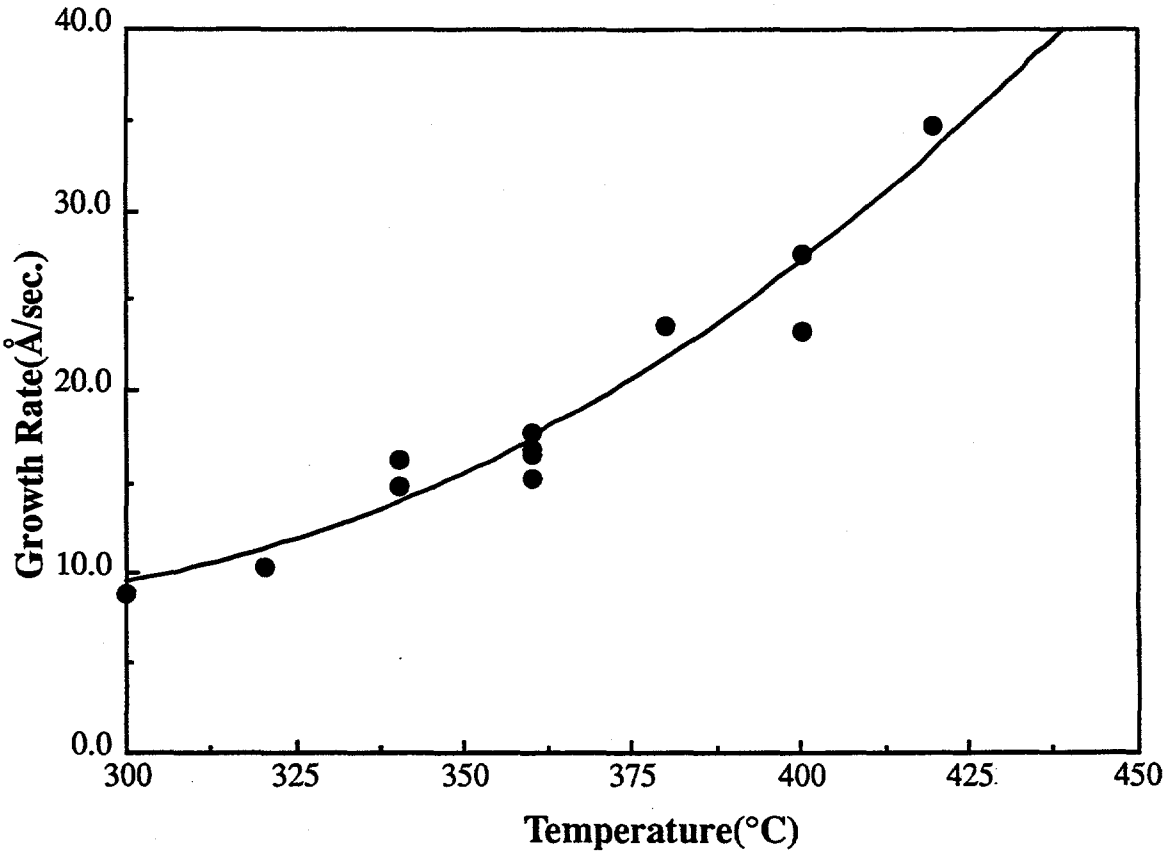

FIG. 2. Peak growth rate dependence on the deposition temperature. The reactant concentrations are the same as in Figure 1.

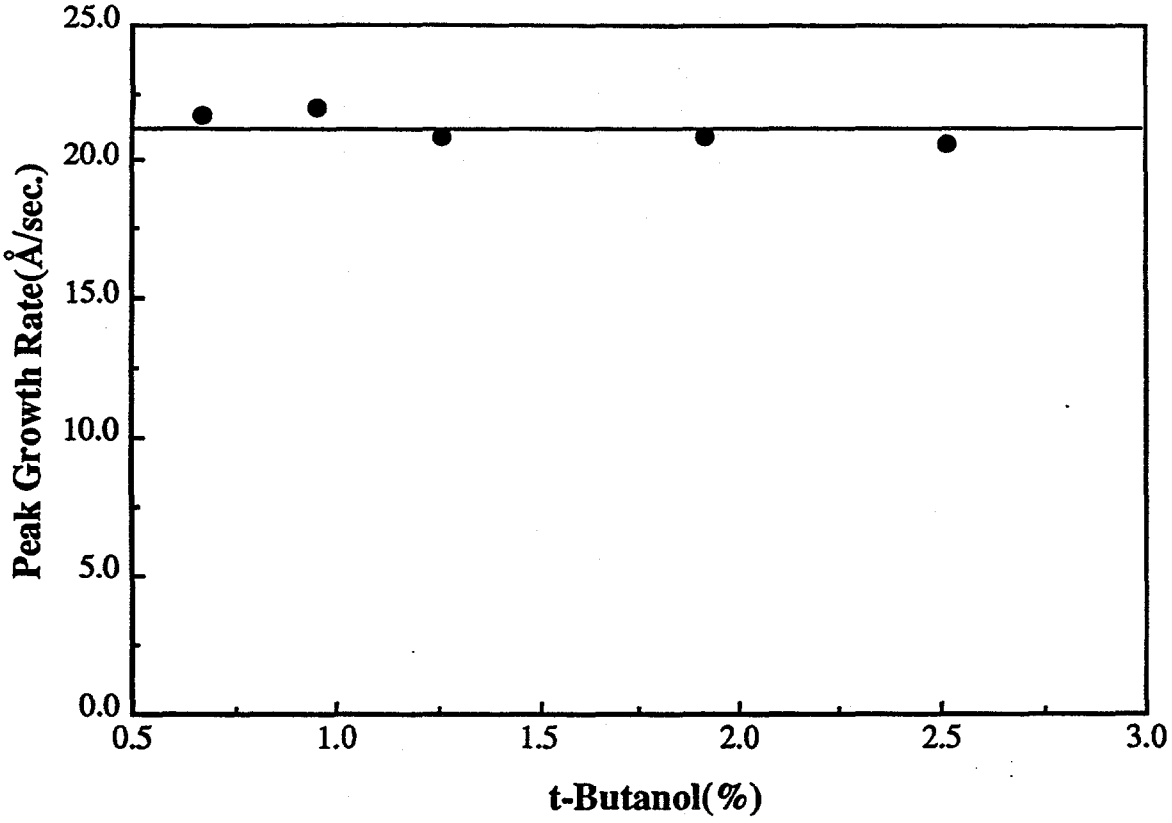

FIG. 3. Growth rate dependence on tert-butanol concentration. The films were deposited at 360°C from 0.07% diethyl zinc and 0.012% diborane.

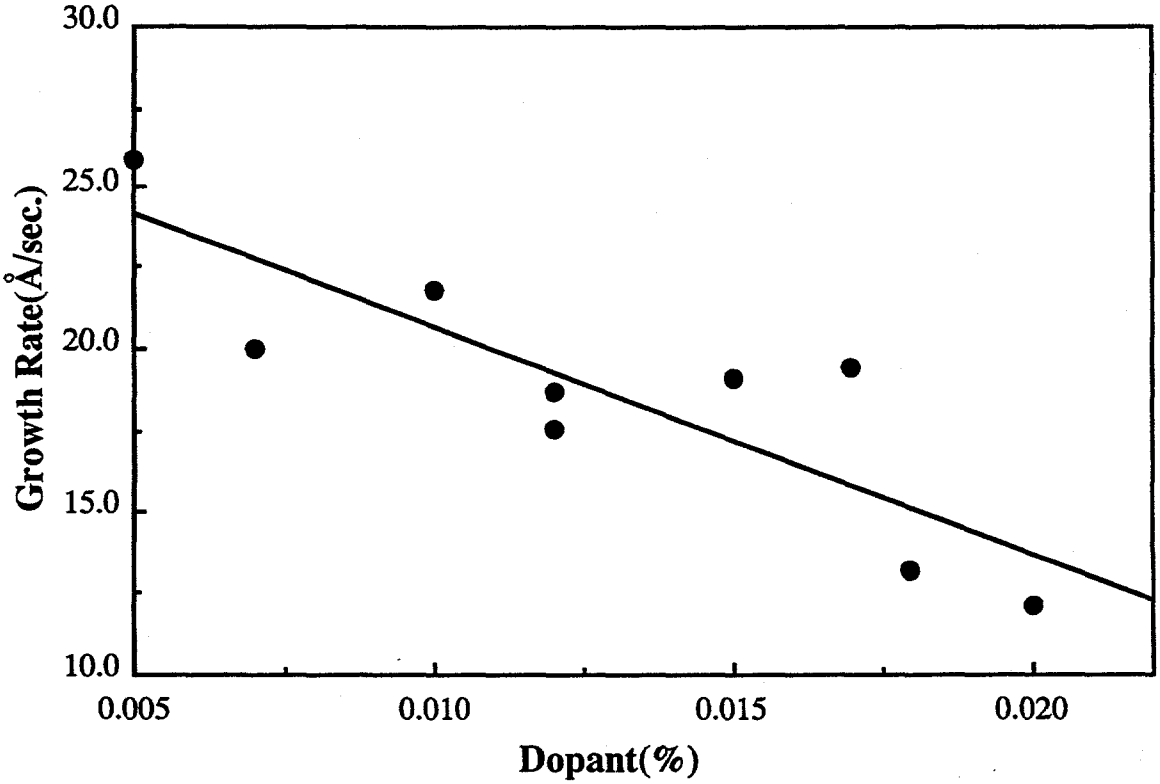

FIG. 4. Peak growth rate dependence on diborane concentration. The films were deposited at 360°C from 0.07% diethyl zinc and 2.4% tert-butanol.

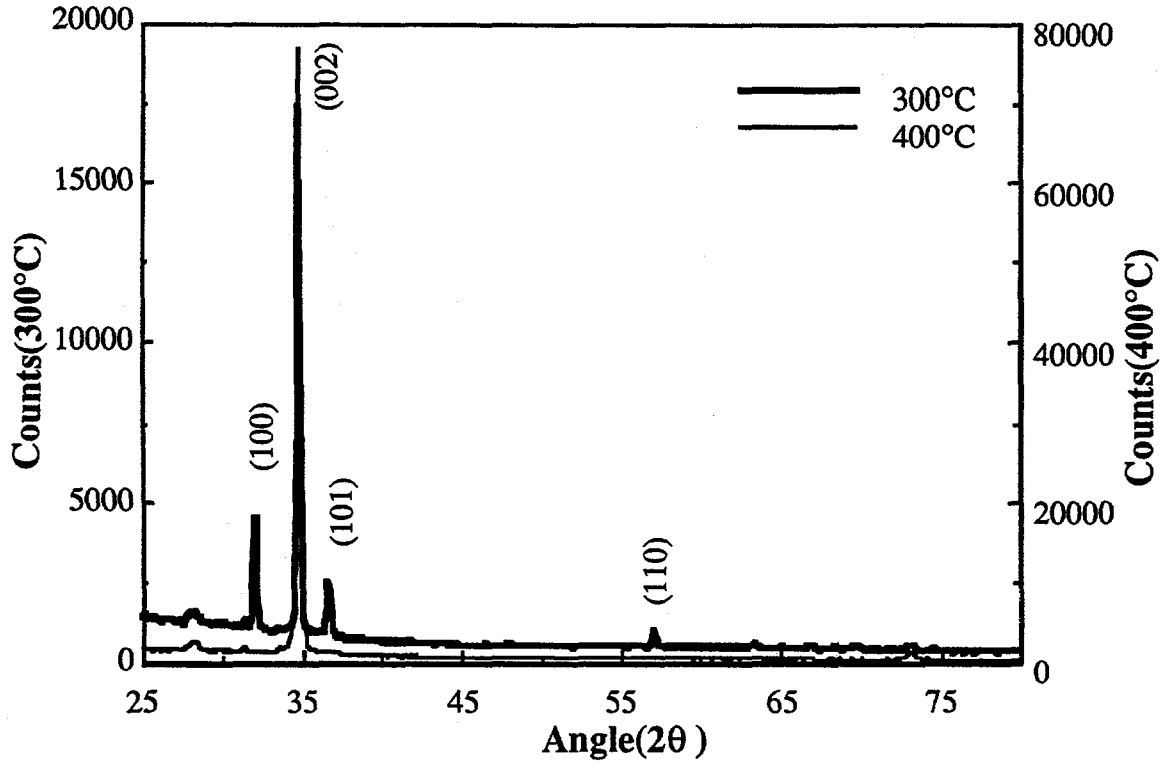

FIG. 5. X-ray diffraction spectra of boron doped zinc oxide films deposited at 300°C and 400°C on soda lime glass substrates.

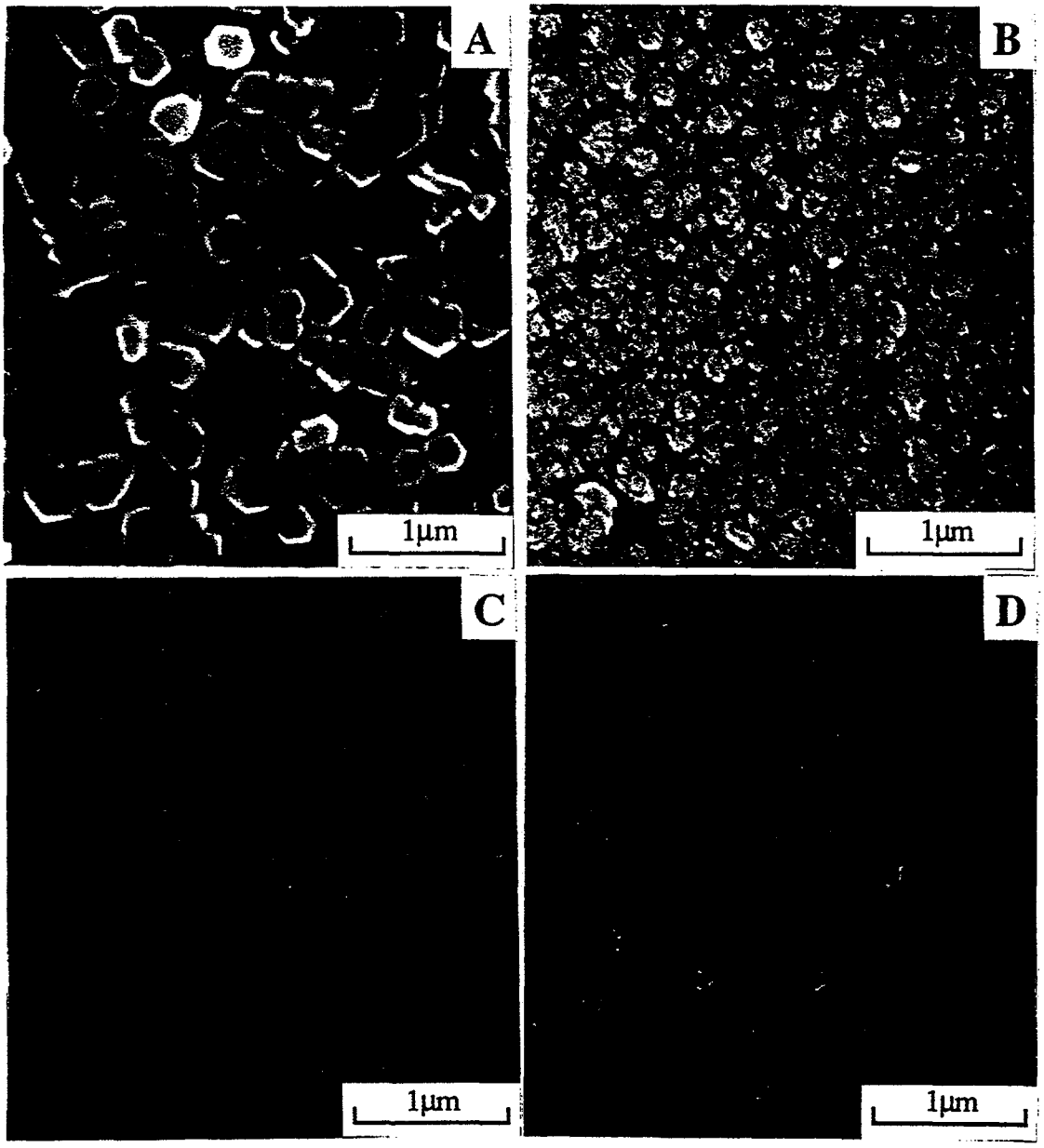

FIG. 6. Scanning electron micrographs of undoped and boron doped zinc oxide films. Sample (a) and (b) were deposited at 400°C and (c) and (d) deposited at 360°C. Sample (a) is undoped and Sample (b), (c) and (d) are doped with 0.012% diborane.

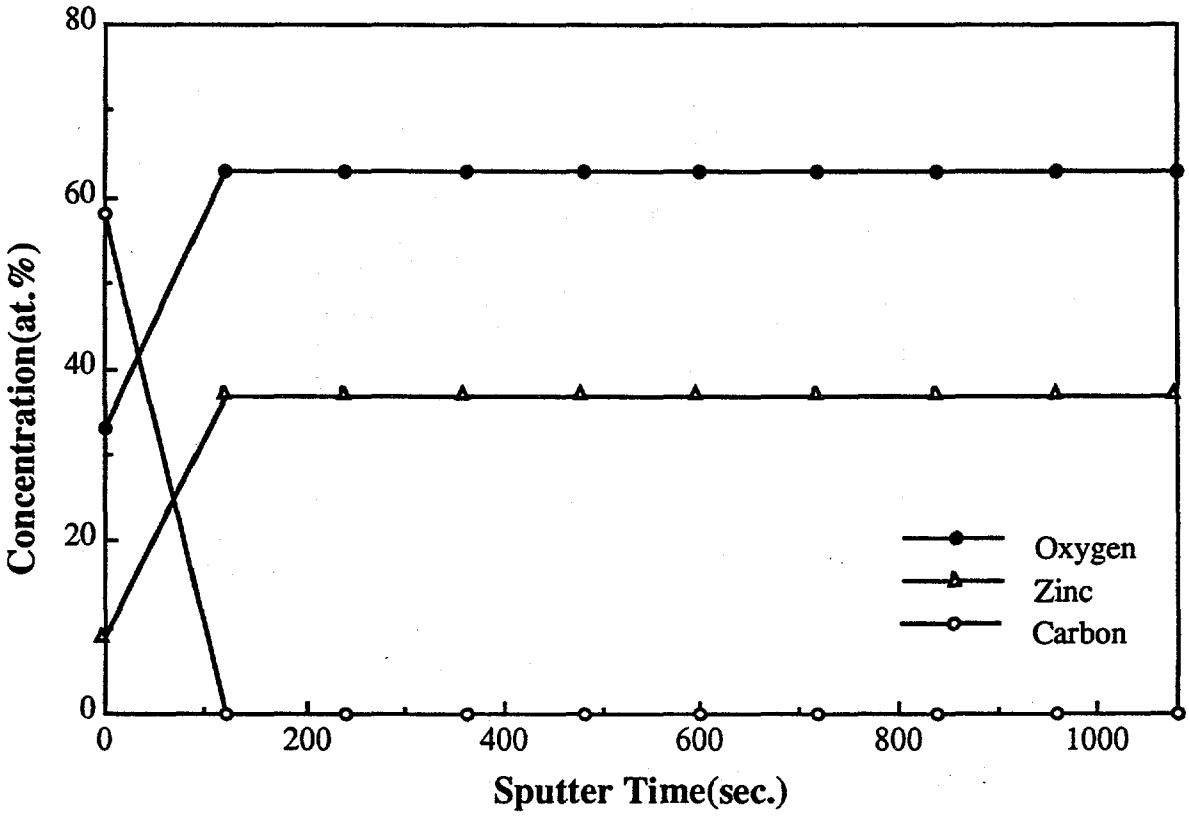

FIG. 7. Depth profile of boron doped zinc oxide film deposited at 360°C from 0.07% diethyl zinc, 2.4% tert-butanol and 0.012% diborane.

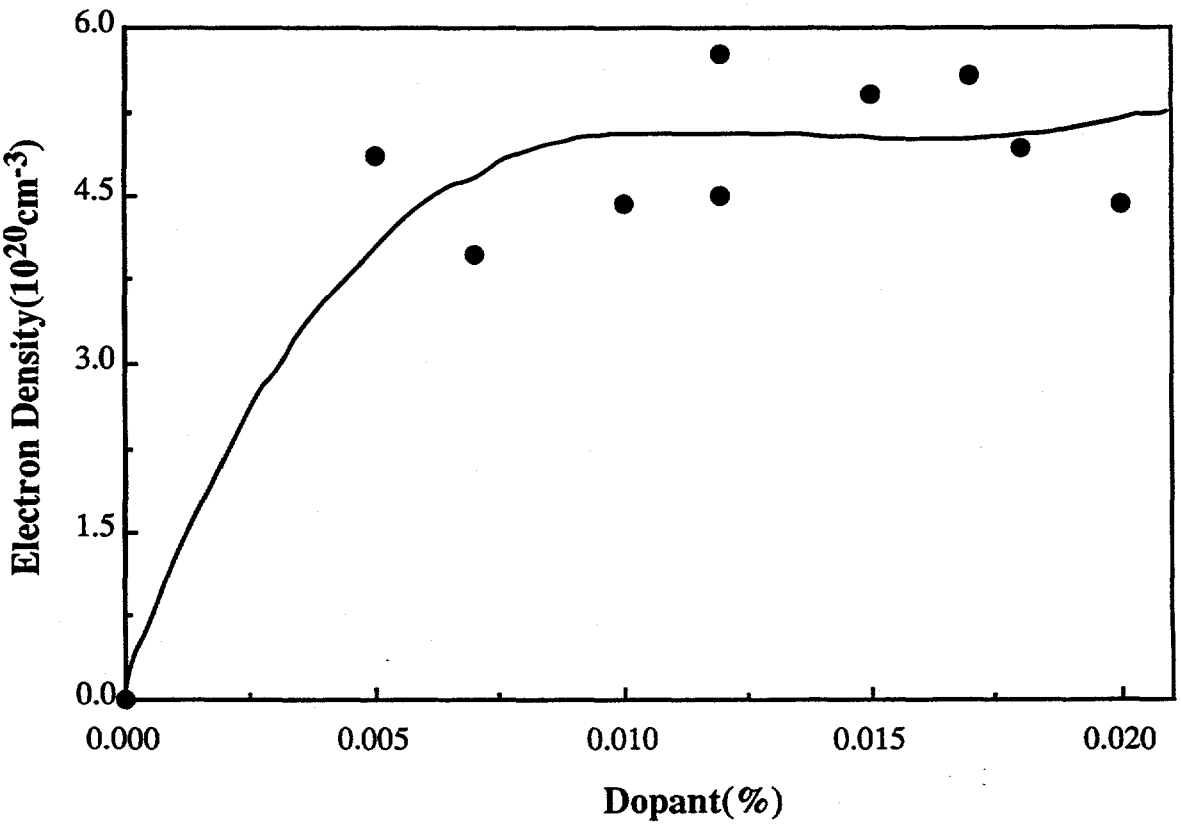

FIG. 8. Electron density dependence on diborane concentration for films deposited at 360°C from 0.07% diethyl zinc and 2.4% tert-butanol.

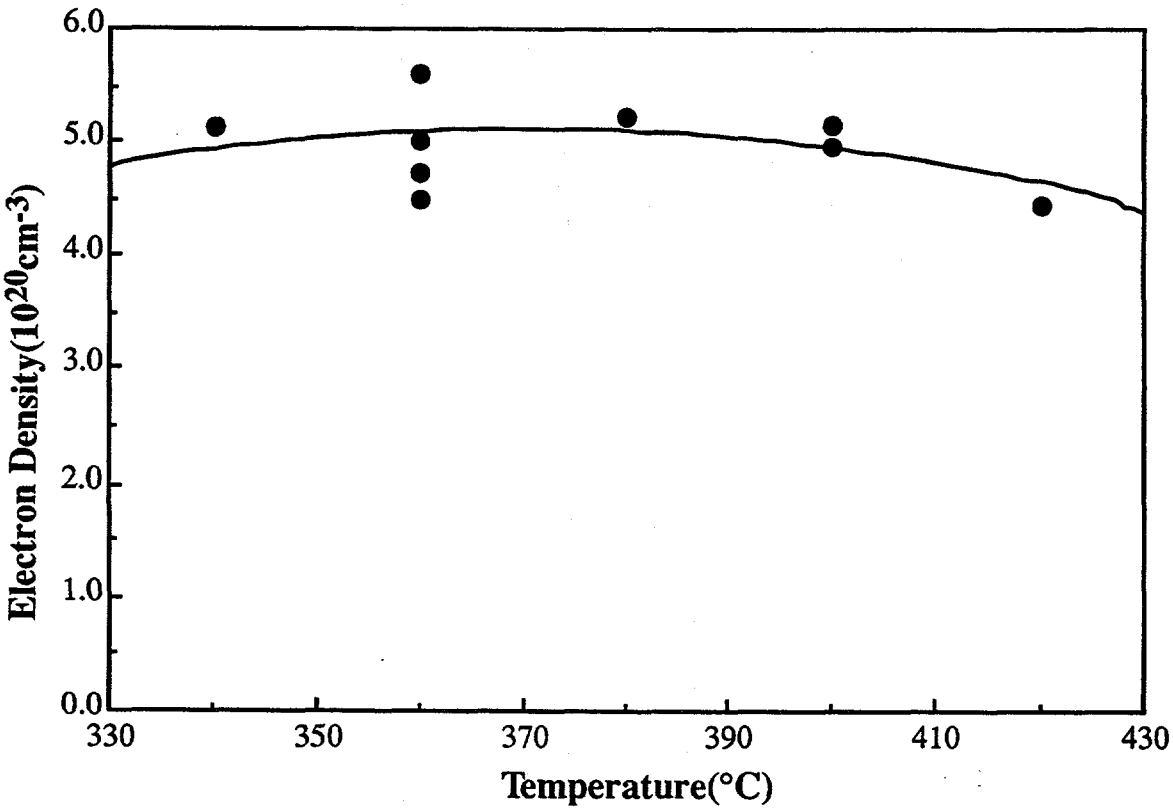

FIG. 9. Electron density as a function of deposition temperature. The films were deposited from 0.07% diethyl zinc, 2.4% tert-butanol and 0.012% diborane.

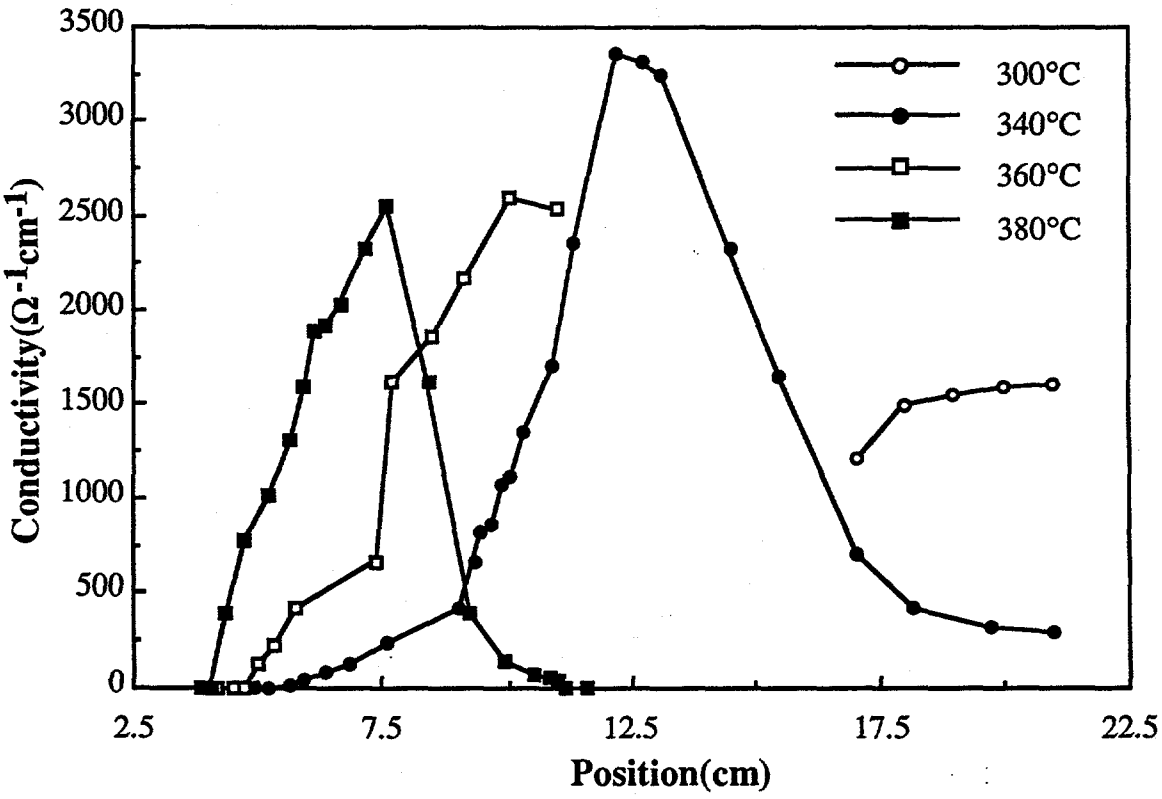

FIG. 10. Conductivity profile for films deposited at different temperatures. The samples are the same as in Figure 1.

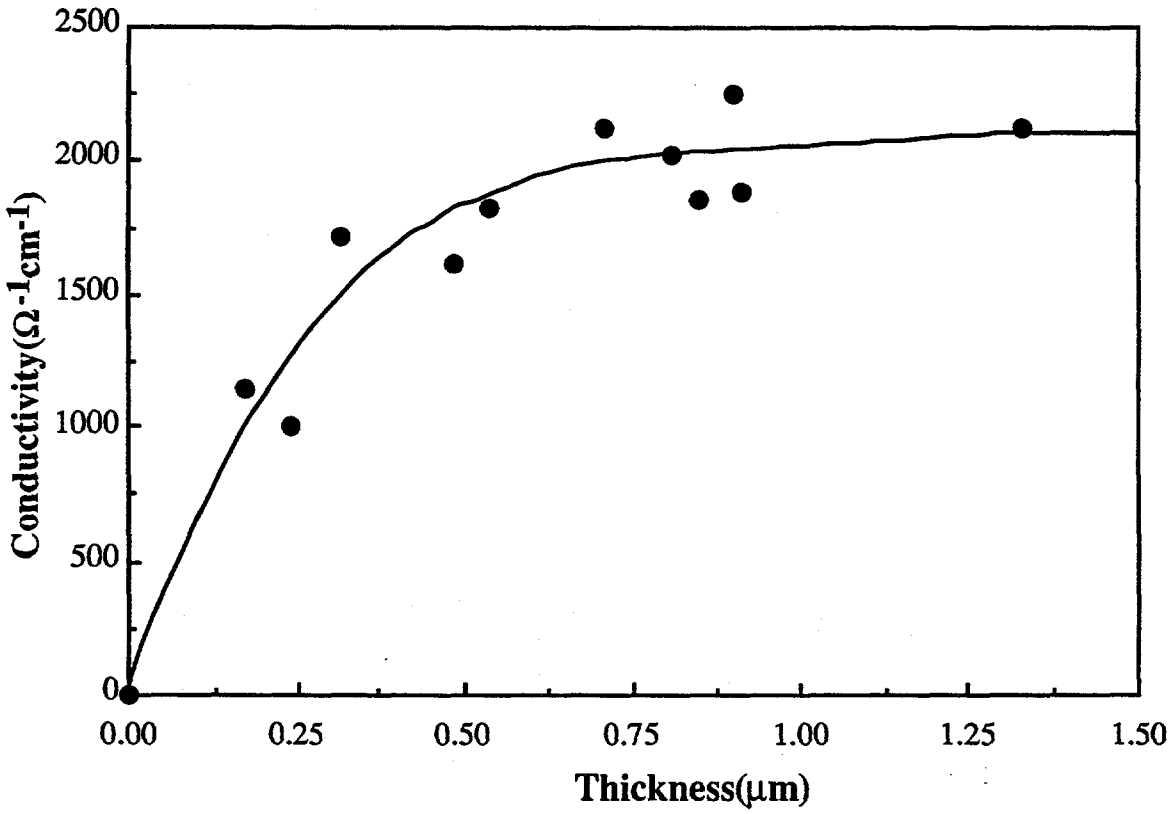

FIG. 11. Conductivity as a function of film thickness. The films were deposited at 360°C from 0.07% diethyl zinc, 2.4% tert-butanol and 0.012% diborane.

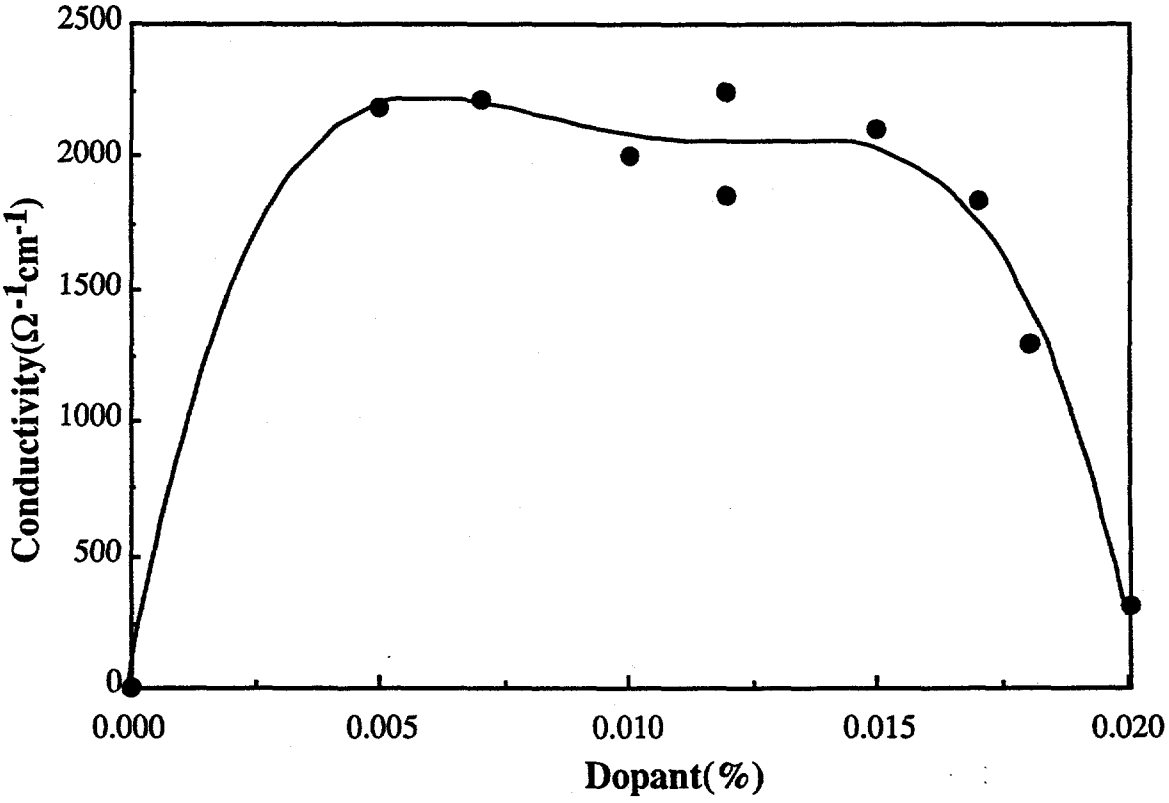

FIG. 12. Conductivity dependence on dopant concentration. The films were deposited at 360°C from 0.07% diethyl zinc and 2.4% tert-butanol with different diborane concentrations.

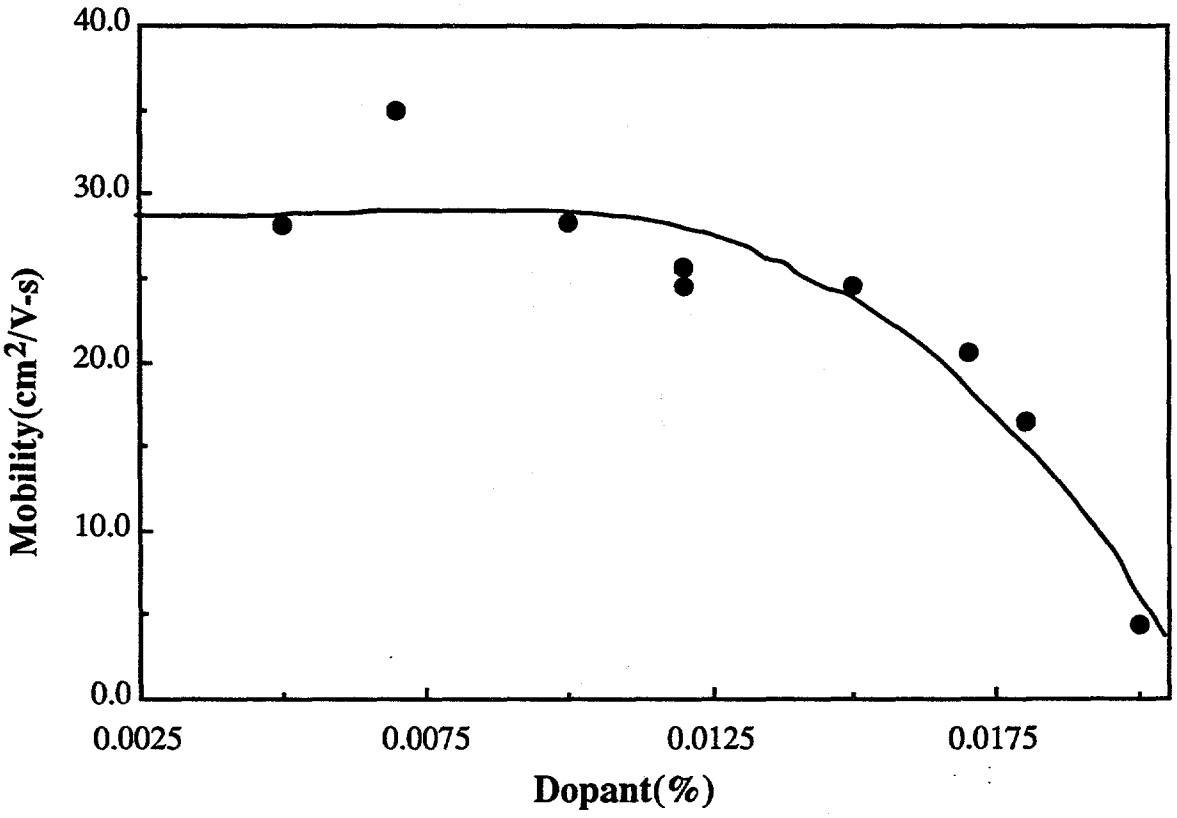

FIG. 13. Mobility dependence on dopant concentration. The films are the same as those in Figure 12.

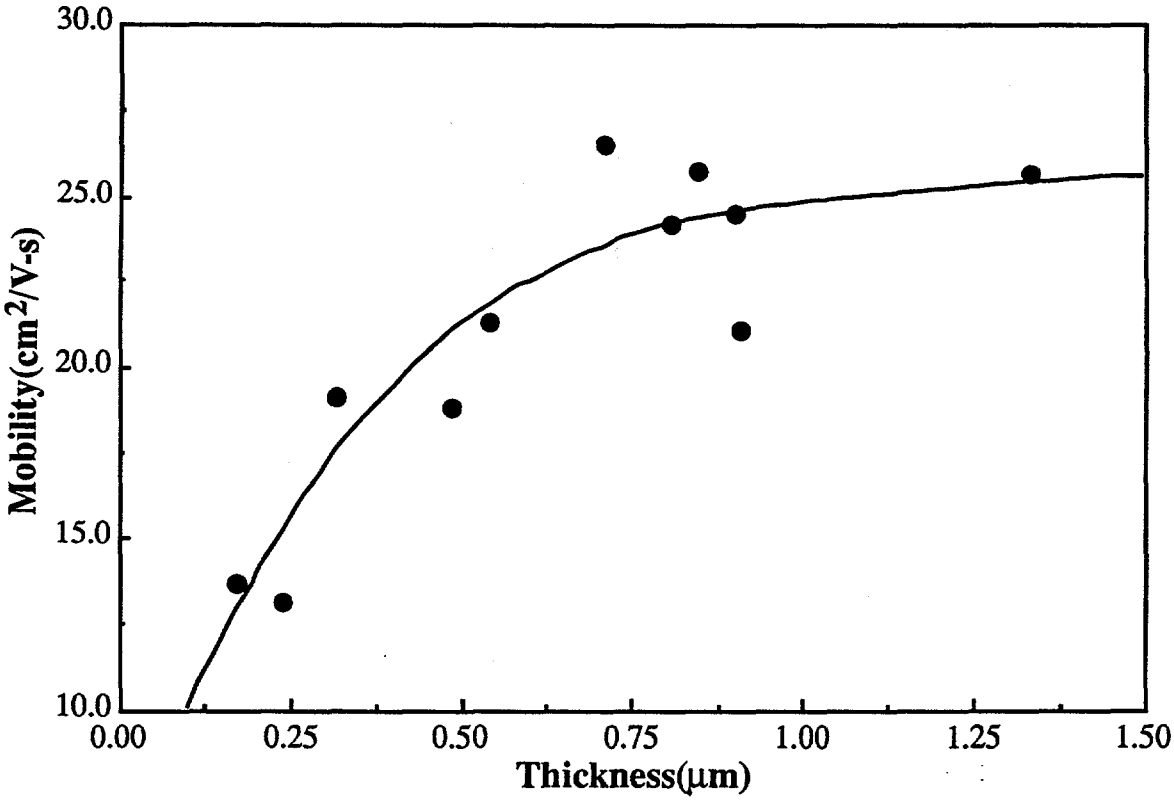

FIG. 14. Mobility dependence on film thickness. The films are the same as those in Figure 11.

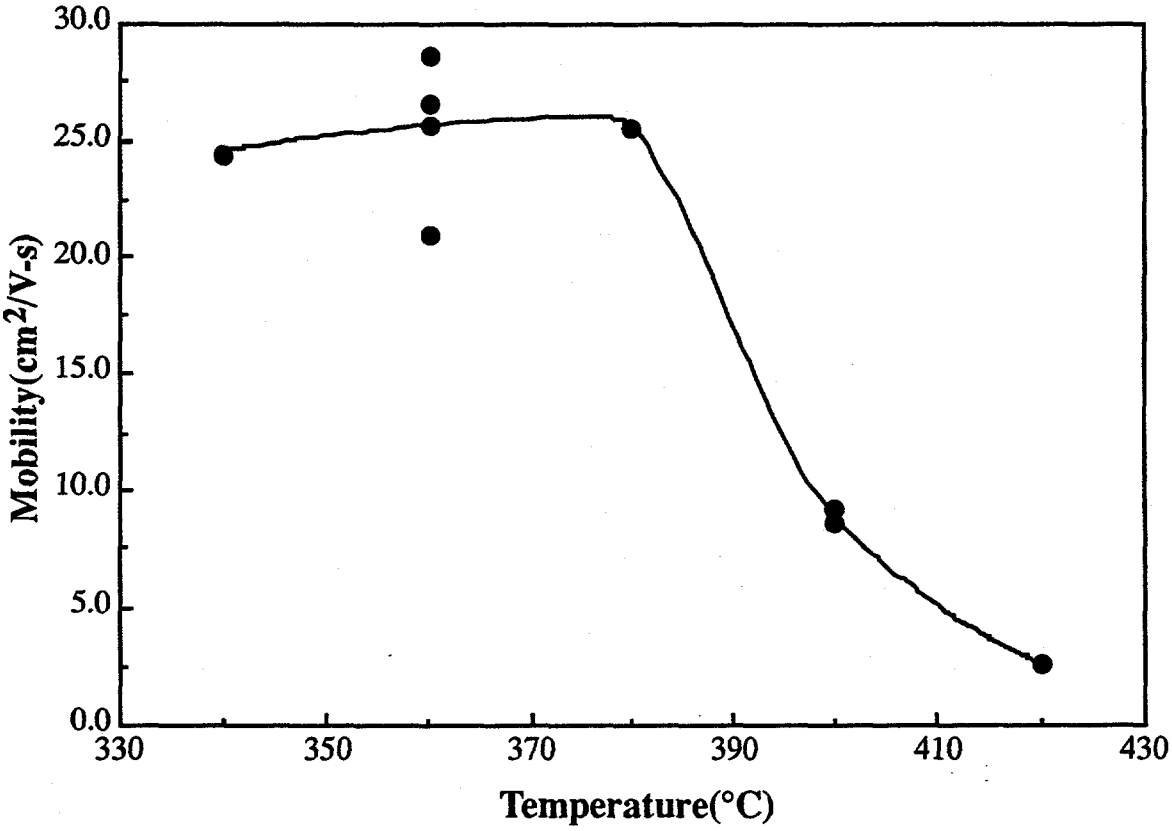

FIG. 15. Mobility dependence on deposition temperature. The films were deposited from 0.07% diethyl zinc, 2.4% tert-butanol and 0.012% diborane.

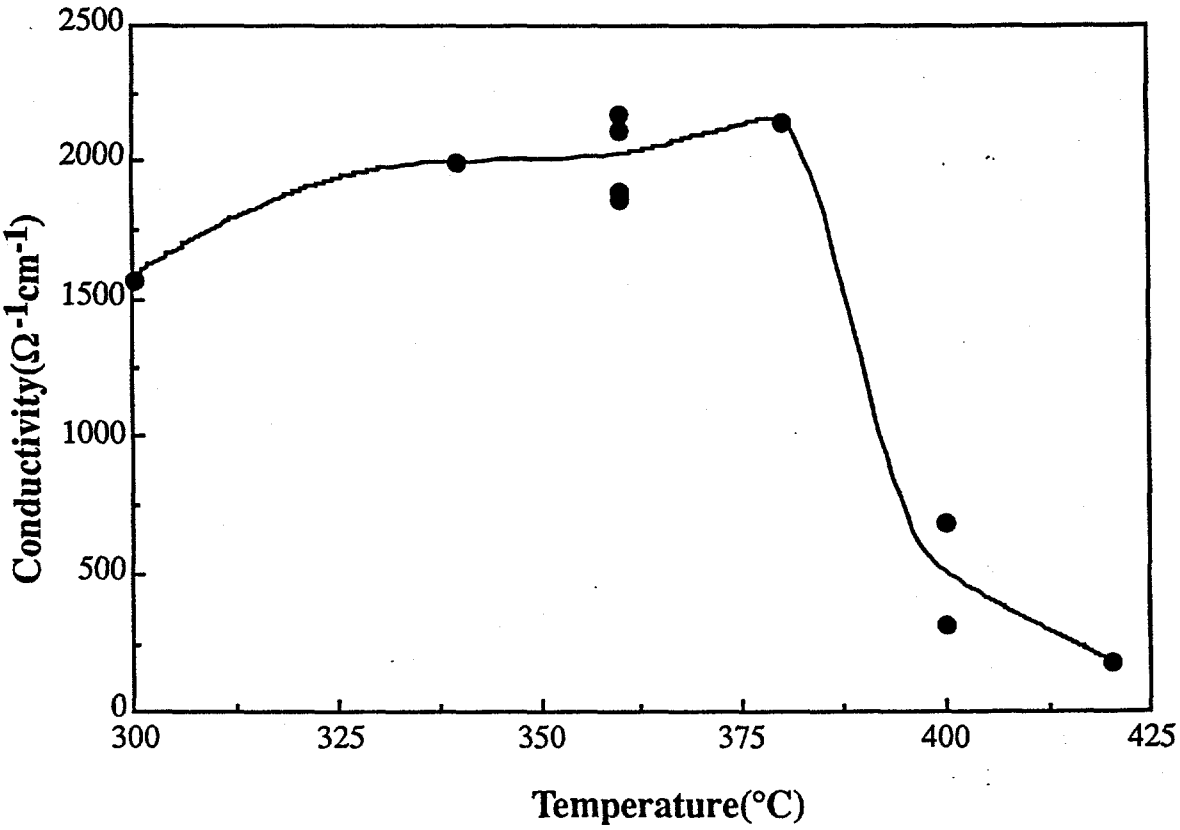

FIG. 16. Conductivity as a function of deposition temperature. The films are the same as those in Figure 15.

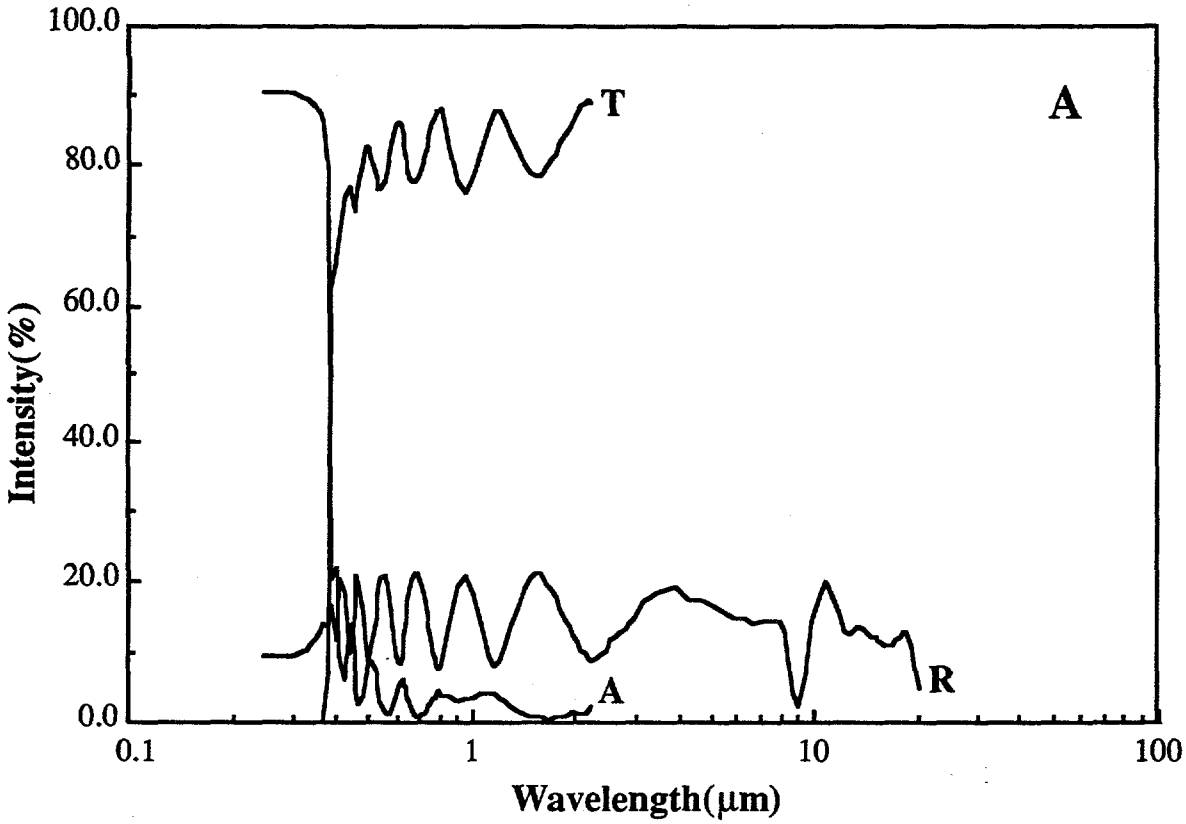
100.0
80.0
60.0
40.0
20.0
0.0
Intensity(%)
T
A
A
R
0.1
1
10
100
Wavelength(μm)

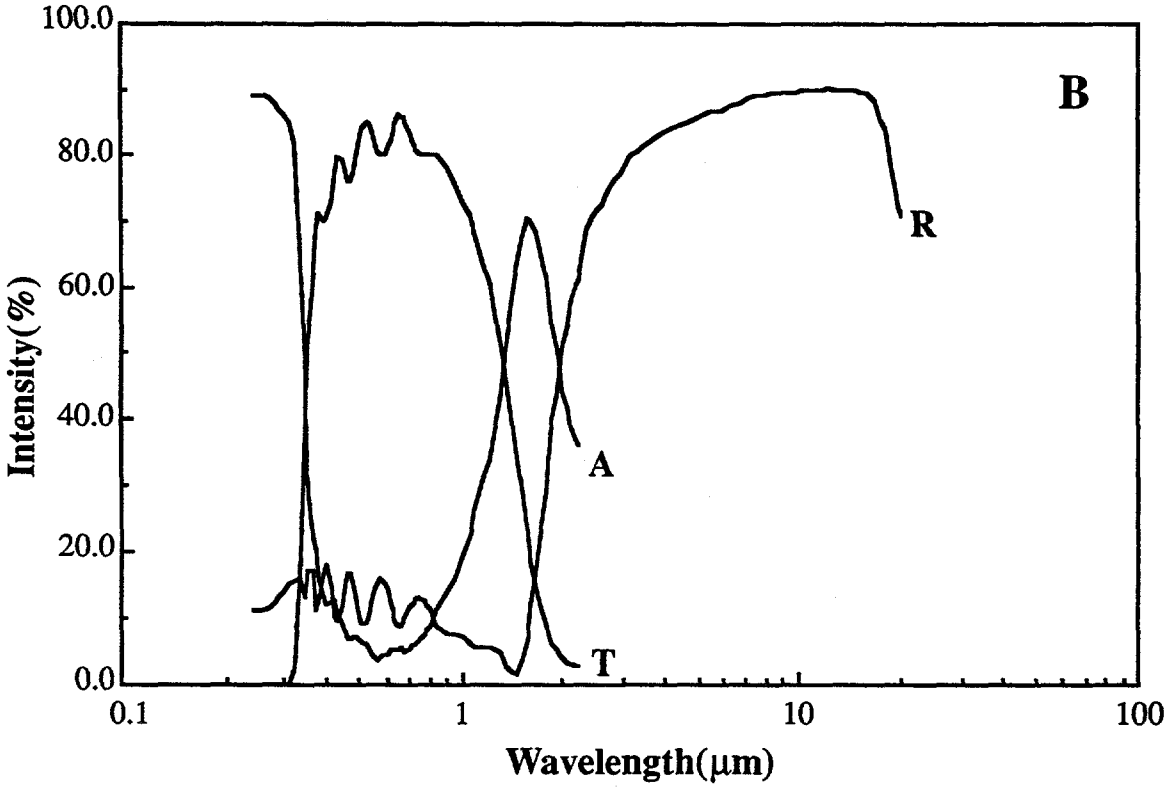
100.0
80.0
60.0
40.0
20.0
0.0
Intensity(%)
B
R
A
T
0.1
1
10
100
Wavelength(μm)

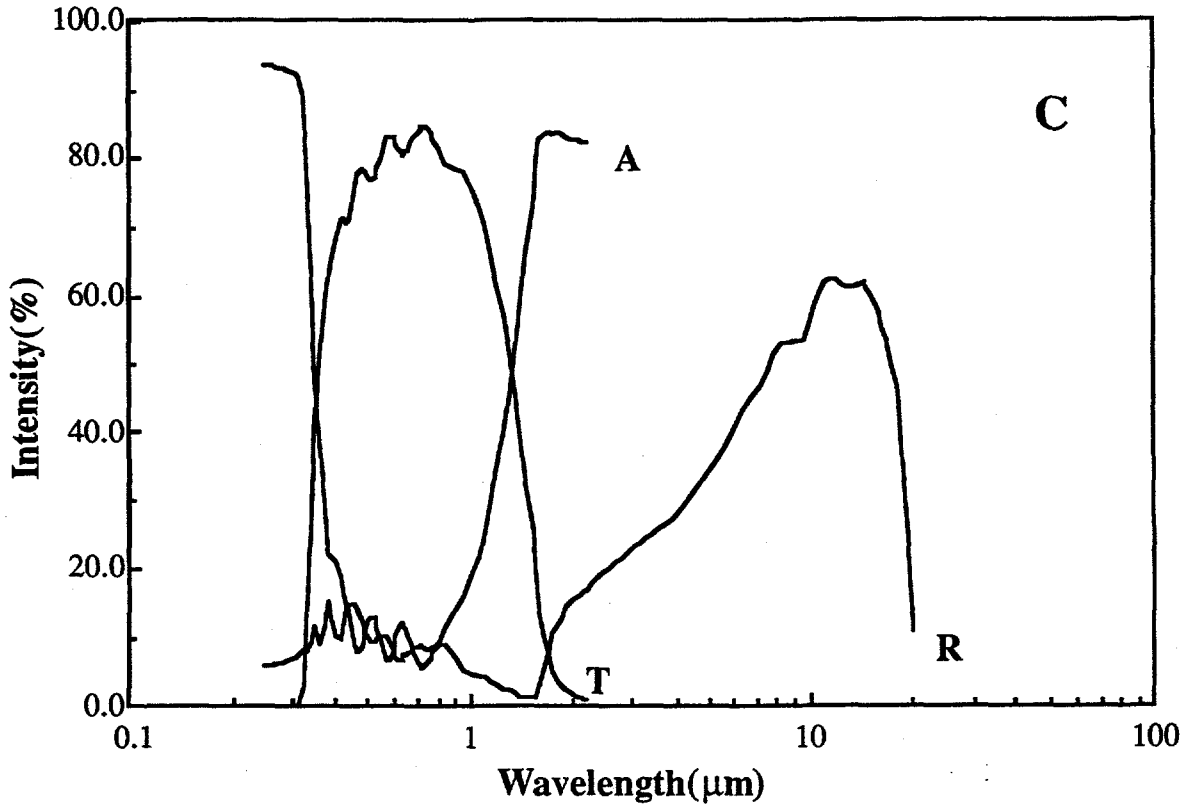

FIG. 17. Transmittance, reflectance and absorbance of three zinc oxide films deposited at 360°C from 0.07% diethyl and 2.4% tert-butanol on soda lime glass substrates. The diborane concentrations are: (a), 0.0%; (b), 0.012%; (c), 0.02%.

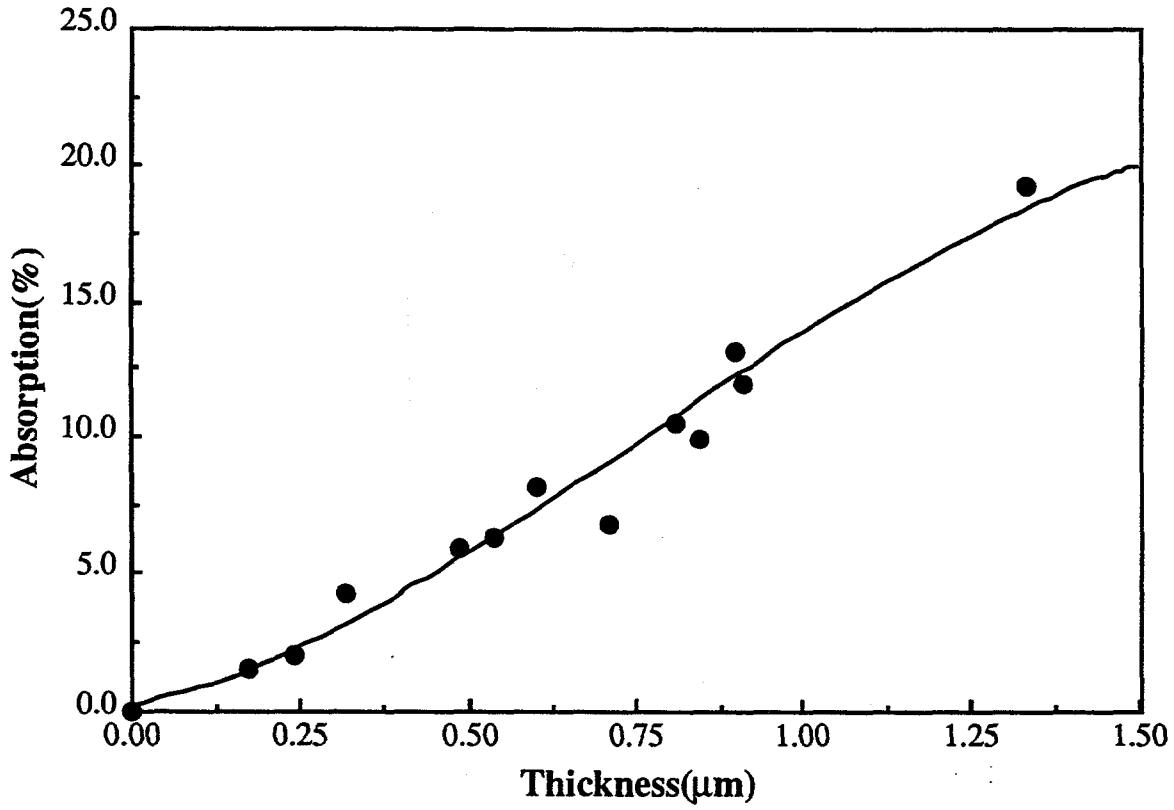

FIG. 18. Average absorption of boron doped zinc oxide film as a function of film thickness. The films were deposited with different deposition times at 360°C from 0.07% diethyl zinc, 2.4% tert-butanol and 0.012% diborane.

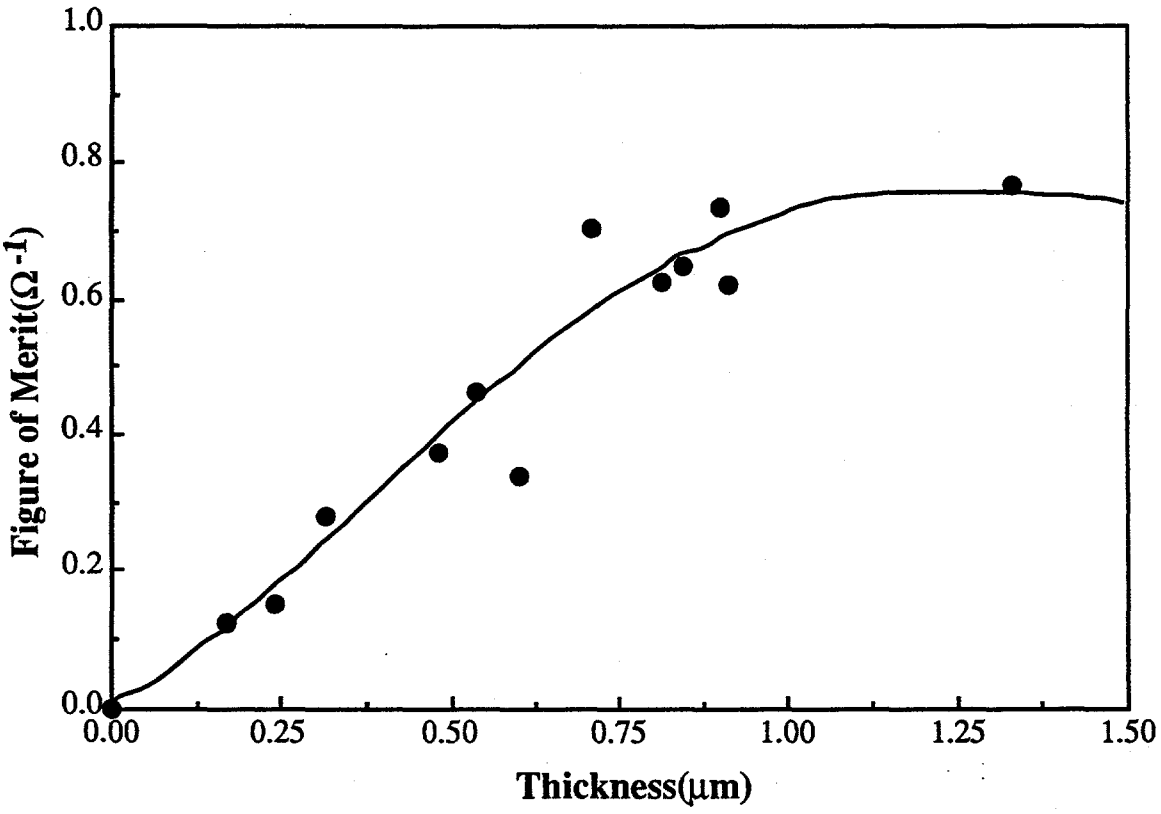

FIG. 19. Figure of Merit dependence on film thickness. The samples were deposited at 360°C from 0.07% diethyl zinc, 2.4% tert-butanol and 0.012% diborane.

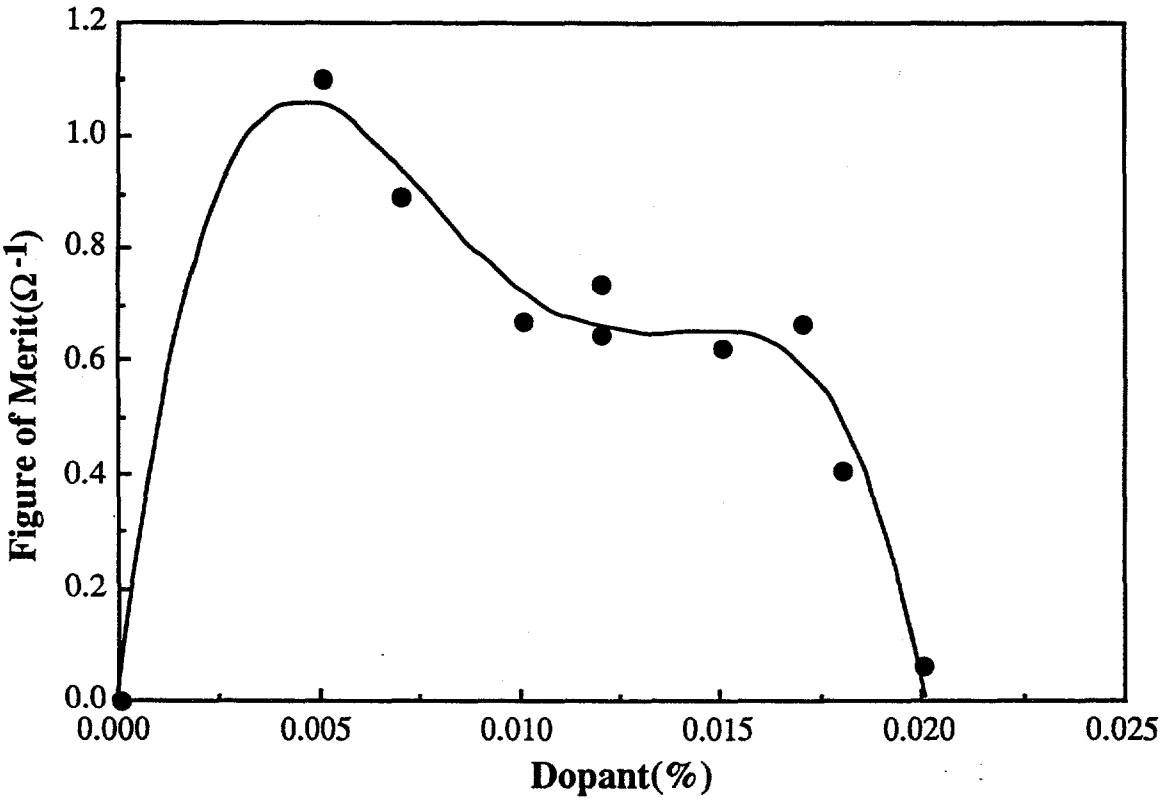

FIG. 20. Figure of Merit dependence on dopant concentration for films with thickness above 0.7 μm. The films were deposited with different dopant concentrations at 360°C from 0.07% diethyl zinc and 2.4% tert-butanol.

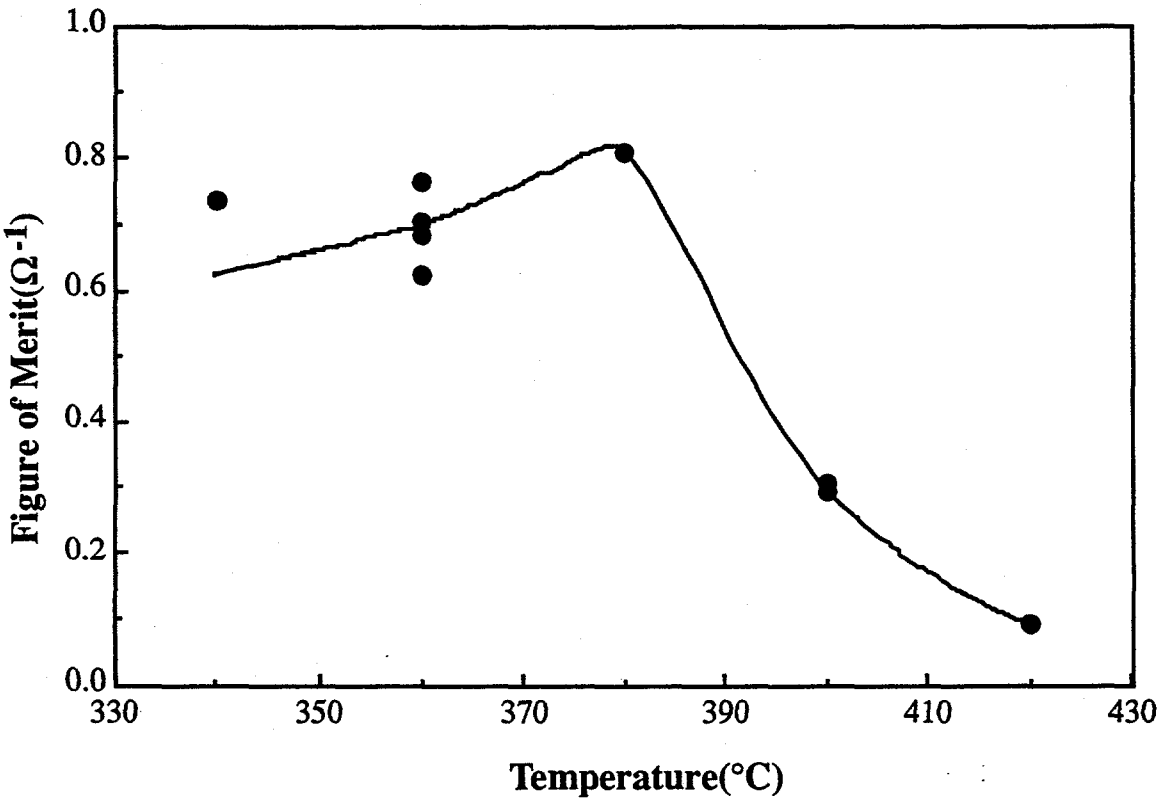

FIG. 21. Figure of Merit dependence on deposition temperature for films with thickness above 0.7 μm. The films were deposited from 0.07% diethyl zinc, 2.4% tert-butanol and 0.012% diborane.

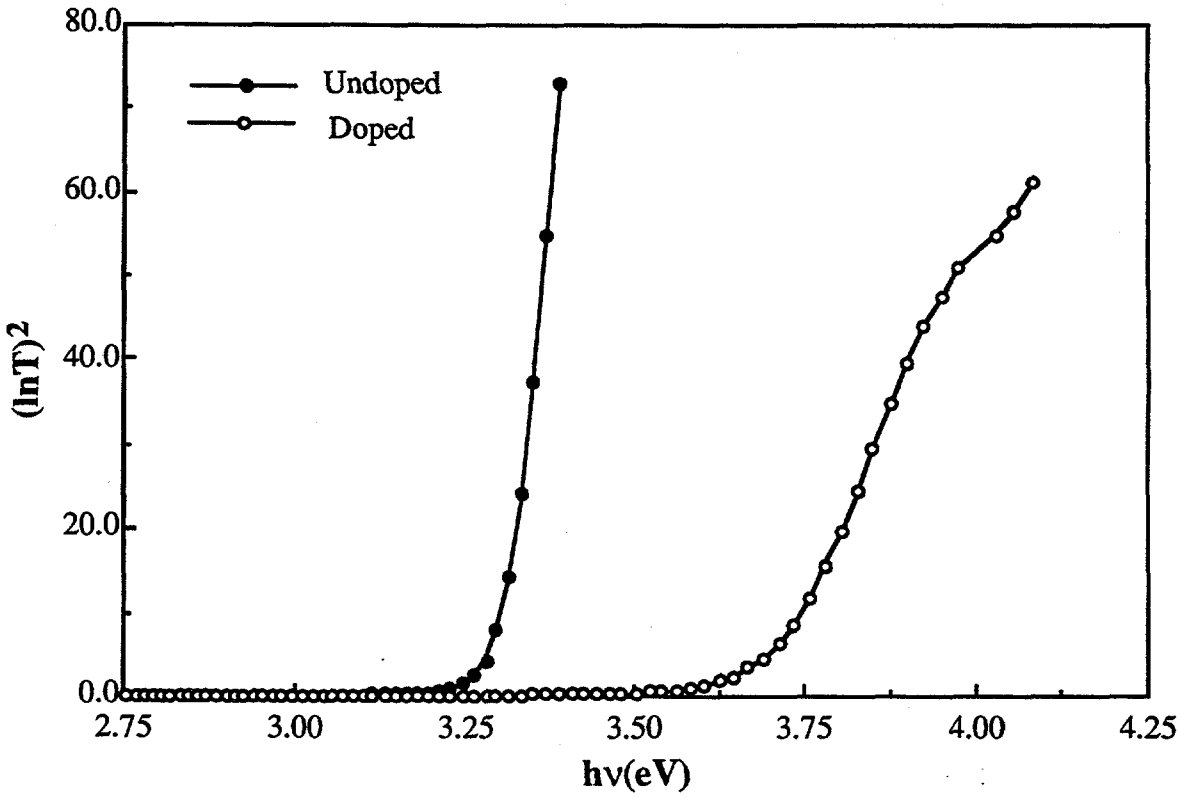

FIG. 22. Spectral absorption coefficients of two zinc oxide samples deposited on quartz substrates at 360°C from 0.07% diethyl zinc and 2.4% tert-butanol. The doped sample was deposited by introduction of 0.012% diborane.

2. TEXTURED ALUMINUM DOPED ZINC OXIDE THIN FILMS FROM ATMOSPHERIC PRESSURE CHEMICAL VAPOR DEPOSITION

ABSTRACT

Aluminum doped zinc oxide films have been deposited on soda lime glass substrates from diethyl zinc, triethyl aluminum and ethanol by atmospheric pressure chemical vapor deposition in the temperature range 367°C to 444°C. Film roughness was controlled by the deposition temperature and the dopant concentration. The films have resistivities as low as 3.0×10^{-4} Ω·cm, infrared reflectances close to 90%, visible transmissions of 85%, and visible absorptions of 5.0% for a sheet resistance of 4.0 Ω/square. The aluminum concentration within doped films measured by electron microprobe is between 0.3 at.% and 1.2 at.%. The electron concentration determined from Hall coefficient measurements is between $2.0 \times 10^{20} cm^{-3}$ and $8.0 \times 10^{20} cm^{-3}$, which is in agreement with the estimates from the plasma wavelength. The Hall mobility, obtained from the measured Hall coefficient and dc resistivity, is between 10.0 $cm^2/V\text{-}s$ and 35.0 $cm^2/V\text{-}s$. Over 90% of the aluminum atoms in the film are electrically active as electron donors. Scanning electron microscope and x-ray diffraction show that the films are crystalline with disk-like structures of diameter 100 nm to 1000 nm and height 30 nm to 60 nm. The films have the desired electrical and optical properties for applications in solar cell technology and energy efficient windows.

I. INTRODUCTION

Zinc oxide and zinc oxide based transparent conductive films have recently gained much attention because they have a number of advantages over the more common indium and tin-based oxide films[1-4]. In the fabrication of a-Si:H solar cells, the most popular materials as transparent electrodes have been indium oxide, indium tin oxide and fluorine doped tin oxide films. Since the fabrication process of a-Si:H normally uses plasma-enhanced chemical vapor deposition, the oxide films must be exposed to a hydrogen plasma. The plasma reduces the oxides to metals, thereby decreasing solar cell efficiency. This oxide degradation process occurs even at low temperature and low plasma power density[5,6]. Another disadvantage of indium oxide and tin oxide films is that tin and indium are expensive. Therefore, it is impractical to use indium and tin oxide films in the mass production of low cost photovoltaic cells. Zinc oxide films, however, are more stable than tin oxide or indium oxide films in the presence of a hydrogen plasma, and zinc is a cheap abundant and nontoxic element. If highly conductive and transparent zinc oxide films could be made with an inexpensive thin film deposition technique, the films could be used as less expensive transparent electrodes.

Zinc oxide is an n-type semiconductor with a hexagonal wurtzite structure and a band gap of about 3.3 eV[7]. Pure zinc oxide is highly transparent in the visible region, but its applications are limited by its low reflectance in the infrared and by its low dc conductivity. Zinc oxide films which are either non-stoichiometric or doped with atoms such as fluorine, boron, aluminum, gallium or indium have high conductivities[1,6,8-12]. The non-stoichiometric films have excellent electrical and optical properties, but they are not very stable at high temperatures. After heat treatments in

vacuum or in inert gas ambients at 400°C, the sheet resistances of the films increased by one to three orders of magnitudes[10]. For practical applications, therefore, undoped ZnO films are inferior to indium or tin based oxide films. On the other hand, doped films can be made to have very stable electrical and optical properties.

Zinc oxide films have been deposited on various substrates by techniques such as metalorganic chemical vapor deposition (MOCVD)[3,8,13], rf magnetron sputtering[10,11,12], reactive sputtering[1] and spray pyrolysis[6]. Metalorganic chemical vapor deposition is especially useful for large scale coatings at high growth rates. The most commonly used precursors in MOCVD are diethyl zinc (DEZ) and dimethyl zinc (DMZ). Although DMZ can react with oxygen at atmospheric pressure to coat substrates over large areas at high growth rates[14,15], it is expensive and reacts violently with air, water or alcohol even at low temperatures. In a laminar flow reactor, it is difficult to use DMZ and water or alcohol at temperatures above 300°C to deposit uniform films over large areas. DEZ is much cheaper than DMZ and has been widely used to deposit both doped and undoped ZnO films at different temperatures by atmospheric[8] and low pressure[13] chemical vapor deposition. The reaction between DEZ and oxygen is difficult to control, and the premature reaction upstream in a flow reactor produces powder even at low temperatures and low reactant concentrations. However, DEZ can be used with different alcohols at different temperatures to deposit uniform films at reasonably high growth rates.

In this chapter we report that aluminum doped zinc oxide films can be deposited in an atmospheric pressure CVD reactor from diethyl zinc (DEZ), ethanol and triethyl aluminum (TEA). The films can be textured to various extents at various temperatures with different TEA concentrations to provide efficient light trapping in solar cells. Resistance and Hall coefficient measurements were used to determine film resistivity, electron concentration and mobility. Optical measurements show that the doped films have high visible transmittance, low visible absorption and high infrared reflectance.

II. EXPERIMENTAL PROCEDURES

Zinc oxide deposition was carried out in an atmospheric-pressure laminar-flow rectangular nickel reactor which has been described previously[8]. High purity helium (99.995%, from Matheson Gas Products) was used as carrier gas for diethyl zinc, triethyl aluminum (DEZ and TEA from Ethyl Corporation) and ethanol (200 proof, from U.S. Industrial Chemicals Co.). Small amounts of water in the ethanol were removed by distillation from magnesium turnings. The DEZ bubbler was kept at 25°C and its vapor pressure at this temperature is about 16.1 Torr. Because TEA has a very low vapor pressure at room temperature (0.042 Torr), its bubbler was heated to about 85°C to achieve high vapor pressure (4.6 Torr). Triethyl aluminum was mixed with DEZ and then diluted by helium before introduction into the reactor. The ethanol bubbler was kept in an oven at 55°C to obtain a high vapor pressure. DEZ and ethanol vapors react quickly, and thus they were introduced into the reactor separately through slit-shaped nozzles, separated by a buffer flow of helium. The gas flow in each line was 4.0 l/min and the total gas flow was 12.0 l/min through a cross section 0.6 cm by 12.0 cm. The reactor was heated from the bottom by a hot plate and its top and bottom temperatures were determined by thermocouples inserted in holes in the side of the reactor. The bottom temperature was taken to be that of the substrate. The temperature difference between the top side of the reactor and the substrate depends on the substrate temperature and varies from 80°C to 100°C when the substrate temperatures are between 367°C and 444°C. The deposition temperature was stabilized to ±1°C. The reactor nozzle was insulated from the heated block by a thin-walled zone of width 3.5 cm and its temperature was kept at about 150°C lower than that of the central part of the reactor. This low temperature zone ensures the establishment of laminar flow by the time the gas reaches the substrate. The soda lime glass substrates were first cleaned with a sodium-free detergent (Detergent 8, from Alconox, Inc.) and then rinsed with deionized water.

Film thicknesses and refractive indices were determined mainly with a Rudolph Research AutoEl-II ellipsometer and a Metricon PC-2000 prism coupler. Ellipsometer measurements are most accurate for film thicknesses above 50 nm and below the full cycle thickness. The full cycle thickness depends on the film refractive index and is about 200 nm for ZnO film with a refractive index about 1.9. The thicknesses and refractive indices of thicker films (above 500 nm) were accurately determined by the prism coupler.

The infrared spectra were taken on a Nicolet Model 800 Fourier Transform spectrometer with a relative reflection attachment, which could measure near normal reflectance (incident angle less than 5°). A gold mirror with a known reflectance was used as the reflectance standard in the wavelength range from 2.0 μm to 20 μm[16]. The near ultraviolet, visible and near infrared spectra were obtained with a Varian 2390 spectrophotometer using an integrating sphere detector which could measure both total and diffuse components of the reflectance and transmittance. The reflectance standard is a barium sulphate plate and its reflectance was taken as 100.0% from 0.2 μm to 2.2 μm. The total reflectance was measured by putting the sample at the same position as the reflectance standard, so the sample beam coming into the sphere at one end of the sphere would hit the sample at opposite end at an incident angle about 5°. The scattered light in all directions was measured by the detector inside the sphere. The total transmittance was measured by letting the sample beam pass through the sample, enter into the integrating sphere through an opening at one end and hit the reflectance standard at the opposite end, which was used to prevent any light from leaking out of the sphere. Diffuse reflectance was measured by allowing the specular component to be reflected out of the integrating sphere. The diffuse transmittance was obtained by letting specularly transmitted light come out of the sphere. The absorption of the light within the film was then found by subtraction of the total reflectance and total transmission from 100.0%. For films with rough surfaces, however, the absorptions are unrealistically high because some light is trapped within the ZnO film and travels in the plane of the film until it is absorbed. In order to provide a better measurement of light absorption during one pass through the ZnO layer, spectra of rough ZnO films were obtained by covering the film surface with a thin layer of liquid of high refractive index (1.74, from Cargille Laboratories). The measured absorptions of films were further corrected for absorption by the liquid, the cover glass and the glass substrate.

The sheet resistance R was measured by using a Veeco FPP-100 Four Point Probe. By assuming that the film is homogeneous in the direction perpendicular to the substrate plane, the film bulk resistivity ρ follows the simple relation $\rho=Rt$, where t is the film thickness. In order to measure Hall coefficients, the film on the substrate was covered by a strip of Scotch tape 0.5 inch wide. The rest of the film on the substrate was etched away by immersing the sample in 4 M hydrochloric acid. The transverse voltage in the presence of a dc current was measured in a constant perpendicular magnetic field by using a Varian V-2300-A electric magnet, which was calibrated by a gaussmeter and found to have an intensity of 10.0 kilogauss. The measurement was repeated by reversing the direction of magnetic field. The magnitudes of two measured voltages were similar but with opposite sign, indicating that the hysteresis effect was negligible. The Hall coefficient R_H was then calculated from the averaged transverse voltage V (in mV), dc current I (in mA), the magnetic field B (in kG) and the thickness of the film t (in μm) according to the formula $R_H=(10.0Vt)/(IB)$.

X-ray diffraction measurements were made on a Philips powder crystallography instrument by using copper K_α radiation. A JEOL JSM-6400 scanning electron microscope (SEM) was used to obtain the crystallite orientation and size. Film compositions were found by a Cameca MBX electron microprobe equipped with a Tracor Northern TN-5502 EDS system and a TN-1310 WDS and stage automation system. The beam voltage, beam current and beam size were 5 kV, 30 nA and 16x16 μm^2, respectively. The standards used for Zn and Al were pure ZnO and $ZnAl_2O_4$. Oxygen concentration was not determined due to interference from the substrate. The surface

composition and depth profile were obtained by an SSX-100 ESCA X-ray photoelectron spectrometer.

III. RESULTS AND DISCUSSION

A. Film deposition

Undoped zinc oxide films were deposited at different temperatures from diethyl zinc and ethanol. The growth rates were found to depend linearly on DEZ concentrations at low DEZ to ethanol ratios when the ethanol concentration was kept constant[8]. In the doping experiments, DEZ and ethanol concentrations were held at 0.05% and 3.0%, respectively. The triethyl aluminum concentration was varied between 0.0% and 0.4% to deposit films with different aluminum concentrations at different temperatures. Figure 1 shows the growth rate profile as a function of deposition temperature. Diethyl zinc, triethyl aluminum and ethanol concentrations were 0.05%, 0.03% and 3.0%, respectively.

In a flow reactor, gas phase reactions change the gas phase composition along the flow direction. The deposition rate is maximized when the flux of film precursors onto the substrate is maximized. When the reactants enter the reactor, gas phase reactions are not fully developed because of the high activation energy of the reactions to form film precursors and therefore the film growth rate is low. As the reactant gas mixture moves down stream, there is a net buildup of film precursors in the gas phase which diffuse to the substrate to form film, and so the film exhibits a rising growth rate. The decline of the growth rate after the peak position corresponds to the depletion of the film precursors in the gas phase. At low temperatures, the reactions to form film precursors are slow and it takes a long time to build maximum film precursor concentrations in the gas phase, and so the deposition is slow and the peak position is further downstream. At high temperatures, gas phase reactions are fast enough to produce maximum film precursor concentrations in a short time. Film growth rate is high, and the peak position appears earlier along the flow direction. Figure 2 shows the peak growth rate as a function of deposition temperature. The peak growth rates were obtained from Figure 1 and were found to increase rapidly with deposition temperatures.

The growth rates also depend on triethyl aluminum concentrations. Figure 3 shows that the growth rates of films deposited at 400°C from 0.05% DEZ and 3.0% ethanol increase slightly with the dopant concentration.

B. X-ray diffraction and scanning electron microscopy

X-ray diffraction measurements showed that undoped films deposited from 0.05% DEZ and 3.0% ethanol in the temperature range 367°C to 444°C all gave strong (002) diffraction peaks. Other peaks with much less intensity were observed, indicating that the films are oriented with their c-axes perpendicular to the substrate plane. The (002) peak width was used to estimate the crystallite dimensions along the c-axis. The Cu K_α radiation contains two lines of wavelength 1.54056 Å and 1.54439 Å with intensity ratio 2:1[7]. ZnO with spacing 2.603 Å along (002) will give two (002) peaks separated by $\Delta(2\theta)=0.088°$ with intensity ratio 2:1. These two peaks were broadened and only one peak could be observed in the spectra because of the small crystallite sizes. In order to find the true peak width B_S corresponding to monochromatic x-rays, a minimization program[17] was used to approximate the measured peak by two gaussian curves with height ratio 2:1, width ratio 1:1 and separated by 0.088. The instrumental broadening was obtained by measuring the diffraction peak width of silicon (111) plane, which has 2θ around 28.5° and is close to ZnO (002) diffraction angle 2θ around 34.5°. There are two well separated silicon (111) diffraction peaks with intensity 2:1, and the width B_0 was found to be 0.072°. The corrected peak

width B can be calculated by the formula $B^2=B_S^2-B_0^2$, and the crystallite dimension t is then estimated according to $t=0.9\lambda/B\cos\theta$, where λ is the x-ray wavelength and θ is the Bragg diffraction angle[18]. The crystallite size along the c-axis was found to lie between 30 nm and 60 nm, depending on the deposition temperature, the dopant concentration, and the position on the substrate.

The average crystallite dimension in the direction perpendicular to the c-axis was determined by scanning electron microscopy (SEM) and was found to be much larger than the average crystallite height estimated by x-ray diffraction. The undoped films consist of disc-like hexagonal structures. The diameter of the "disc" varied from about 500 nm for films deposited at 367°C to about 1000 nm for films deposited at 444°C. Figure 4 (a) and (b) show two undoped ZnO samples deposited from 0.05% DEZ and 3.0% ethanol at 367°C and 420°C, respectively. The sample shown in Figure 4 (a) has many small and big disc-like crystallites. These small crystallites make the film appear to be mixed with "dust" because the SEM does not have enough resolution to show these small crystallites clearly. Sample B has sharper edges on its crystallites than sample A. The hexagonal planes of the films deposited at all temperatures were somewhat tilted, which indicates that the crystallites are not completely oriented with their c-axes perpendicular to the substrate plane.

The addition of aluminum to zinc oxide films has a strong influence on the film morphology. The doped films deposited at high temperatures are usually less rough than the undoped films. However, at very high temperatures (444°C), when the growth rate is very fast, the morphology difference between doped and undoped films becomes less obvious and they all look very "milky" and are therefore very rough. The dopant triethyl aluminum tends to create more nucleation centers during the deposition process and so the doped films have small crystallite sizes. Figure 4 (c) and (d) are electron micrographs of samples deposited at 367°C and 420°C from 0.05% DEZ, 0.03% TEA and 3.0% ethanol. Sample C has a spheroidal structure with a diameter of about 100 nm. Although sample D still has a disc-like structure, its crystallite diameter is only about 200 nm, which is about five times smaller than the crystallite diameter of undoped films deposited at the same temperature. Figure 4 (d) also suggests that the doped film is more oriented than the undoped film.

The crystallite sizes of the film also depend on film thickness. When the film was deposited for only a short time, there were many nucleation centers on the substrate which would produce many small crystallites in the film. These small crystallites do not have time to grow into large crystallites, and the thin film therefore has smaller crystallite sizes than the thick films. Figure 5 (a) and (b) show the electron micrographs of two samples deposited at 400°C from 0.05% DEZ, 0.03% TEA and 3.0% ethanol. The thicknesses of samples A and B are 270 nm and 840 nm, respectively. Sample A has spheroidal crystallites with diameters of about 50 nm. Sample B contains not only small spheroidal crystallites but also big, highly oriented crystallites with diameters above 100 nm.

C. Microprobe analysis and film composition

Electron microprobe analysis shows that the aluminum concentration in the doped films varies from 0.3 to 1.2 at.% for highly conductive ZnO films. The aluminum concentration is inhomogeneous along the gas flow direction. The position of peak growth rate is usually not the same as the position of highest aluminum concentration. Figure 6 shows the aluminum distribution along the gas flow direction for films deposited at different temperatures with 0.05% DEZ, 0.03% TEA and 3.0% ethanol. The aluminum concentrations along the gas flow direction are between 0.5 at.% and 1.0 at.% for films deposited at all four temperatures. Although the gas phase reaction is faster at high temperatures, the rate of aluminum incorporation into the film does not increase, so the aluminum concentration in the film does not increase either. Instead, triethyl

aluminum can produce powders at high temperatures. Figure 7 shows the dependence of aluminum to zinc ratio in the film on the aluminum to zinc ratio in the gas phase. The films were deposited at 400°C with 0.05% DEZ and 3.0% ethanol and the samples came from position 9.5 cm down stream from the reactor nozzle. Higher triethyl aluminum concentration in the gas phase leads to higher aluminum concentration in the film. The aluminum concentration in the film does not increase linearly with the aluminum concentration in the gas phase because some aluminum atoms produce powder on the upper side of the reactor.

X-ray photoelectron spectroscopy (XPS) detected carbon, oxygen and zinc on the surface. No other impurities were detected. Some hydrogen may also be present in the films, but it is impossible to use XPS to detect hydrogen. After the surface layer was sputtered away, only oxygen and zinc could be detected and the carbon content decreased to less than 0.5 at.%. The large amount of carbon on the film surface interferes with the quantitative analysis of the film composition. The surface layer must be sputtered away, but the preferential sputtering makes quantitative analysis unreliable. Therefore, no attempt was made to determine film composition by XPS.

D. Electrical properties

The film conductivity was determined from the measured sheet resistance R and the thickness of the film. Since the film composition and crystallite sizes are different from place to place and from one deposition temperature to another, the film conductivity is not uniform along the gas flow direction, and conductivity at the same position on the substrate is different from one deposition temperature to another. Figure 8 gives the conductivity distribution along the gas flow direction for films deposited at different temperatures with 0.05% DEZ, 0.03% TEA and 3.0% ethanol. The corresponding aluminum distribution is given in Figure 6. These data show that the film conductivity varies not only with the aluminum concentration in the films but also with the sample location on the substrate. Figure 9 shows the peak conductivity dependence on the deposition temperature for the same samples used in Figure 8. The position of peak conductivity is different from the position of peak growth rate and from the position of highest aluminum concentration. Although the films deposited at lower temperatures contain almost the same amount of aluminum as those deposited at higher temperatures, their conductivities are much smaller. The conductivity dependence on aluminum concentration is shown in Figure 10. The films were deposited at 400°C with 0.05% DEZ, 3.0% ethanol and different triethyl aluminum concentrations. The conductivity increases very rapidly with the increase of aluminum concentration in the film. Small amounts of aluminum introduce large number of free electrons in the doped films and the conductivity therefore increases. Figure 10 also shows that when the aluminum concentration in the film is above 0.45 at.%, any further increase of aluminum concentration does not further increase the conductivity. This can be explained by the formation of non-conductive aluminum oxide from the extra aluminum atoms and the achievement of equilibrium between the aluminum atoms contributing conduction electrons and those producing aluminum oxide. If the aluminum concentration were made very high, the film conductivity would be expected to drop again because of the large amount of non-conductive aluminum oxide in the film.

Table I shows the effect of film thickness on conductivity. The films were deposited at 400°C from 0.05% DEZ, 0.03% TEA and 3.0% ethanol, and the deposition time was varied so as to deposit films with different thicknesses. The samples were located at 7.0 cm from reactor nozzle (at the center of the substrate), and the aluminum concentrations were found to be about 1.0 at.% for all the samples. The ionized impurity scattering frequencies for those samples therefore should all be very close to each other. Very thin films have a lower conductivity and the conductivity increases as the films become thicker. When the film thickness is above 700 nm, the conductivity is almost a constant, and does not increase with the film thickness. The scanning electron micrographs (Figure 5) show that the thicker films have bigger crystallite sizes, and that the grain boundary scattering of free electrons in thicker films is less than that in thinner films.

Since the conductivity is inversely proportional to the electron scattering frequency[19], the conductivity of thicker films is higher than that of the thinner films. When the films become very thick (thickness above 700 nm), the grain boundary scattering frequency becomes less important. The conductivity is then limited by the ionized impurity scattering frequency and becomes less dependent upon the thickness of the films.

TABLE I. The thickness t, resistivity ρ, plasma wavelength λ_p, absorption A, electron density N_e and mobility μ determined from the measured Hall coefficients and from optical analysis for aluminum doped ZnO films deposited at 400°C from 0.05% DEZ, 0.03% TEA and 3.0% ethanol. The samples were located 7.0 cm from the reactor nozzle.

				Electrical		Optical		
Sample	t (μm)	ρ ($10^{-4}\Omega$.cm)	λ_p (μm)	N_e (10^{20}/cm^3)	μ (cm^2/V-s)	N_e (10^{20}/cm^3)	μ (cm^2/V-s)	A (%)
2049	0.25	8.26	1.13	6.74	11.2	8.21	9.2	1.8
2050	0.42	6.31	1.28	5.91	16.8	5.82	17.0	2.0
2051	0.54	5.27	1.33	6.73	17.6	5.27	22.4	2.7
2052	0.70	4.45	1.38	7.78	18.1	4.83	29.1	5.2
2053	0.85	4.64	1.45	6.45	20.9	4.34	31.0	4.2

Aluminum is an n-type dopant which replaces zinc atoms in the film and increases the free electron density. The measured Hall coefficient R_H can be used to calculate the free electron density N_e of the films by the formula $N_e=1/(R_H e)$, where e is the electron charge. The Hall mobility μ_H can be obtained from the measured Hall coefficient R_H and the film conductivity σ, according to the following relation: $\mu_H=R_H\sigma$. Whereas lightly doped single crystal ZnO mobilities are typically around 180 cm^2/V-s[7], the mobilities of the polycrystalline aluminum doped ZnO films vary from 10.0 to 35.0 cm^2/V-s, which is in the same range as that of the fluorine doped zinc oxide films[8,14]. These lower values can be expected because the conduction electrons inside polycrystalline ZnO films undergo grain boundary scattering. As the crystallite sizes become larger, the grain boundary scattering has less influence on the conduction electrons and the film mobility should increase. Table I also shows that the mobility increases with the film thickness.

Aluminum atoms in the films produce not only conduction electrons but also ionized impurity scattering centers. Figure 4 shows that the crystallite sizes decrease as the aluminum is incorporated into the film. When the film is very thick, the scattering frequency should be dominated by ionized impurity scattering; the grain boundary scattering has only a minor effect. High aluminum concentration in the film does not always increase the free electron concentration since the aluminum atoms must replace zinc atoms inside the crystallites to contribute conduction electrons. The extra aluminum atoms could not occupy the correct places inside the zinc oxide crystallites because of the limited solubility of aluminum inside ZnO. The ionic radius of aluminum is smaller than that of zinc, and the excess aluminum may occupy interstitial positions and deform the crystal structure. Some aluminum may also form aluminum oxide between small zinc oxide crystallites. In the low aluminum concentration range, free electron density increases as more aluminum is introduced into the film. The scattering by the ionized impurities, the defects in the crystal and the grain boundaries increases as the aluminum concentration becomes higher, and results in lower film mobilities. Figure 11 shows the mobility and electron density dependence on the aluminum concentration for films deposited at 400°C from 0.05% DEZ and 3.0% ethanol with different triethyl aluminum concentrations. The samples were taken at the position 9.5 cm on the substrate. As the aluminum concentration increases, the electron concentration increases and the mobility decreases.

Table II. Comparison of aluminum doped ZnO properties at different deposition temperatures. The thickness was determined by a prism coupler and the electron concentration and mobility were determined from the measured Hall coefficients. The films were deposited from 0.05% DEZ and 3.0% ethanol. The TEA concentration used for film deposited at 367°C was 0.03% and for other samples it was 0.02%. All the samples were taken from 9.5 cm on the substrate.

Sample	Td (°C)	t (μm)	R (Ω/sq)	Zn (at.%)	Al (at.%)	N_e (10^{20}/cm^3)	μ (cm^2/V-s)	η_{DE} (%)
2047	370	0.68	10.2	49.2	0.8	5.7	15.8	86
2040	400	0.84	8.48	47.3	0.4	3.9	22.3	118
2060	420	0.58	11.0	46.6	0.4	3.6	26.7	109
2058	444	0.55	12.4	45.7	0.4	2.9	31.4	87

The deposition temperature strongly influences both the gas phase reaction and the movement of dopant atoms to the positions in which they are electrically active. The doping efficiency, defined as the ratio of the number of free electrons in the film to the aluminum concentration, gives the fraction of aluminum atoms that are electrically active in the film. The doping efficiency can be calculated from the free electron concentration of the film, the aluminum percentage and the ZnO density, which is taken to be the bulk density 5.606 gram/cm^3. An aluminum atom replacing zinc atom in the ZnO crystal produces only one free electron, while an aluminum atom occupying an interstitial position might produce up to three free electrons. Which position aluminum atoms occupy depends on many factors, such as the aluminum concentration, the deposition temperature and the sample location on the substrate. Table II shows the doping efficiency of four samples deposited at different temperatures from 0.05% DEZ and 3.0% ethanol with different dopant concentrations. All the samples were chosen from position 9.5 cm on the substrate. Each aluminum atom was assumed to contribute one electron. The doping efficiency above 100.0% may result either from the contribution of more than one free electron from some aluminum atoms or from experiment errors in the measurements of the aluminum and electron concentrations. The film thickness, sheet resistance, electron concentration, film mobility and film composition are also shown in Table II. Since the deposition temperature changes the growth profile and therefore the peak growth rate position, it can be expected that the film properties listed in the table above do not reflect those of the peak growth position. Since the peak position was located at 9.5 cm from the reactor nozzle for deposition at 400°C, only sample B with the highest mobility was taken from the peak position. As deposition temperature increases or decreases from 400°C, however, the peak position moves away from the position 9.5 cm, and the doping efficiency decreases.

E. Optical properties

The free electrons in the doped films modify some of the film's optical properties. In the infrared, films behave like metals and have high reflectance. In the visible, however, the films are highly transparent, and their spectra are like those of dielectrics. The crossover between these two behaviors is the plasma wavelength, which moves to shorter wavelength as the free electron density in the films increases. Since the reflectance of doped ZnO films at the plasma wavelength is always very small (less than 5%), the extinction coefficient κ must be close to zero, and the following approximations are valid:

$$R_{min} \approx \frac{(n-1)^2}{(n+1)^2} \approx 0. \qquad (1)$$

Therefore, the refractive index n at the plasma wavelength should be close to 1.0, and the real part of the dielectric function $\varepsilon_1 \approx n^2 \approx 1$. Drude theory[19] predicts that the free electron concentration N_e is related to the plasma frequency ω_p by the following relation:

$$\omega_p^2 = \frac{N_e e^2}{\varepsilon_0 m_e^*(\varepsilon_\infty - 1)} - \gamma^2, \tag{2}$$

where ε_∞ is the high frequency dielectric function, γ is the Drude scattering frequency, e is the electron charge, ε_0 is the permittivity of vacuum, and m_e^* is the effective mass of electrons in the conduction band. For aluminum doped ZnO films produced by sputtering, the literature values[1] of ε_∞ and m_e^* are 3.85 and $0.28m_e$, where m_e is the free electron mass. The Drude scattering frequency can be taken as frequency-independent for qualitative analysis and can be found from the dc resistivity by the following formula:

$$\gamma = \rho \frac{N_e e^2}{m_e^*}. \tag{3}$$

Formulas (2) and (3) are coupled equations and the electron concentration can be found when the plasma frequency and the film resistivity are known. The film mobility is related to the scattering frequency and effective electron mass through

$$\mu = \frac{e}{\gamma m_e^*}. \tag{4}$$

Table I lists the electron density and mobility determined from measured Hall coefficients and from optical analyses. The plasma wavelength becomes longer as the film becomes thicker, indicating that the thicker films have lower electron concentrations. Since the films were deposited at approximately the same conditions with only different deposition times, the main difference between samples is their crystallite sizes. Although the electron density in an individual crystallite may be the same for samples with different thicknesses, the thicker films with larger crystallite sizes tend to be more porous and the measured electron density of the film will therefore be smaller. There is some discrepancy between the results obtained from optical analysis and from Hall coefficient measurements. Drude theory assumes a constant scattering frequency in the whole spectra range, however, the actual scattering frequency is frequency-dependent. A better theory, using a resistivity network model to take into account both ionized impurity scattering and grain boundary scattering to model the reflectance and transmittance data, will predict the resistivity, electron concentration and film mobility more accurately [20].

The spectra of undoped and aluminum doped ZnO films deposited at different temperatures are shown in Figure 12. The samples were chosen from the position 9.5 cm on the substrate. Sample A and B were deposited at 367°C and sample C at 420°C with 0.05% DEZ and 3.0% ethanol. The doped films B and C were deposited by introducing 0.035% TEA into the reactant gas mixture. Samples A and B are smooth and the interference fringes of their reflectance and transmittance spectra have deep valleys and tall crests. However, sample C looks very "milky" and the film has a rough surface. The interference fringes of its spectra have shallow valleys and crests, which is typical for rough films. The undoped film is transparent throughout the whole visible and near infrared range and has a plasma wavelength in the infrared (around 8.2 μm). Although the doped films are still transparent in the visible, the high free electron concentrations in the films make them opaque to near infrared and infrared light. The plasma wavelengths of samples B and C lie in the near infrared at 1.28 μm and 1.23 μm, respectively. The optical

behavior of doped samples in the infrared is dominated by free electrons. The maximum infrared reflectances of samples B and C are 82% and 90%. The measured reflectance of undoped film in the infrared is strongly influenced by phonons and the reflectance spectrum of the glass substrate, which has a broad reflection peak at 9.5 μm with intensity about 40% .

The absorption $A(\lambda)$ obtained from reflectance and transmittance depends slightly on the wavelength in the visible range. For solar cell applications, the appropriate average absorption A is calculated from

$$A = \frac{\int d\lambda \Psi(\lambda) A(\lambda)}{\int d\lambda \Psi(\lambda)}, \qquad (5)$$

where $\Psi(\lambda)$ is the solar irradiance spectrum for 1.5 air mass multiplied by the spectral sensitivity of a typical solar cell. This average absorption is very close to a simple geometrical average. Table I includes the absorptions of samples with different thicknesses. Usually the absorption increases as the film thickness increases. In solar cell applications, films require a low absorption in the visible range and a high dc conductivity. The performance of the transparent conducting films can be ranked according to a quantity called the Figure of Merit, which is defined[16] as $\sigma/\alpha = -1/(R \ln T)$, where σ is the bulk conductivity, α is the absorption coefficient, R is the sheet resistance in Ω/square and T is the average fractional transmittance from 400 nm to 800 nm. This definition is different from that used by Madan[21] who used bulk resistivity ρ instead of sheet resistance R. Although films with high electron concentrations tend to have low resistivities, their transmittance is lower than that of the films with low electron concentrations. Most samples have a Figure of Merit between 0.5 Ω^{-1} to 1.0 Ω^{-1}. Figure 13 (a) shows the Figure of Merit dependence on the film thickness. Since only the crystallite sizes are different for films with different thicknesses, the dependence of Figure of Merit on film thickness must result from the size differences among samples. The Figure of Merit dependence on the deposition temperature is given in Figure 13 (b). The maximum Figure of Merit was obtained for films deposited at 420°C. Figure 13 (c) shows that the aluminum concentration also influences the Figure of Merit, which first increases rapidly with the increase of aluminum concentration, and then becomes a constant at high aluminum concentrations. The best Figure of Merit for aluminum doped ZnO films was found to be 1.55 Ω^{-1}. The film was deposited at 420°C with 0.05% DEZ, 0.04% TEA and 3.0% ethanol, and the sample was located at 9.5 cm on the substrate. The aluminum concentration in this film was 0.84 at.%, and the film resistivity, electron density, mobility and thickness were found to be 3.0×10^{-4} Ω·cm, 8.8×10^{20} cm^{-3}, 23.3 $cm^2/V\text{-}s$, and 790 nm, respectively. The film has only a 5% absorption loss, along with a sheet resistance of 3.8 Ω/square.

The diffuse transmission spectra provide a useful way to characterize film roughness, which can improve the efficiency of amorphous silicon solar cells by increasing the amount of light-trapping. A recent paper by Gordon et al.[22] presented results that only a small amount of roughness characterized by 5% diffuse transmission at 632 nm is necessary to achieve optimal cell performance. Figure 14 (a) shows the diffuse transmittance of three different samples deposited at 400°C from different triethyl aluminum concentrations. The samples were located 9.5 cm from the reactor nozzle. The dopant tends to decrease crystallite size; small crystal sizes will lead to a smooth film surface. The undoped film has the largest crystal size and thus has highest diffuse transmittance. Figure 14 also shows that the optimal triethyl aluminum concentration for films deposited at 400°C is about 0.026%. The temperature dependence of diffuse transmittance is shown in Figure 14 (b). The samples were deposited from 0.05% DEZ, 0.01% TEA and 3.0% ethanol. Since crystallite sizes also increase as the deposition temperature becomes higher, the

sample deposited at a higher temperature is expected to have higher diffuse transmittance. For a gaussian roughness model, the root mean square roughness σ of the film is related to the diffuse reflectance R_d and total reflectance R_0 through[23]

$$R_0 - R_d = R_0 \exp\left(- \frac{(4\pi\sigma)^2}{\lambda^2} \right) \qquad (6)$$

The sample deposited at 400°C which gives 5% diffuse transmittance was found to have a rms roughness of about 28 nm, approximately the same as the crystallite height determined by x-ray diffraction methods.

VI. CONCLUSIONS

Aluminum doped ZnO films have been successfully deposited from diethyl zinc, triethyl aluminum and ethanol at various temperatures. Film thickness is not uniform along the gas flow direction and there is a maximum growth rate, indicating that the film is produced from some intermediate film precursors. The film growth rate increases with the dopant concentration and with the deposition temperature. X-ray diffraction and scanning electron microscopy reveal that the films are oriented with their c-axes perpendicular to the substrate. The film crystallites have disc-like structures with diameter between 100 nm and 1000 nm and height between 30 nm and 60 nm. The aluminum concentration in the film, determined from electron microprobe analysis, varies from 0.3 at.% to 1.2 at.%, depending on the dopant gas flow, the deposition temperature and the position along the gas flow direction. The electron concentration, determined form Hall coefficient measurements, was between 2.0×10^{20} cm^{-3} and 8.0×10^{20} cm^{-3}, in agreement with the estimates from the plasma wavelength. The measured dc conductivity is between 3.0×10^{-4} Ω·cm and $8.0 \times 10^{-4}\Omega$·cm. The Hall mobility calculated from the measured Hall coefficient and the film conductivity is in the range 10.0 cm^2/V-s to 35.0 cm^2/V-s. The doping efficiency, calculated by assuming every aluminum atom contributed one electron was nearly 100%, indicating that most aluminum atoms are electrically active. When the deposition temperature was below 420°C, the dopant TEA changed the roughness of the films by decreasing the crystallite size. As the temperature was increased to 444°C, the dopant was found to have less influence on the crystallite size, and the roughness of the films did not change appreciably with doping. Textured films with desired electrical and optical properties can be deposited by controlling the deposition temperature and the dopant concentration. The films with best performance for solar cell applications can be deposited at 400°C from 0.05% DEZ, 0.026% TEA and 3.0% ethanol, with a 5% diffuse transmission at 632 nm, indicating a roughness of about 28 nm. Films with a sheet resistance of 4 Ω/square have visible transmission above 85% when the influence from surface roughness is eliminated by covering the film with a thin layer of high refractive index oil. The doped films with a high electron concentration give high infrared reflectance (close to 90%). We conclude that the highly conductive and transparent aluminum doped zinc oxide films deposited in an atmospheric pressure reactor are suitable for efficient transparent electrodes in solar cells.

References

[1]Z. C. Jin, I. Hamberg, and C. G. Granqvist, J. Appl. Phys. **64**, 5117 (1988).

[2]J. B. Yoo, A. L. Fahrenbruch, and R. H. Bube, J. Appl. Phys. **68**, 4694 (1990).

[3]C. K. Lau, S. K. Tiku, and K. M. Lakin, J. Electrochem. Soc. **127**, 1843 (1980).

[4]M. J. Vellekoop, A. Venema, C. C. G. Visser, and P. M. Sarro, Ceramic Bull. **69**, 1503 (1990).

[5]R. Banerjee, S. Ray, N. Basu, A. K. Batabyal, and A. K. Barua, J. Appl. Phys. **62**, 912 (1987).

[6]A. F. Aktaruzzaman, G. L. Sharma, and L. K. Malhotra, Thin Solid Films **198**, 67 (1991).

[7]D. R. Lide, *Handbook of Chemistry and Physics*, 71st ed. (CRC Press, Boca Raton, Florida, 1991).

[8]J. Hu and R. G. Gordon, Solar Cells **30**, 437 (1991).

[9]P. S. Vijayakumar, K. A. Blaker, R. D. Wieting, B. Wong, A. T. Halani, and C. Park, U.S. Patent 4,751,149 (1988).

[10]T. Minami, H. Nanto, and S. Takata, Jpn. J. Appl. Phys. **23**, L280 (1984).

[11]B. H. Choi, H. B. Im, J. S. Song, and K. H. Yoon, Thin Solid Films **194**, 712 (1991).

[12]S. N. Qiu, C. X. Qiu, and I. Shih, Solar Energy Mater. **15**, 261 (1987).

[13]S. Oda, H. Tokunaga, N. Kitajima, J. Hanna, I. Shimizu, and H. Kokado, Jpn. J. Appl. Phys. **24**, 1607 (1985).

[14]J. Hu and R. G. Gordon, Mater. Res. Soc. Symp. Proc. **202**, 457 (1991).

[15]F. T. J. Smith, Appl. Phys. Lett. **43**, 1108 (1983).

[16]J. W. Proscia., Ph.D. thesis, Harvard University, (1988).

[17]W. H. Press, B. P. Flannery, S. A Teukolsky, and W. T. Vetterling, *Numerical Recipies* (Cambridge, New York, 1986).

[18]B. D. Cullity, *Elements of X-ray Diffraction*, 2nd ed. (Addison-Wesley, Reading, MA, 1978).

[19]I. Hamberg and C. G. Granqvist, J. Appl. Phys. **60**, R123 (1986).

[20]J. Hu and R. G. Gordon, to be published.

[21]R. E. I. Schropp and A. Madan, J. Appl. Phys. **66**, 2027 (1989).

[22]R. G. Gordon, J. W. Proscia, G. B. Ellis, Jr., and A. E. Delahoy, Solar Energy Mater. **18**, 263 (1989).

[23]H. E. Bennett and J. O. Porteus, J. Opt. Soc. Am. **51**, 123 (1961).

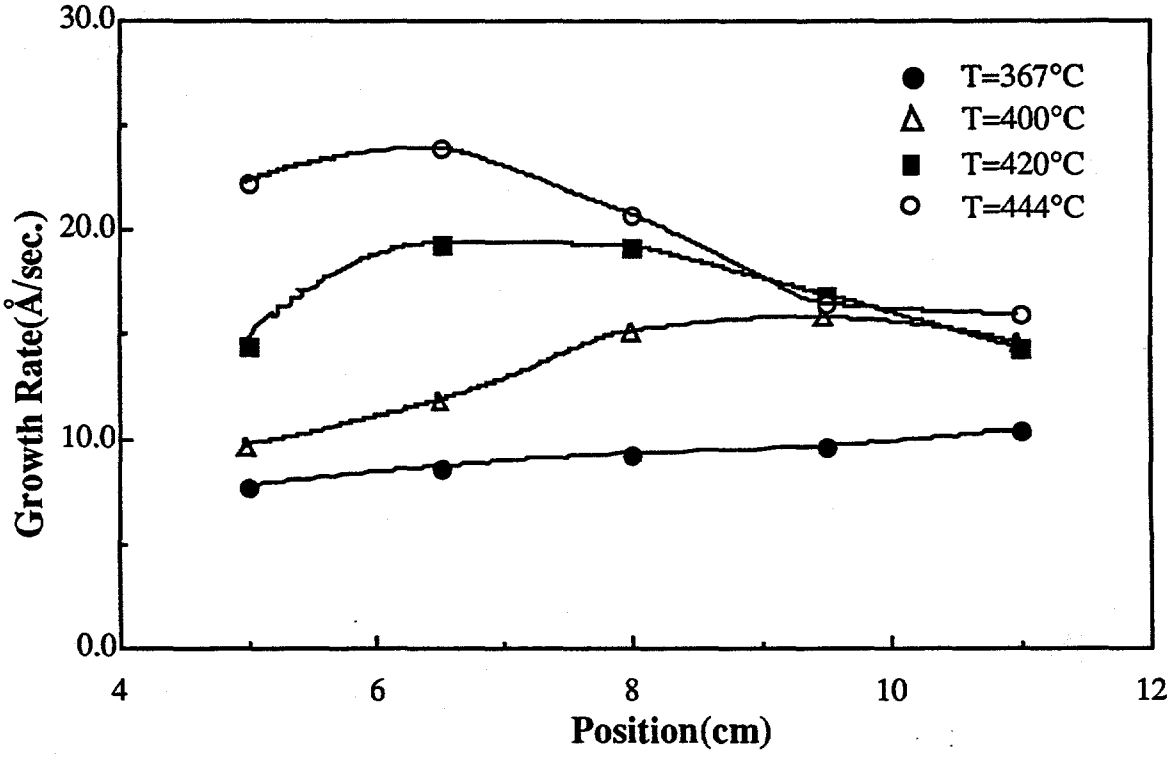

FIG. 1. Growth rate profile as a function of deposition temperature. The reactant gas mixture contains 0.05% DEZ, 0.03% TEA and 3.0% ethanol.

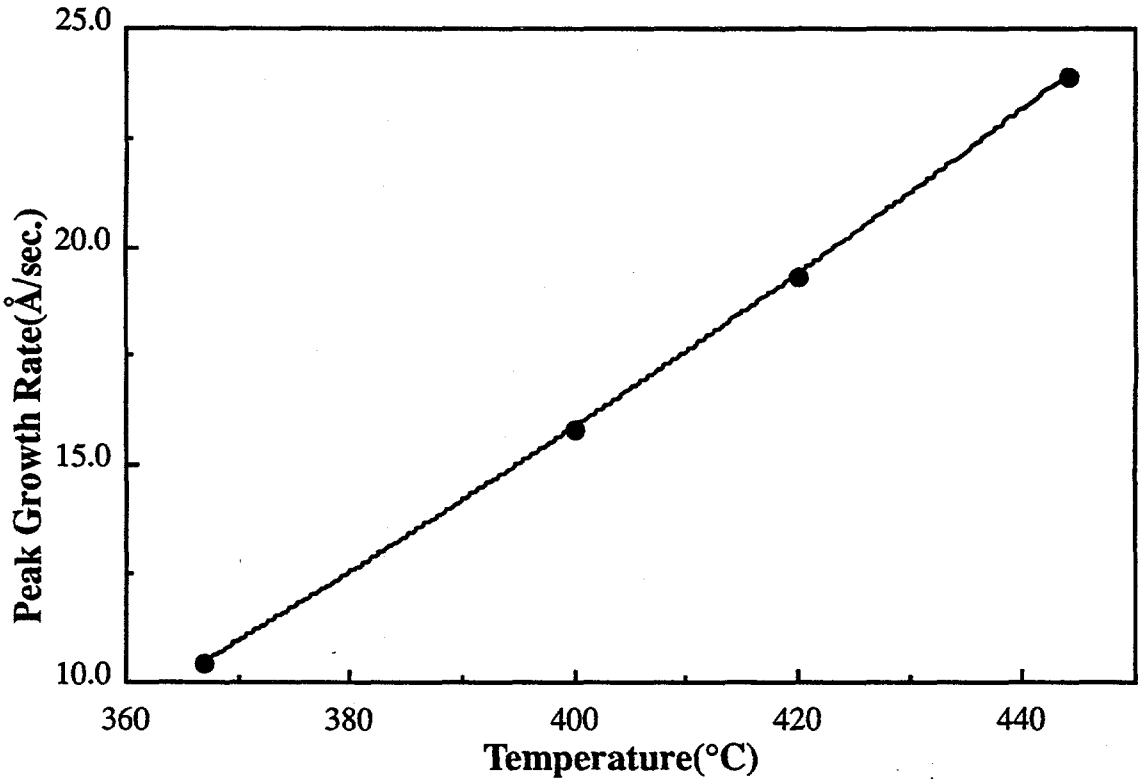

FIG. 2. Peak growth rate dependence on deposition temperature. The samples were the same as in Fig. 1.

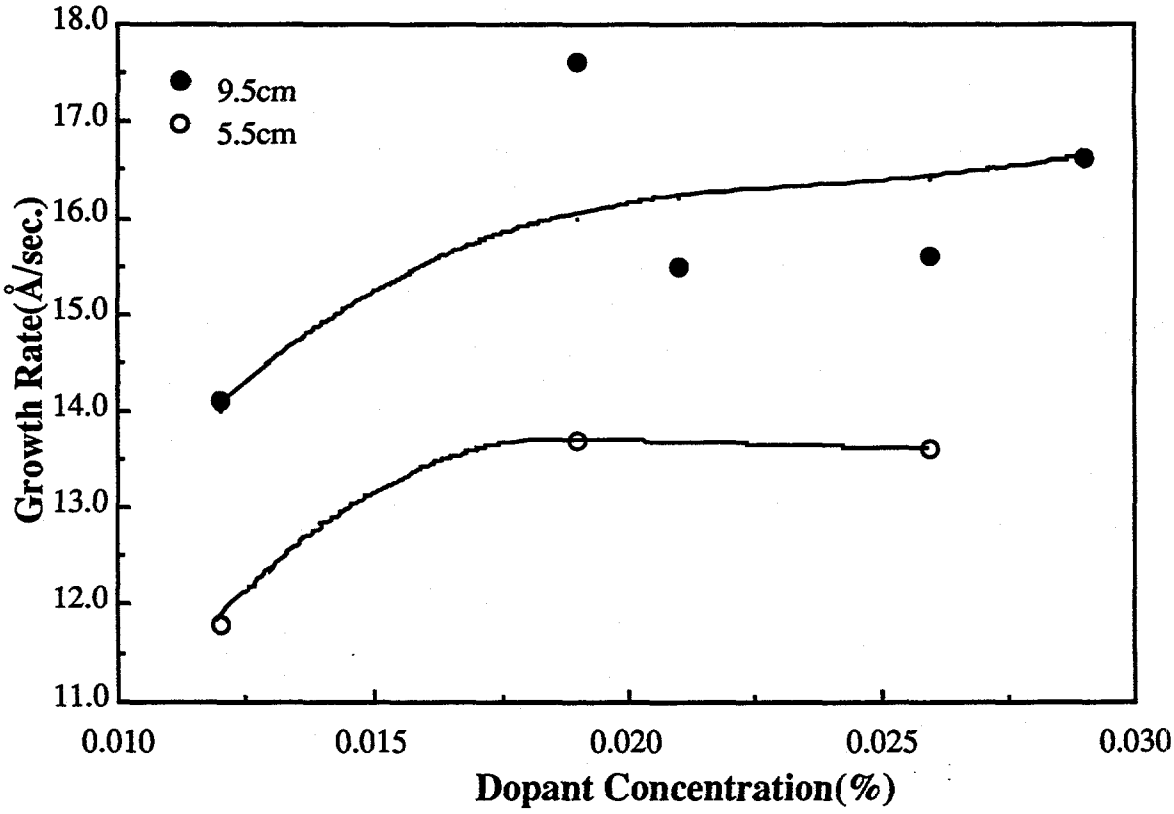

FIG. 3. Dependence of growth rates at position 5.5 cm and 9.5 cm from the reactor nozzle on dopant concentrations. The films were deposited at 400°C from 0.05% DEZ and 3.0% ethanol.

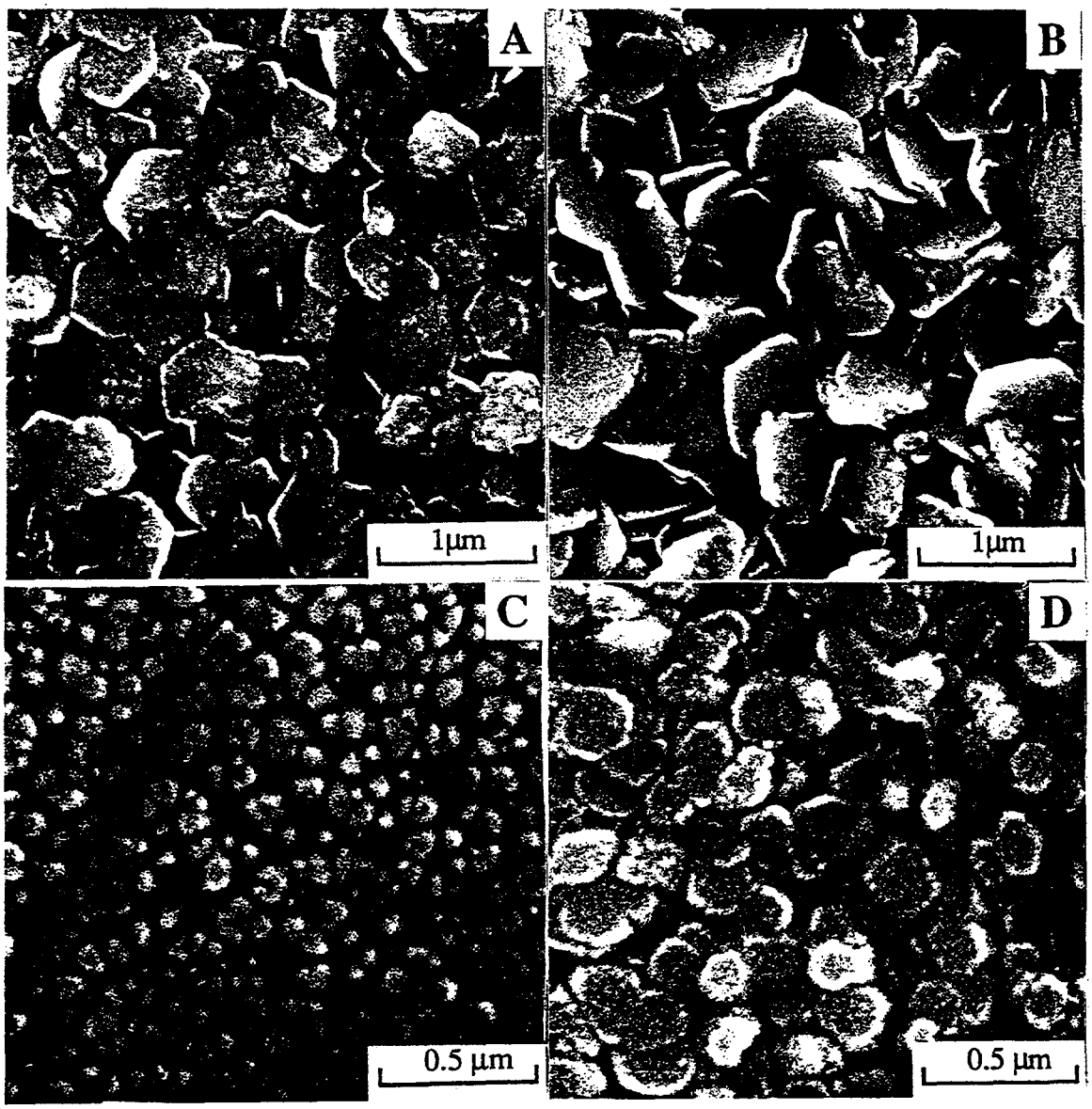

FIG. 4. Scanning electron micrographs of undoped ZnO films deposited at 367°C (a) and at 420°C (b) from 0.05% DEZ and 3.0% ethanol. The aluminum doped films deposited at 367°C and 420°C from 0.05% DEZ, 0.03% TEA and 3.0% ethanol are shown in (c) and (d).

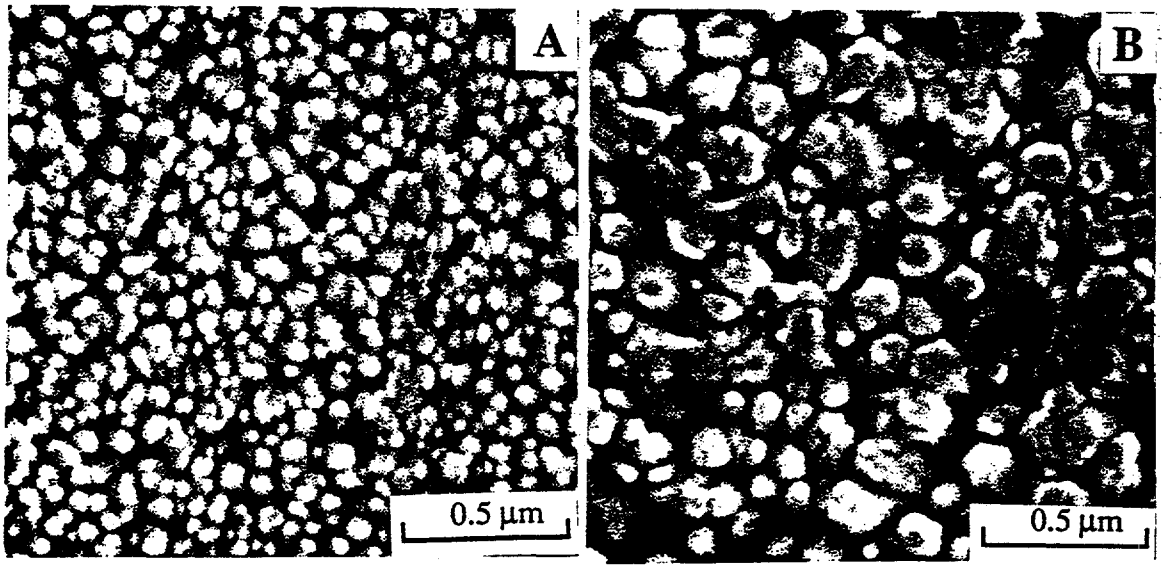

FIG. 5. Scanning electron micrographs of aluminum doped ZnO films deposited at 400°C from 0.05% DEZ, 0.03% TEA and 3.0% ethanol. The samples shown in (a) and (b) have thicknesses of 270 nm and 840 nm and are located at 7.0 cm from the reactor nozzle.

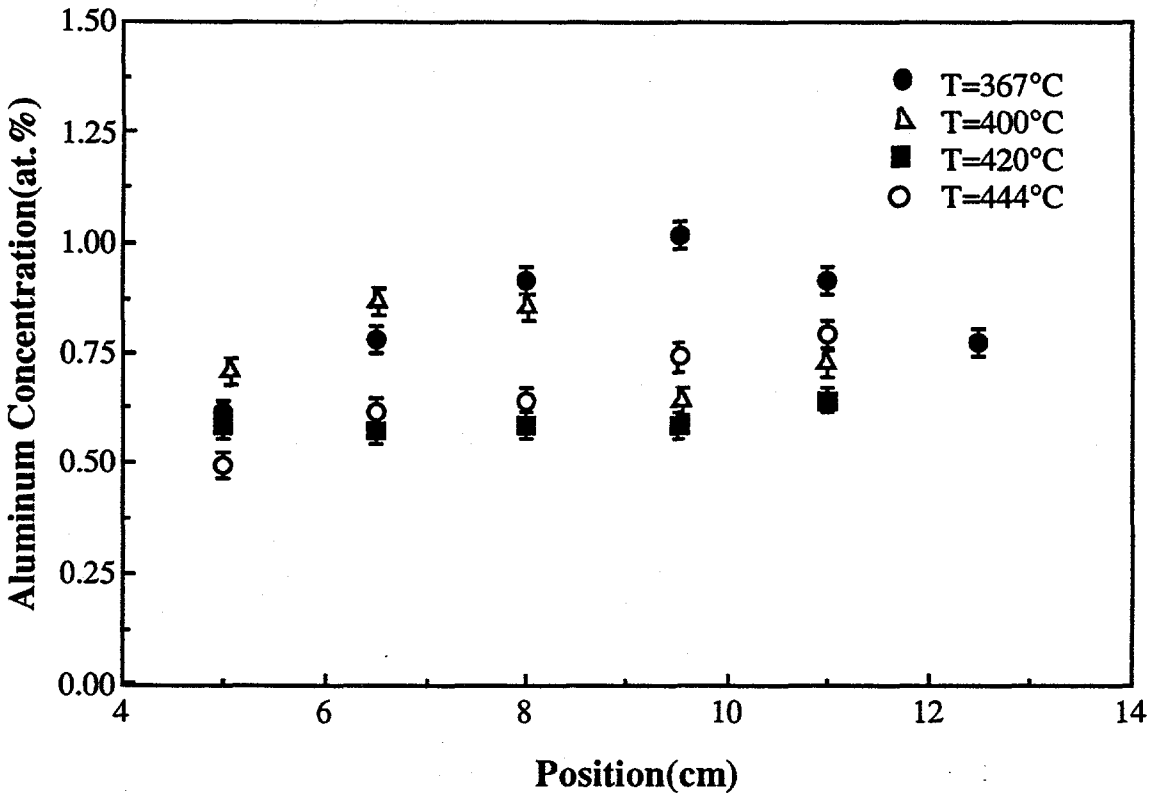

FIG. 6. Aluminum distribution along gas flow direction for films deposited at different temperatures from 0.05% DEZ, 0.03% TEA and 3.0% ethanol.

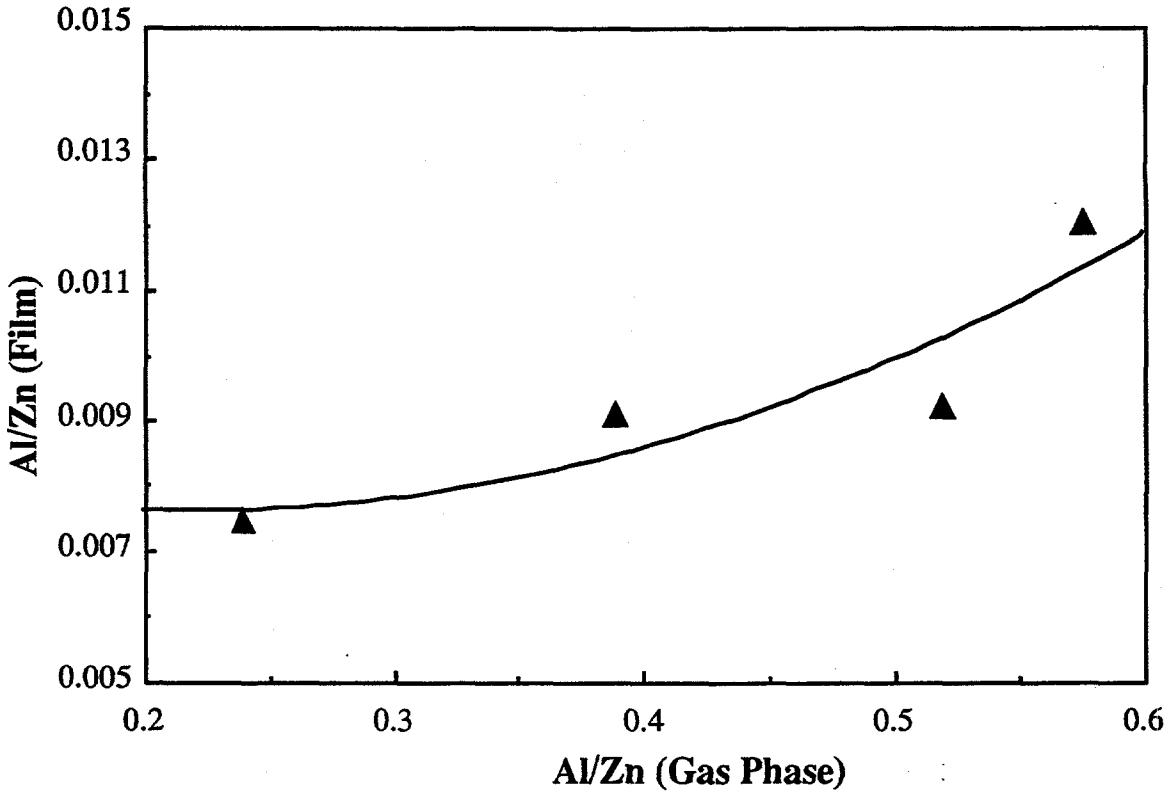

FIG. 7. Dependence of aluminum over zinc ratio in the films on aluminum over zinc ratio in the gas phase. The films were deposited at 400°C from 0.05% DEZ and 3.0% ethanol and the samples were located at 9.5 cm from the reactor nozzle.

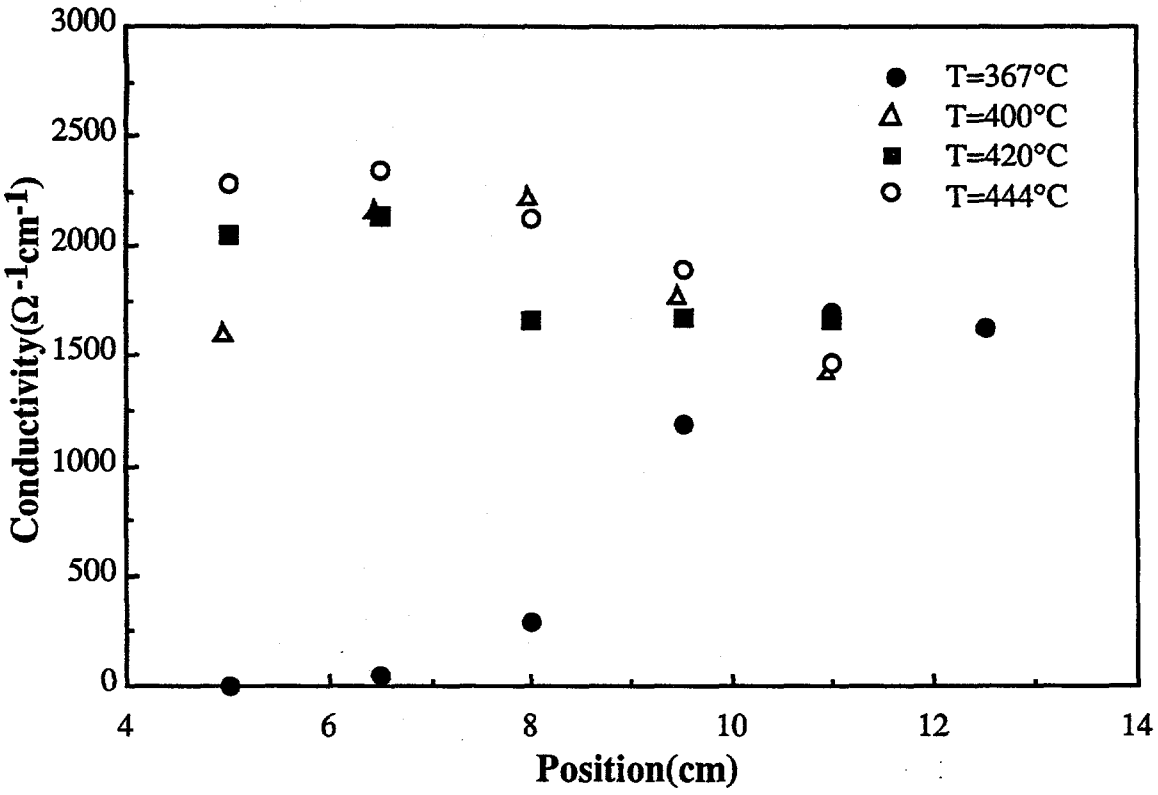

FIG. 8. Conductivity distribution along gas flow direction for films deposited at different temperatures from 0.05% DEZ, 0.03% TEA and 3.0% ethanol.

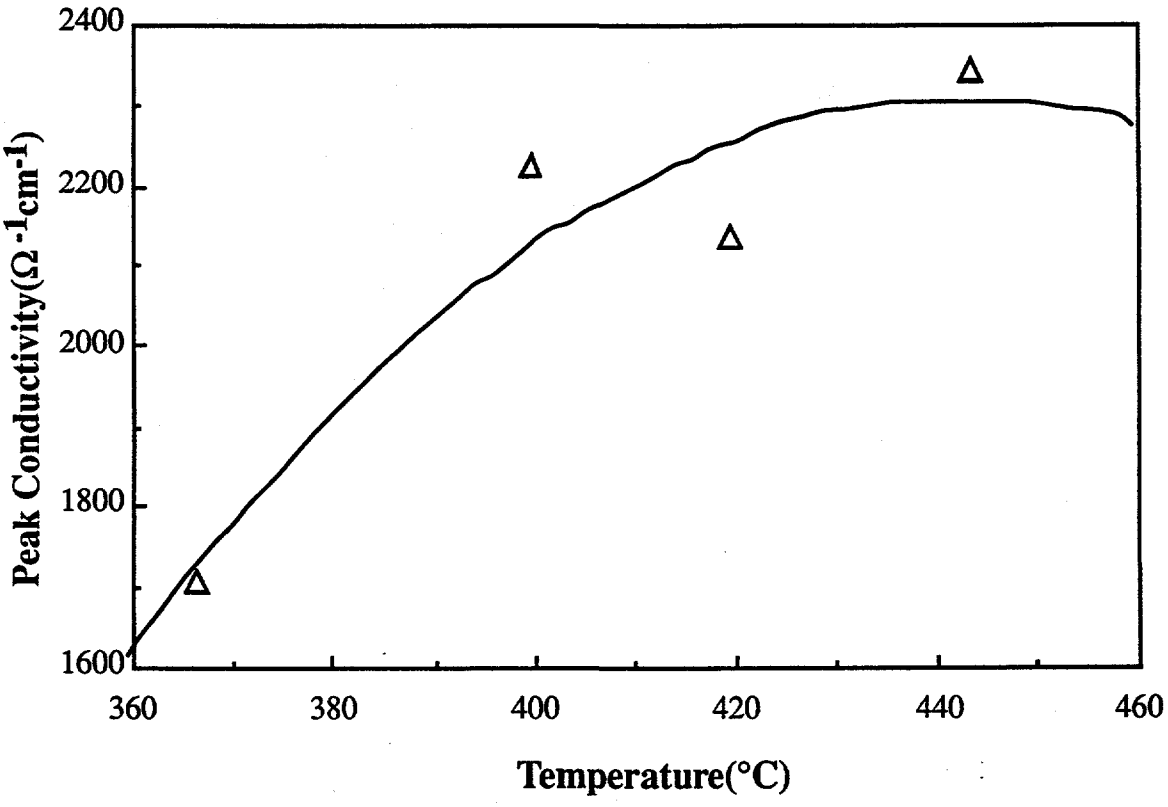

FIG. 9. Peak conductivity as a function of deposition temperature. The samples are the same as in Fig. 8.

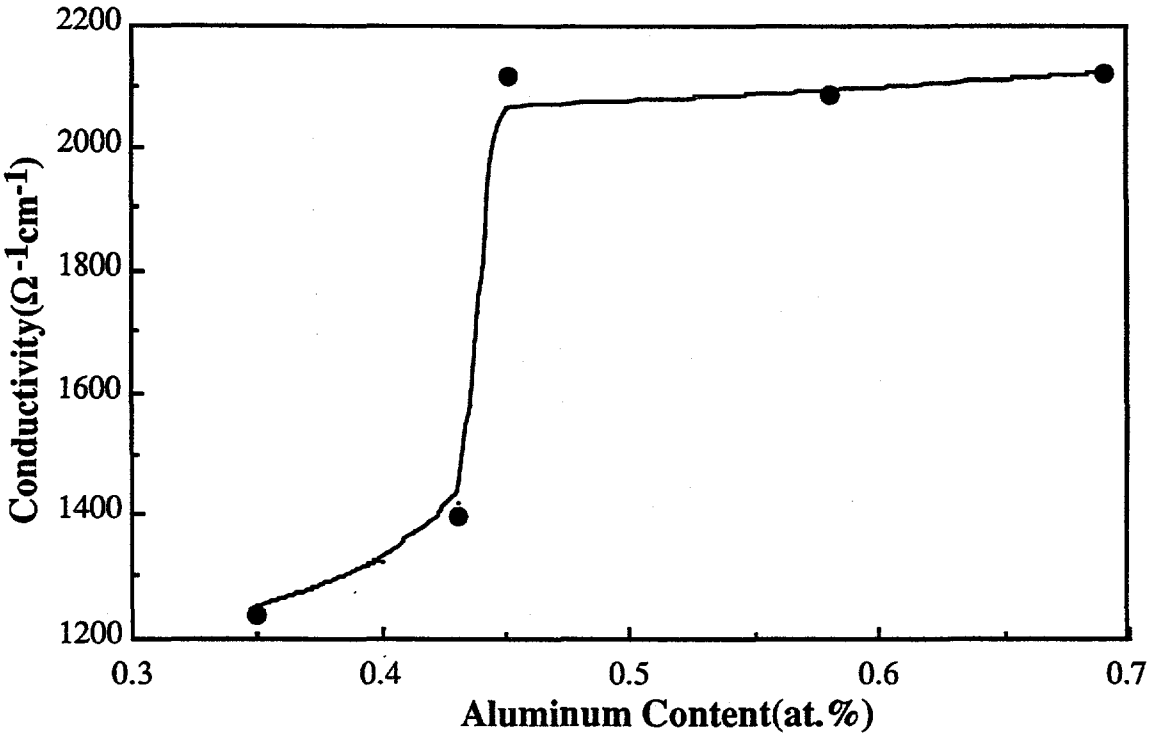

FIG. 10. Conductivity dependence on aluminum content for films with thickness above 700 nm. The films were deposited at 400°C from 0.05% DEZ and 3.0% ethanol with different TEA concentrations.

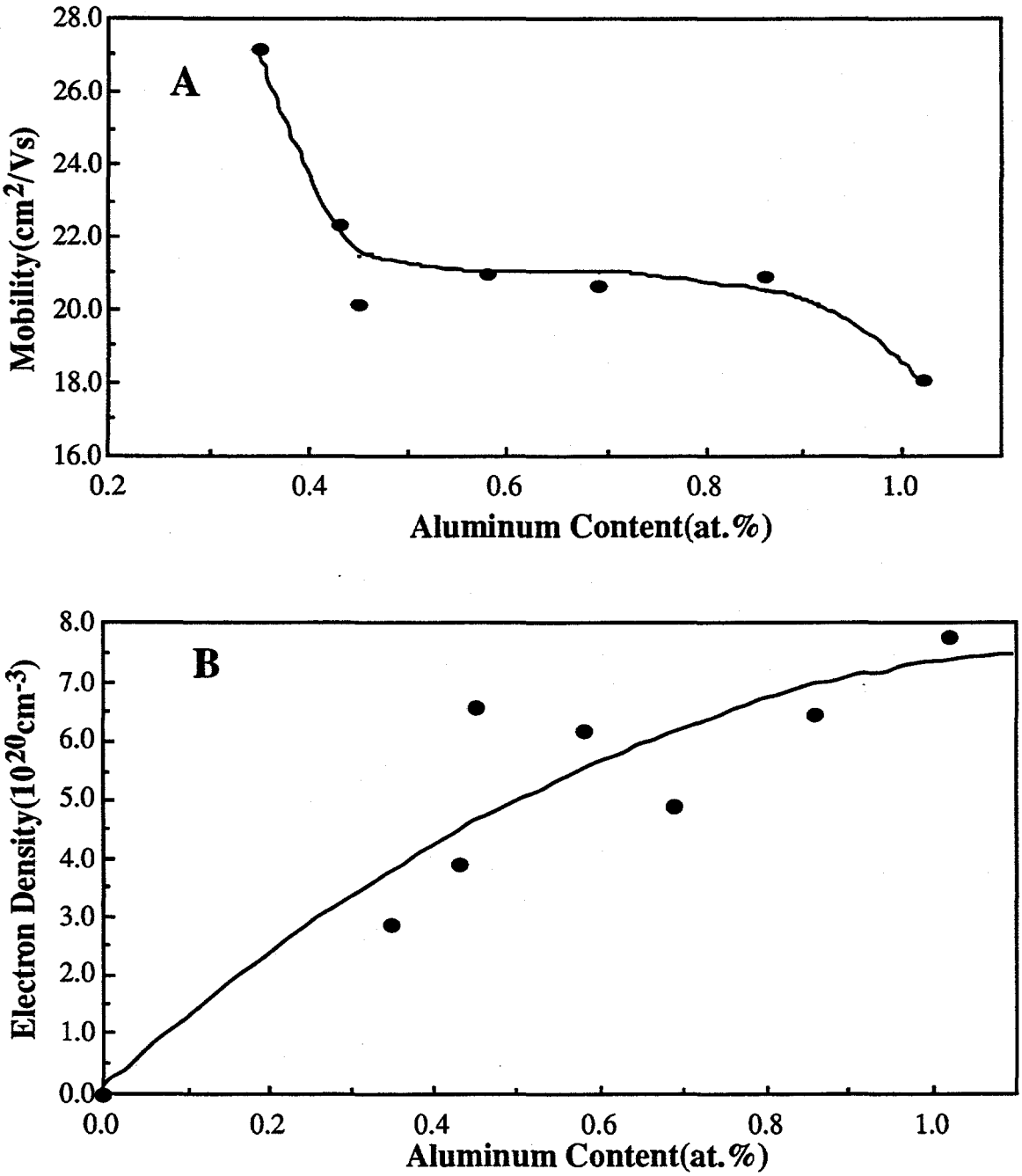

FIG. 11. Mobility (a) and electron density (b) of films with thickness above 700 nm as a function of aluminum concentration. The films were deposited at 400°C from 0.05% DEZ and 3.0% ethanol and the samples were located at 9.5 cm from the reactor nozzle.

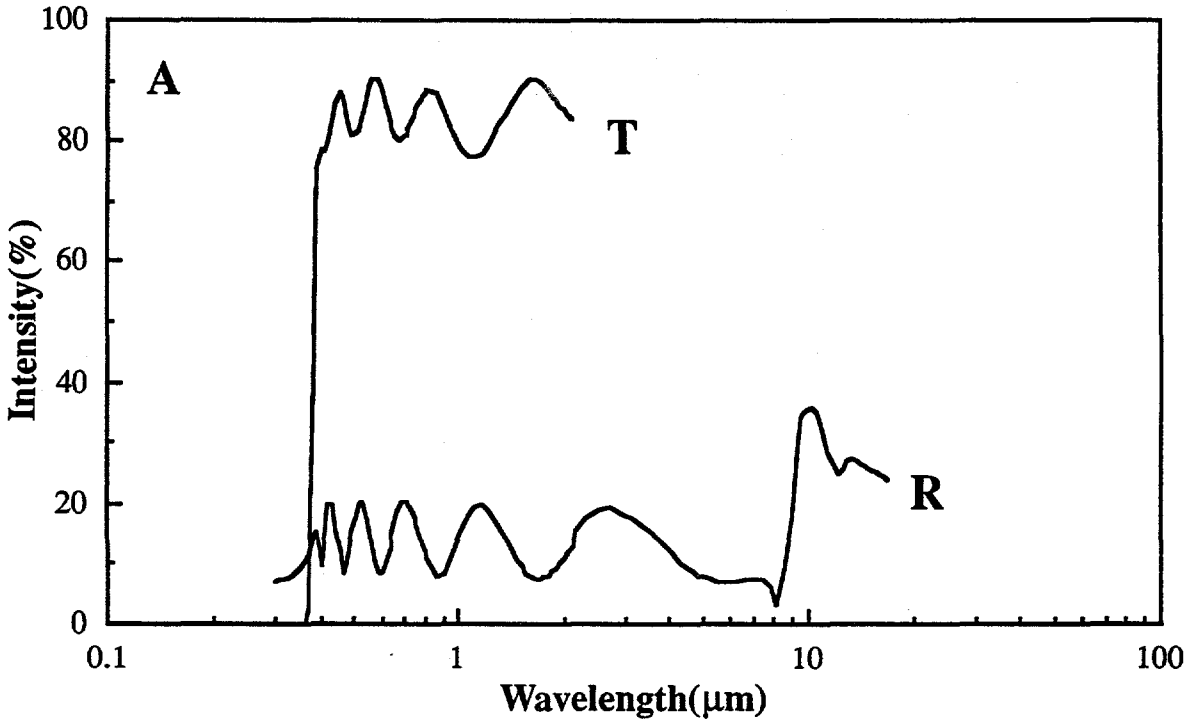
A
T
R
100
80
60
40
20
0
Intensity(%)
0.1
1
10
100
Wavelength(μm)

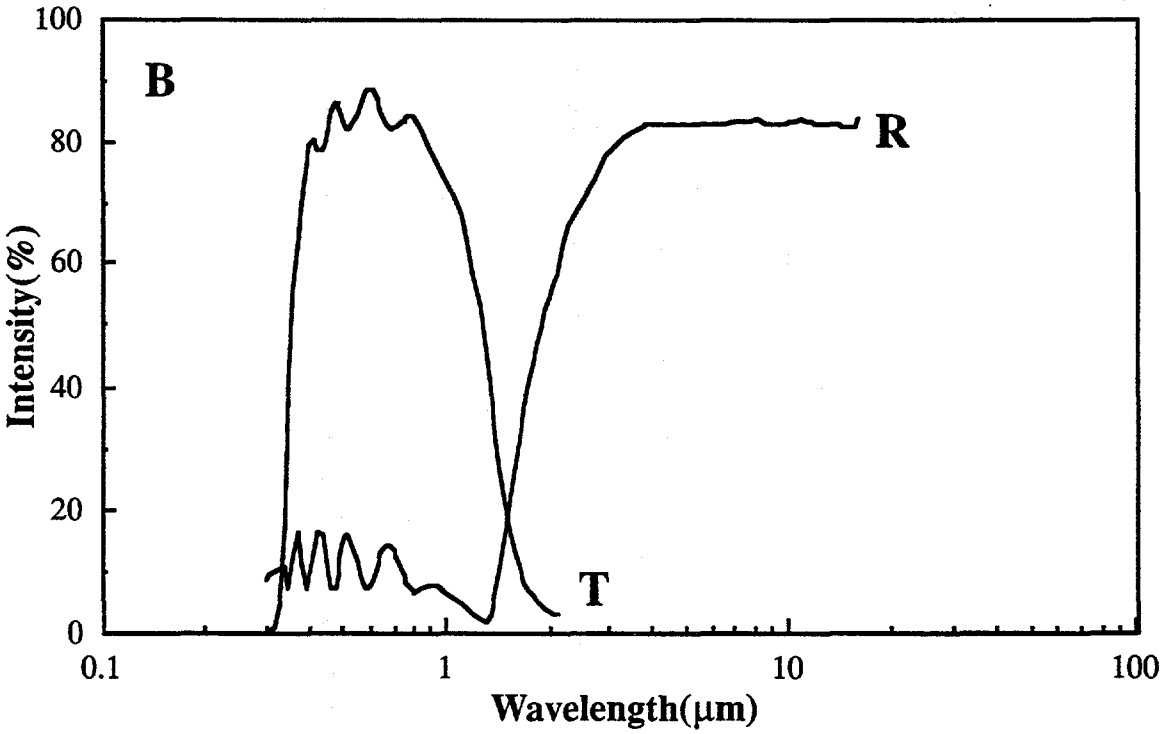
B
R
T
100
80
60
40
20
0
Intensity(%)
0.1
1
10
100
Wavelength(μm)

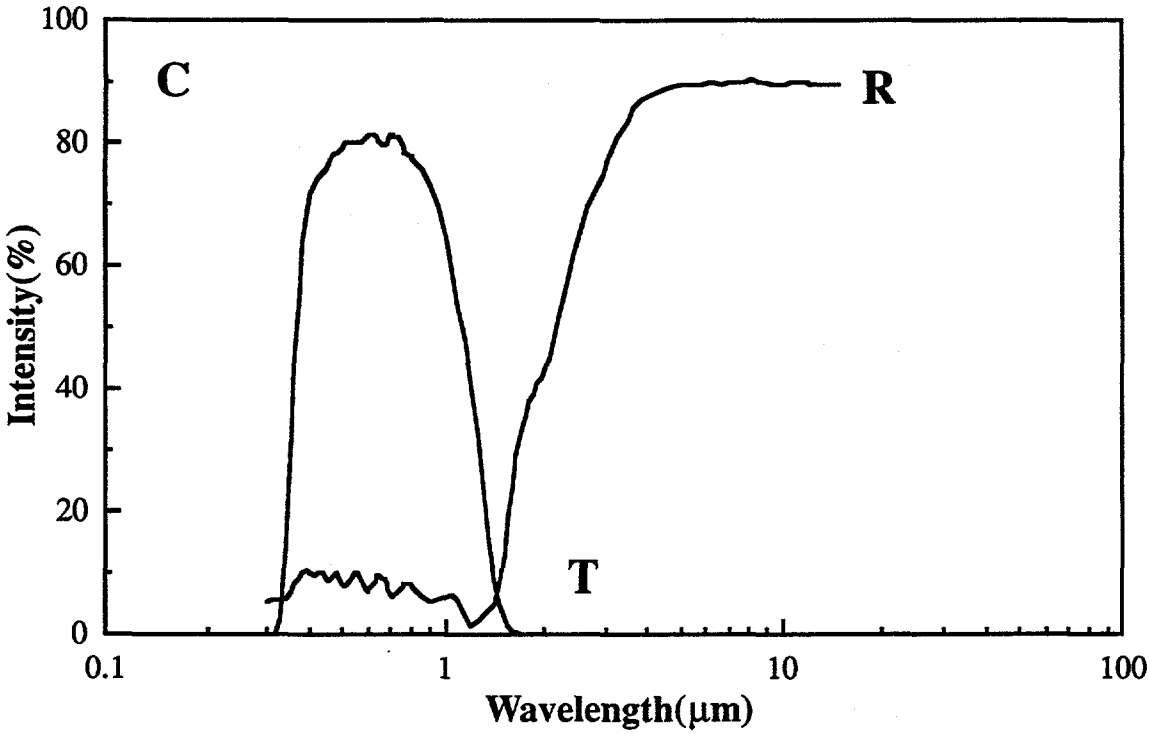

FIG. 12. (a) and (b) Normal transmittance T and near normal reflectance R of undoped and aluminum doped ZnO films deposited at 367°C and (c) at 420°C from 0.05% DEZ and 3.0% ethanol. The doped samples (b) and (c) were deposited by introducing 0.035% TEA into the gas phase. All three samples were located at 9.5 cm from the reactor nozzle.

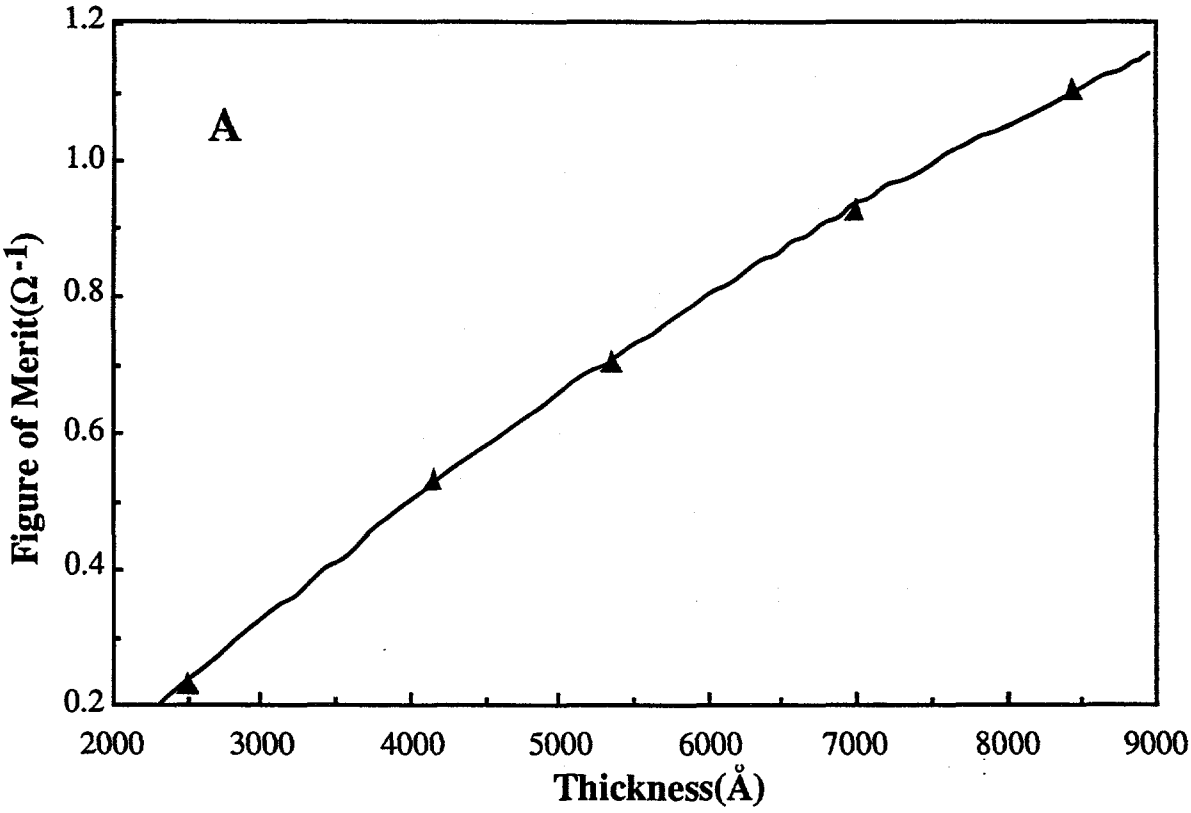
A
Figure of Merit(Ω-1)
1.2
1.0
0.8
0.6
0.4
0.2
2000
3000
4000
5000
6000
7000
8000
9000
Thickness(Å)

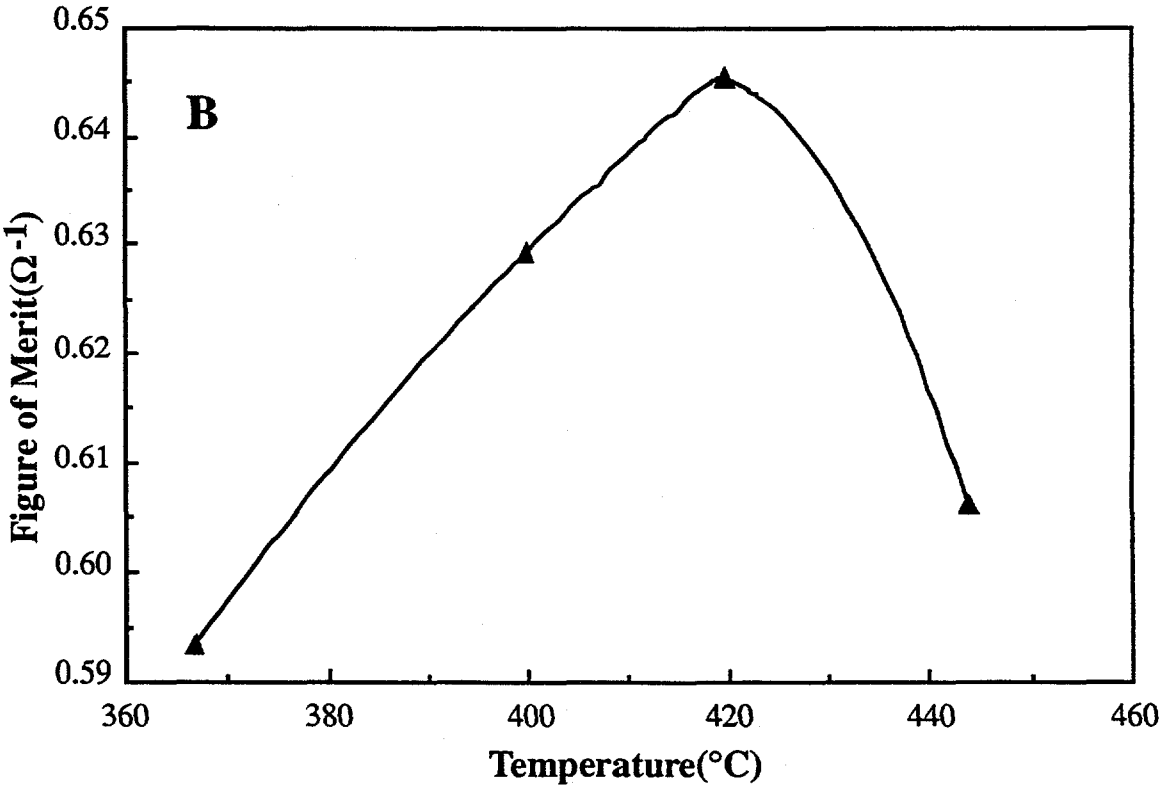
B
Figure of Merit(Ω-1)
0.65
0.64
0.63
0.62
0.61
0.60
0.59
360
380
400
420
440
460
Temperature(°C)

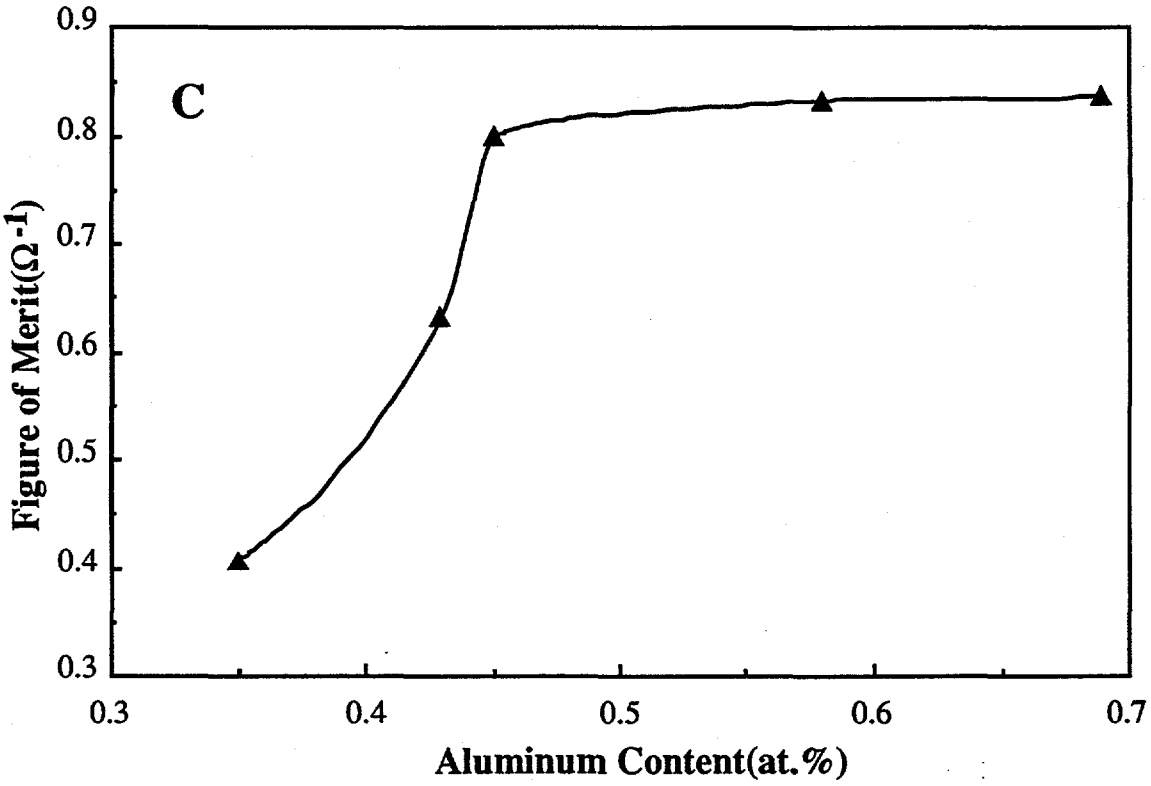

FIG. 13. (a) Figure of merit σ/α dependence on film thickness, (b) on deposition temperature, (c) on aluminum content. The DEZ and ethanol concentrations used for all the samples were 0.05% and 3.0%. The films in (a) were deposited at 400°C with 0.03% TEA and were taken from 7.0 cm on the substrate. The films in (b) were also deposited from 0.03% TEA and were taken from 9.5 cm on the substrate. The films in (c) were deposited at 400°C with various TEA concentrations and the samples were located at 9.5 cm from reactor nozzle.

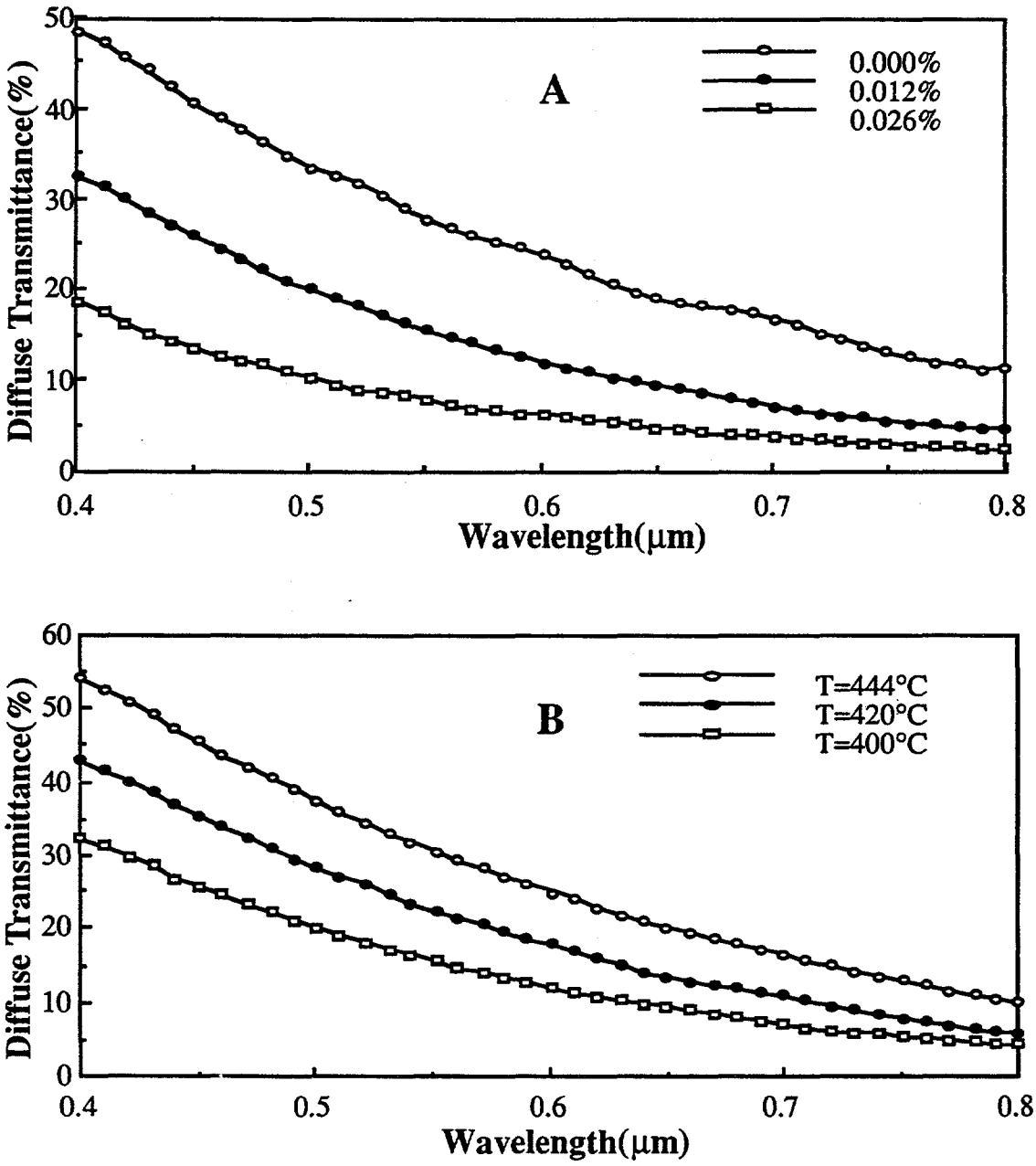

FIG. 14. Diffuse transmittance spectra of ZnO films. (a) Diffuse transmittance dependence on dopant concentration. (b) Diffuse transmittance dependence on the deposition temperature. The films in (a) were deposited at 400°C from 0.05% DEZ and 3.0% ethanol and the films in (b) were deposited from 0.05% DEZ, 0.01% TEA and 3.0% ethanol. All the samples were located at 9.5 cm from the reactor nozzle.

3. ATMOSPHERIC PRESSURE CHEMICAL VAPOR DEPOSITION OF GALLIUM DOPED ZINC OXIDE THIN FILMS FROM DIETHYL ZINC, WATER AND TRIETHYL GALLIUM

ABSTRACT

Gallium doped zinc oxide films have been deposited in the temperature range 150°C to 470°C from 0.05% diethyl zinc, 0.8% water and various triethyl gallium concentrations. The films are polycrystalline with crystallite sizes varying between 275 Å and 500 Å for undoped films and between 125 Å and 400 Å for doped films. Only those films deposited above 430°C are highly oriented, and have their c-axes perpendicular to the substrate plane. The electron density, conductivity and mobility always increase with temperature. Thicker films have higher conductivity and mobility than thinner films. The refractive index is reduced from 1.96 to 1.73 when the electron density is increased from zero to 3.7×10^{20} cm^{-3}. A film deposited at 370°C with 3.0 at.% gallium and a thickness of 0.62 μm has a conductivity of 2075 $\Omega^{-1}cm^{-1}$, an electron density of 9.3×10^{20} cm^{-3}, and a mobility of 13.9 cm^2/Vs. The plasma wavelength of this film is 1.15 μm and the film has a maximum infrared reflectance close to 85%. For films deposited at 370°C with a gallium concentration of about 2.5 at.%, the ratio of conductivity to visible absorption coefficient increases from 0.03 Ω^{-1} to 1.25 Ω^{-1} when the film thickness increases from 0.11 μm to 1.2 μm. A film deposited at 470°C with a gallium concentration of 2.4 at.% and a thickness of 0.66 μm has a sheet resistance of 3.6 Ω/square and an average visible absorption of 6.8%. When the gallium concentration is less than 5.0 at.%, the band gap widening approximately follows the Burstein-Moss relation.

I. INTRODUCTION

Zinc oxide is a wide band gap n-type semiconductor with a hexagonal wurtzite structure. It has potential applications in liquid crystal displays, energy-efficient windows and solar cell technology [1-5]. Zinc oxide has a few advantages over the most commonly used transparent and conductive oxide films such as indium tin oxide (ITO) or fluorine doped tin oxide films. Both indium and tin are relatively expensive metals whereas zinc is cheap and abundant [6]. Zinc oxide has a higher visible transmittance than other conductive oxide films and is also known to be more resistant to the reduction by a hydrogen-containing plasma, which exists in the fabrication of process of some optoelectronic devices such as solar cells [7,8].

Pure zinc oxide film usually has low conductivity because of the low electron density in the film. Although non-stoichiometric zinc oxide films have been made to have high conductivity and high visible transmittance, they are not very stable at high temperatures [9]. Doped zinc oxide films, on the other hand, can be made to have very stable electrical and optical properties. Zinc oxide films can be doped with the Group VII element fluorine [10,11] or the Group III elements boron [12], aluminum [1,5,8,9,13-16], gallium [17,18], and indium [19-21].

The deposition of zinc oxide films has been achieved by metalorganic chemical vapor deposition (MOCVD) [10-12,22-29], rf magnetron sputtering [1,4,5,9,16-18,20], dc magnetron sputtering

[2,13,19], ion beam sputtering [14,15], and spray pyrolysis [8,21]. Magnetron sputtering has been widely used to deposit aluminum, gallium and indium doped zinc oxide films. We recently reported the deposition of aluminum doped zinc oxide films by atmospheric pressure metalorganic chemical vapor deposition [29]. The fluorine and boron doped zinc oxide films have been prepared only by metalorganic chemical vapor deposition.

Metalorganic chemical vapor deposition is especially useful for large scale coatings at high growth rates. Doped films can be deposited by introducing the dopant into the gas phase, and the extent of doping can easily be controlled by the concentration of dopant in the gas phase. The most commonly used organometallic zinc precursors are diethyl zinc (DEZ) [10,12,22,23,26,29] and dimethyl zinc (DMZ) [11,24,25,27,28]. The oxidant can be pure oxygen, water, alcohol, nitrous oxide (N_2O), carbon dioxide or even some oxygen-containing cyclic compounds such as furan (C_4H_4O), tetrahydrofuran (C_4H_8O), and tetrahydrophyran ($C_5H_{10}O$). Plasma and light are sometimes used to increase the film growth rate and to lower the deposition temperature [23,28].

In this chapter the deposition of gallium doped zinc oxide films by atmospheric pressure chemical vapor deposition from diethyl zinc (DEZ), water and triethyl gallium (TEG) will be presented. Also discussed is the influence of the dopant concentration and deposition temperature on the structural, electrical and optical properties of the films.

II. EXPERIMENTAL PROCEDURES

Zinc oxide films were deposited on soda lime glass substrates and silicon substrates in an atmospheric pressure chemical vapor deposition system which has been described previously [10]. High purity helium (99.995%, from Matheson Gas Products) was used as carrier gas for diethyl zinc (from Ethyl Corporation), deionized water and triethyl gallium (99.0%, from Strem Chemicals, Inc.). The DEZ bubbler was heated slightly to 25°C and its vapor pressure at this temperature is about 16.1 torr. The triethyl gallium bubbler was kept at 18°C. We used triethyl gallium (TEG) rather than trimethyl gallium (TMG) because triethyl gallium has a much lower vapor pressure than trimethyl gallium, making it easier to control the extent of doping . The vapor pressure of TEG and TMG at 18°C are 3.9 torr and 166 torr, respectively. Triethyl gallium vapor was pre-mixed with DEZ vapor and then diluted with more helium before flowing into the reactor. The water bubbler was kept in an oven at 45°C to obtain a vapor pressure of 72 torr. Diethyl zinc and water were introduced into the reactor through slit-shaped nozzles, separated by a buffer flow of helium. The gas flow in each line was 4.0 l/min and the total gas flow was 12.0 l/min through a cross section of 0.6x12.0 cm^2. The reactor was heated from the bottom by a hot plate and the top and bottom temperatures were determined by thermocouples inserted in holes in the side of the reactor. The temperature of the substrate was assumed to be the same as the bottom temperature. The temperature difference between the top side of the reactor and the substrate depended on the substrate temperature and varied from 30°C to 110°C for the substrate temperatures between 150°C and 470°C. The deposition temperature was stabilized to ±1°C. The reactor nozzle was insulated from the heated block by a thin-walled zone of width 3.5 cm and the nozzle temperature was maintained at about 150°C lower than that of the central part of the reactor. This low temperature zone ensured the establishment of laminar flow before the gas mixture reached the substrate. The soda lime glass substrates were first cleaned with a sodium-free detergent (Detergent 8, from Alconox, Inc.) and then rinsed with deionized water. The silicon substrates were dipped into 1:1 sulfuric acid and 30% hydrogen peroxide solution for 10 minutes and then rinsed with deionized water.

Film thicknesses and refractive indices at λ=6328 Å were determined with a Metricon PC-2000 prism coupler. The prism coupler gives accurate results for the thickness and the refractive index when the film thickness is above 0.6 μm. The refractive indices of thinner films were not

determined, and the thicknesses of thinner films were measured with an Tencor Alpha-Step 200 profilometer. The sheet resistance R was measured with a Veeco FPP-100 Four Point Probe. The film bulk resistivity ρ was obtained from $\rho=Rt$, where t is the film thickness. The electron density and mobility were obtained from the measured Hall coefficient. The sample preparation and Hall coefficient measurement procedures have been described previously [29].

The near normal infrared reflectance was measured on a Nicolet Model 7199 Fourier Transform spectrometer with a relative reflection attachment. A gold mirror with a known reflectance was used as the reflectance standard in the wavelength range between 2.0 μm and 20 μm [30]. The near ultraviolet, visible and near infrared spectra were obtained with a Varian 2390 spectrophotometer using an integrating sphere detector which could measure both the total and diffuse components of the reflectance and transmittance. The reflectance standard was a barium sulphate plate and its reflectance was taken as 100.0% between 0.2 μm and 2.2 μm. The absorption within the film was then found by subtraction of the total reflectance and total transmittance from 100.0%. The measured absorption was further corrected for absorption by the glass substrate.

X-ray diffraction measurements were made on a Philips powder crystallography instrument with copper K_α radiation. A JEOL JSM-6400 scanning electron microscope (SEM) was used to obtain the crystallite orientation and size. Film composition was found by a Cameca MBX electron microprobe equipped with a Tracor Northern TN-5502 EDS system and a TN-1310 WDS and stage automation system. The beam voltage, beam current and beam size were 5 kV, 30 nA and 16x16 μm^2, respectively. The standards used for zinc and gallium were pure ZnO and $Y_3Ga_5O_{12}$. Oxygen concentration was not determined due to interference from the substrate and the existence of hydrogen in the film. Rutherford backscattering and forward recoil spectra (RBS and FRS) were obtained on a General ionics Model 4117 spectrometer. The Helium ion beam energy was 2.0 MeV. The standard for hydrogen concentration calibration was a piece of gold coated Kapton ($C_{22}H_{10}N_2O_5$).

III. RESULTS AND DISCUSSION

A. Film deposition

Zinc oxide films were deposited on soda lime glass substrates and silicon substrates in the temperature range 150°C to 470°C from 0.05% diethyl zinc and 0.8% water. Since diethyl zinc reacts rapidly with water even at 150°C, the position of film peak growth is located in the cold zone. All of the samples taken for analysis were from the after-peak positions on the substrates. The deposition temperature and dopant concentration influences the growth rate profile. Figure 1 shows the growth rate profiles at four different temperatures with a triethyl gallium concentration of 0.0032%. The peak positions at all temperatures were located in the cold zone and could not be seen in Figure 1. The profile moves towards the reactor nozzle as the temperature is increased. Triethyl gallium only slightly changes the film growth rate profile when the dopant concentration in the gas phase is below 0.009%. However, as the dopant concentration increased above 0.009%, the growth rate profile changed dramatically. Figure 2 shows growth rate profiles for films deposited with two different dopant concentrations. The film doped with a higher triethyl gallium concentration had a higher growth rate at the same position on the substrate and was spread downstream more than the film deposited with a lower triethyl gallium concentration.

B. Film structure and crystallite size

X-ray diffraction measurements showed that the zinc oxide films deposited in the temperature range 150°C to 470°C were crystalline. Both doped and undoped films deposited at 150°C gave strong (100) and (110) diffraction peaks, but no (002) diffraction peak. For deposition temperatures between 260°C and 400°C, (100), (002) and (101) diffraction peaks were found for doped and undoped films. The relative intensities of these three peaks depend on the deposition temperature and the dopant concentration. Figure 3 shows x-ray diffraction spectra of three films deposited at 370°C with different dopant concentrations. Sample (a) was undoped and its (101) diffraction peak was the strongest. Sample (b) was doped with 0.0032% triethyl gallium and its strongest peak was (100) and its weakest peak was (002). Sample (c) was doped with 0.009% triethyl gallium and its (002) diffraction peak disappeared completely from the spectrum. The dopant triethyl gallium make a film less oriented along its c-axis. The intensity of (110) diffraction peak at $2\theta=56.8°$ increases with dopant concentration. When the deposition temperature was above 430°C, both doped and undoped films were highly oriented with their c-axes perpendicular to the substrate plane. For these films, only (002) diffraction peak had any significant intensity.

The (002) diffraction peak width was used to estimate the crystallite dimension along the c-axis. The Cu $K\alpha$ radiation contains two lines of wavelength 1.54056 and 1.54439 Å with an intensity ratio of 2:1 [6]. Zinc oxide with a spacing of 2.603 Å along (002) direction will give two (002) diffraction peaks separated by $\Delta(2\theta)=0.088°$ with intensity ratio of 2:1. These two diffraction peaks were broadened and only a single peak could be observed in the spectra because the crystallites were small. In order to find the true peak width B_S corresponding to a monochromatic x-ray, a minimization program [31] was used to approximate the measured peak by two Gaussian curves with a height ratio of 2:1, width ratio of 1:1, and separated by 0.088. The instrumental broadening was obtained by measuring the silicon (111) diffraction peak width, which has 2θ around 28.5° and is close to the zinc oxide (002) diffraction angle 2θ around 34.5°. There were two well separated silicon (111) diffraction peaks with an intensity of 2:1, and the width B_0 was found to be 0.033°. The corrected peak width B was calculated from the observed width B_S by the formula $B^2 = B_S^2 - B_0^2$, and the crystallite dimension t was then estimated according to $t = 0.9\lambda/B\cos\theta$, where λ is the x-ray wavelength and θ is the Bragg diffraction angle [32]. Figure 4 shows that the crystallite size always increases with deposition temperature and the undoped films have larger crystallite size than the doped films.

Scanning electron micrographs of zinc oxide films are shown in Figure 5. Samples (a) and (b) were deposited at 350°C and samples (c) and (d) at 430°C. Samples (a) and (c) were undoped and samples (b) and (d) were doped with 0.0032% triethyl gallium. The thicknesses of all four samples are around 0.6 μm. Sample (a) contains many large crystallites mixed with many small crystallites. Since the scanning electron microscope does not have a high enough resolution, these small crystallites look like "powder". The large crystallites do not have sharp edges. For the films deposited at 430°C, there are many small crystallites on top of large crystallites. Figure 5 (c) shows that the small and large crystallite sizes are around 50 nm and 100 nm, respectively. Triethyl gallium decreases crystallite size and changes crystallite orientation. The doped samples (b) and (d) both contain large crystallites mixed with "powder". Sample (b) has crystallites almost completely tilted with their c-axes parallel to the substrate plane. Sample (d) has its crystallites oriented with their c-axes perpendicular to the substrate plane.

The film crystallite size also depends on film thickness. With the deposition begins, there are many nucleation centers on the substrate and small crystallites are produced. When the films are deposited for only a short time, the small crystallites on the substrate are not able to grow into large crystallites, and therefore the thinner films have smaller crystallites than the thicker films. Figure 6

shows the electron micrographs of two gallium doped zinc oxide samples. The thicknesses of sample (a) and (b) are 0.11 μm and 1.2 μm. Sample (a) has such a small crystallite size that the scanning electron microscope is not able to give sharp images. Sample (b) shows that the large crystallites with disk structure are tilted and the small crystallites still look like "powder".

C. Film composition

Electron microprobe analysis showed that the gallium concentration in the film depended on triethyl gallium concentration and the deposition temperature. In a flow reactor, gas phase reactions change the gas phase composition along the flow direction. The gallium concentration is therefore inhomogeneous along the gas flow direction. The position of highest conductivity usually is not the same as the position of highest gallium concentration. Figure 7 shows the gallium distribution along the gas flow direction for films deposited with two different triethyl gallium concentrations. The film with a higher triethyl gallium concentration had a higher gallium concentration in the film. Figure 8 shows that the gallium to zinc ratio in the film is nearly equal to the gallium to zinc ratio in the gas phase. Those films were deposited at 370°C and the measurements were made at the most conductive part on the substrate. The gallium concentration in the film first increases almost linearly with dopant concentration in the gas phase and then levels off at very high dopant concentrations. The gallium concentration in the film can be made up to 10 at.% when the triethyl gallium concentration is about 0.015% in the gas phase. Figure 9 shows the gallium distribution along the gas flow direction as a function of deposition temperature. Because gas phase reactions are faster at higher temperatures, the incorporation rate of gallium into the film increases with temperature, and so the higher temperature leads to a higher gallium concentration in the film for constant triethyl gallium concentration in the gas phase.

Rutherford backscattering and forward recoil spectra were obtained for films deposited on silicon substrates at different temperatures from 0.05% diethyl zinc, 0.8% water and 0.0032% triethyl gallium. Figure 10 shows the RBS spectrum of a film deposited at 370°C. The oxygen signal is located on top of the broad silicon substrate signal. The slight increase of the silicon signal counts towards low channels is due to the detector. The oxygen to zinc atomic ratio determined from the spectrum is about 1.15. The hydrogen concentration determined from FRS is about 8.1 at.%. The gallium signal cannot be found in the RBS spectrum because of its low concentration and its proximity to the zinc signal. A film deposited with the same conditions on soda lime glass substrate was found to have a gallium concentration of about 2.5 at.%. FRS spectra of films deposited at different temperatures are given in Figure 11. The hydrogen concentration in the film decreases as the deposition temperature increases. The estimated hydrogen concentration decreased from 15.3 at.% for the film deposited at 150°C to 7.4 at.% for the film deposited at 470°C.

TABLE I. The deposition temperature T_d, thickness t, sheet resistance R, zinc and gallium concentrations, plasma wavelength λ_p, electron density N_e and mobility μ determined from the measured Hall coefficient and from optical analysis for gallium doped zinc oxide films deposited at different temperatures from 0.05% diethyl zinc, 0.8% water and 0.0032% triethyl gallium. The films were chosen from the most conductive part on the substrates.

							Electrical		Optical	
	T_d	t	R	Zn [a]	Ga [b]	λ_p	N_e	μ	N_e	μ
Sample	(°C)	(μm)	(Ω/sq)	(at.%)	(at.%)	(μm)	(10^{20}/cm^3)	(cm^2/Vs)	(10^{20}/cm^3)	(cm^2/Vs)
2211	200	0.56	11000	38.6	2.9		0.7	0.1		
2200	260	0.57	128	41.7	3.5	1.55	4.0	2.1		
2188	350	0.64	14.2	41.6	2.5	1.32	7.9	8.8	5.8	11.9
2179	400	0.67	6.0	43.7	2.5	1.04	8.2	19.1	8.5	18.3
2182	430	0.66	4.2	42.2	2.5	1.00	10.6	21.4	9.1	24.9
2185	470	0.66	3.6	40.6	2.4	1.02	10.6	24.6	8.5	30.6

[a]The estimated error is ±1.2 at.%.
[b]The estimated error is ±0.2 at.%.

D. Electrical properties

Gallium is an n-type dopant that is presumed to replace zinc atoms in the film thereby increaseing the free electron density. The ionic radii of Ga^{3+} and Zn^{2+} are 0.62 Å and 0.74 Å [6]. The measured Hall coefficient R_H can be used to calculate the free electron density N_e of the film by the formula $N_e = 1/(R_H e)$, where e is the electron charge. Figure 12 shows that the electron density first increases with gallium concentration and then decreases at high gallium concentrations. The electron density peaks at about 9.3×10^{20} cm^{-3} when the gallium concentration is about 3.0 at.%. Similar behavior has been observed for tin doped indium oxide films [33]. Table I shows that the electron density also increases with temperature.

As a small amount of gallium is introduced into the film, the gallium is ionized into Ga^{3+} and replaces Zn^{2+}. One free electron is produced from one zinc atom replacement. The electron density therefore increases with gallium concentration. At high gallium concentrations, the free electron density decreases because an increasing number of dopant atoms form some kind of neutral defect, and these neutralized gallium atoms do not contribute free electrons. The ionized impurity scattering should also first increase with gallium concentration until peak electron density is reached and then decrease with gallium concentration. The amount of electrically active gallium in the film is measured by the doping efficiency, which is defined as the ratio of the number of free electrons in the film to the gallium concentration. 100% doping efficiency would correspond to one free electron from each gallium atom. The doping efficiency can be calculated from the electron density in the film, the gallium concentration, and the zinc oxide density which is taken to be the bulk density of 5.606 g/cm^3. Figure 12 also shows that the doping efficiency decreases with gallium concentration, indicating that more gallium atoms are neutralized at higher gallium concentrations. The deposition temperature strongly influences both the gas phase reactions and the movement of dopant atoms to the positions in which they are ionized and are electrically active. Figure 13 shows the temperature dependence of the doping efficiency for films deposited from 0.05% diethyl zinc, 0.8% water and 0.0032% triethyl gallium. The doping efficiency is close to zero for films deposited at 150°C, and increases to about 53% when the deposition temperature is increased to 470°.

The film conductivity was obtained from the measured sheet resistance and the thickness of the film. The film conductivity is not uniform along the gas flow direction because of the nonuniformity of the film composition and thickness. The conductivity at the same position on the substrate varies with dopant concentration and deposition temperature. Figure 14 shows the conductivity distribution along the gas flow direction for films deposited at 370°C from 0.0032% and 0.0107% triethyl gallium. When the dopant concentration was above 0.009%, the film was spread out over large areas on the substrate and the conductivity was more uniformly distributed along the gas flow direction.

The effect of film thickness on conductivity is given in Figure 15. The electron density and the ionized impurity scattering frequency should be the same for all samples. Since the thicker films have larger crystallite sizes, the grain boundary scattering in thicker films is smaller than in thinner films. The total scattering frequency γ follows Matthiessen's rule [34] and is equal to the sum of ionized impurity scattering frequency γ_i and grain boundary scattering frequency γ_g, $\gamma = \gamma_i + \gamma_g$. The total scattering frequency is therefore smaller for thicker films than for thinner films. The conductivity σ is related to the scattering frequency γ and the electron density N_e by the following relation:

$$\sigma = N_e e^2/m_e^*\gamma, \qquad (1)$$

where e is the electron charge, m_e^* is the effective mass of conduction electrons. The thicker films have a smaller scattering frequency and therefore a higher conductivity. As the film becomes very thick, the scattering will be dominated by ionized impurity scattering. The total scattering frequency will not change appreciably with a further increase in film thickness and the conductivity will become constant for thicker films.

The peak conductivity dependence on gallium concentration in the film is shown in Figure 16. The films are the same as those in Figure 12. The conductivity first increases rapidly with gallium concentration because of the increase of free electron density. A maximum conductivity of 2075 $\Omega^{-1}cm^{-1}$ was obtained at a gallium concentration of 3.0 at.%. The dopant concentration in the gas phase was 0.0036%. Any further increase in gallium concentration first decreases conductivity to a minimum of about 490 $\Omega^{-1}cm^{-1}$ at 5.3 at.% gallium and then slightly increases conductivity to 870 $\Omega^{-1}cm^{-1}$ at a gallium concentration of about 9.5 at.%.

Conductivity profiles along the gas flow direction are given as a function of deposition temperature in Figure 17. The conductivity is more uniformly distributed for films deposited at lower temperatures; however, films deposited at higher temperatures have higher conductivities. The peak conductivities for films deposited at 370°C and 325°C could be found in Figure 17. For a film deposited at 470°C, the peak conductivity is as high as 4310 $\Omega^{-1}cm^{-1}$ and its position is very close to the cold zone of the reactor. In contrast, the film deposited at 260°C has a peak conductivity of only 140 $\Omega^{-1}cm^{-1}$ and its position is farther away from the reactor nozzle. Figure 18 shows that the peak conductivity increases with temperature. The films are the same as those in Figure 17. At very low temperatures, there is large amount of hydrogen in the film. Some of the hydrogen may exist in the form of non-conductive zinc hydroxide and the conductivity is therefore lower for films with higher hydrogen concentrations. Higher temperatures lead to larger crystallites and thus smaller grain boundary scattering frequency. Films deposited at higher temperatures have lower scattering frequencies and therefore higher conductivities. Table I shows that the film deposited at 470°C has a lower sheet resistance than the film deposited at 430°C, although they have the same thickness and electron density.

The Hall mobility μ_H is related to the Hall coefficient R_H and the film conductivity σ by the following relation: $\mu_H = R_H\sigma$. Whereas the mobility of lightly doped single crystal zinc oxide is around 180 cm^2/Vs [6], the polycrystalline gallium doped zinc oxide mobility is usually below 25 cm^2/Vs, which is lower than that of fluorine doped zinc oxide films [10]. The mobility is related to the scattering frequency γ and the effective electron mass m_e^* through

$$\mu_H = e/\gamma m_e^*, \tag{2}$$

where e is the electron charge. Figure 19 shows that the mobility depends on film thickness. The films are the same as those in Figure 15. As the film becomes very thick, the scattering frequency becomes dominated by ionized impurity scattering. Therefore, the mobility becomes constant for very thick films.

The mobility depends on gallium concentration, as shown in Figure 20. The mobility first increases with gallium concentration and has a peak value of 13.9 cm^2/Vs at a gallium concentration of 3.0 at.%. As the gallium concentration increases further, the mobility decreases to a minimum of 5.4 cm^2/Vs at a gallium concentration of 4.3 at.%. Any further increase of gallium concentration leads to an increase in film mobility because of the neutralization of dopant atoms and therefore the decrease of ionized impurity scattering frequency.

Since larger crystallites are formed at higher temperatures, free electrons in the films deposited at higher temperatures have less scattering from grain boundaries and from internal defects than in those films deposited at lower temperatures. The film mobility increases with deposition temperature, as shown in Table I.

E. Optical properties

The optical properties of zinc oxide films were modified by doping. Figure 21 shows that the refractive index (λ = 6328 Å) depends on electron density. The refractive index decreases from 1.96 to 1.73 when the electron density increases from zero to 3.7×10^{20} cm^{-3}. Further increase of electron density until 9.3×10^{20} cm^{-3} does not change film refractive index appreciably. Pure zinc oxide crystal has a refractive index of 2.008 [6]. The undoped zinc oxide films usually have refractive index between 1.95 and 2.00. The classical Drude theory can be used to calculate film refractive index from the measured electron density and conductivity. The dielectric function $\varepsilon = \varepsilon_1 + i\varepsilon_2$ is related to the scattering frequency γ and the electron density N_e through [35]

$$\varepsilon_1(\omega) = \varepsilon_\infty - [\omega_N^2/(\omega^2 + \gamma^2)], \tag{3}$$

$$\varepsilon_2(\omega) = (\gamma/\omega)[\omega_N^2/(\omega^2 + \gamma^2)], \tag{4}$$

$$\omega_N^2 = N_e e^2/\varepsilon_0 m_e^*, \tag{5}$$

where ω is the angular frequency of incident light, ε_∞ is the high frequency dielectric constant, ε_0 is the permitivity of vacuum, e is the electron charge, m_e^* is the effective mass of conduction electrons, ω_N is the unscreened plasma frequency. For doped zinc oxide films, the literature values of the parameters are: $\varepsilon_\infty = 3.85$, $m_e^* = 0.28m_e$ [5]. The scattering frequency γ can be obtained from the electron density and conductivity through equation (2). The complex dielectric

constant can be calculated from equations (3) - (5). The complex refractive index N = n + ik is related to the complex dielectric constant by the following equations:

$$n = [((\varepsilon_1^2 + \varepsilon_2^2)^{1/2} + \varepsilon_1)/2]^{1/2}, \quad (6)$$

$$k = [((\varepsilon_1^2 + \varepsilon_2^2)^{1/2} - \varepsilon_1)/2]^{1/2}. \quad (7)$$

Figure 21 shows that the calculated refractive index n decreases steadily with electron density.

Since free electrons in the film change the refractive index and the extinction coefficient, the optical spectra of zinc oxide films will also be modified by free electrons. In the infrared, the films behave like metals and have high reflectance. In the visible, however, the films are highly transparent and their spectra are like those of dielectrics. The transition between these two behaviors is at the plasma wavelength, which moves to a shorter wavelength as the free electron density in the films increases. Since the doped zinc oxide films always have a very small reflectance at the plasma wavelength (less than 5%), the extinction coefficient k should be close to zero, and the following approximation is valid:

$$R_{min} \approx (n-1)^2/(n+1)^2 \approx 0. \quad (8)$$

Therefore, the refractive index n at plasma wavelength should be close to 1.0 and the real part of dielectric constant $\varepsilon_1 \approx n^2 \approx 1.0$. From equation (3), the plasma frequency ω_p is related to the electron density by the following relation:

$$\omega_p^2 = N_e e^2/\varepsilon_0 m_e^*(\varepsilon_\infty - 1) - \gamma^2. \quad (9)$$

Formula (1) and (9) are coupled equations and the electron density can be determined when the plasma frequency and the film conductivity are known. The mobility can then be calculated with equation (2). The calculated electron density and mobility from the plasma wavelength and conductivity are shown in Table I. No solution for the electron density and mobility could be found for films deposited at 200°C and 260°C because these films have a very low dc conductivity and therefore a high scattering frequency. Drude theory, which assumes a constant scattering frequency in the whole spectral range, does not apply to those films with high scattering frequencies and low electron densities because the actual scattering frequency decreases with frequency, following a power law relation in the high frequency range. There are discrepancies between the calculated and the measured refractive indices. A more rigorous theory using a resistivity network model to take into account both ionized impurity scattering and grain boundary scattering will model the refractive index and extinction coefficient in the spectra range 0.3 μm to 20 μm more accurately [36].

Figure 22 (a) shows the reflectance and transmittance spectra of a gallium doped zinc oxide film deposited at 370°C from 0.05% diethyl zinc, 0.8% water and 0.0107% triethyl gallium. The gallium concentration in the film is 7.6 at.%. The film thickness, conductivity, electron density and mobility are 0.63 μm, 730 $\Omega^{-1}cm^{-1}$, 5.0×10^{20} cm^{-3} and 9.5 cm^2/Vs, respectively. The plasma wavelength of this film is at 1.45 μm. The optical behavior in the infrared is dominated by free electrons, and the film has a maximum infrared reflectance close to 75%. For films deposited at 370°C, we found that the electrical and optical properties are optimized with a gallium concentration of 3.0 at.%. This gallium concentration was obtained when the film was deposited from 0.0036% triethyl gallium in the gas phase. Figure 22 (b) shows the optical spectra of this sample with a thickness of 0.62 μm. The interference fringes of the reflectance and transmittance in the visible

have shallow valleys and crests because of the thickness nonunformity of the sample. The plasma wavelength of this film is at 1.15 μm and the film has a maximum infrared reflectance close to 85%. The film conductivity, electron density, and mobility are 2075 $\Omega^{-1}cm^{-1}$, $9.3x10^{20}$ cm^{-3}, 13.9 cm^2/Vs, respectively.

The absorption $A(\lambda)$ obtained from the reflectance and transmittance depends slightly on the wavelength in the visible region. For solar cell applications, the appropriate average absorption A is calculated from

$$A = \frac{\int d\lambda \psi(\lambda) A(\lambda)}{\int d\lambda \psi(\lambda)}, \tag{10}$$

where $\psi(\lambda)$ is the solar irradiance spectrum at one air mass multiplied by the spectral sensitivity of a typical solar cell. This average absorption is very close to a simple arithmetic average. The visible absorption depends on film thickness, as shown in Figure 23. The films are the same as those in Figure 15. The absorption increases with film thickness. In solar cell applications, films require low visible absorption and high dc conductivity. The performance of transparent conducting films can be ranked according to a quantity called the Figure of Merit, which we define as the ratio of conductivity σ to absorption coefficient α, $\sigma/\alpha = -1/(R\ln T)$, where R is the sheet resistance, and T is the average fractional transmittance between 400 nm and 800 nm. The Figure of Merit in the Drude approximation can be expressed as:

$$\sigma/\alpha = 4\pi^2 c^3 n \varepsilon_0 / \lambda^2 \gamma^2, \tag{11}$$

where c is the speed of light in vacuum, n is the refractive index, λ is the wavelength. The Figure of Merit depends strongly on scattering frequency. Figure 24 (a) shows that the Figure of Merit depends on film thickness. The films are the same as those in Figure 15. Since the grain boundary scattering frequency γ decreases with film thickness, the Figure of Merit increases with film thickness. Figure 24 (b) shows that the Figure of Merit depends on deposition temperature. The scattering frequency also decreases with deposition temperature and so the Figure of Merit increases with deposition temperature.

The optical absorption coefficient of a direct band gap semiconductor near the band edge, for photon energy hv greater than the band gap energy E_g of the semiconductor, is given by the following equation [35]:

$$\alpha = A(h\nu - E_g)^{1/2}, \tag{12}$$

where A is a constant. At the absorption edge, the film transmittance $T \approx \exp(-\alpha t)$, where t is the film thickness [19]. By plotting $(\ln T)^2$, which is proportional to α^2, versus photon energy hv, the band gap E_g can be found from extrapolation. In heavily doped zinc oxide films, the lowest states in the conduction band are occupied by free electrons and the valence electrons require extra energy to be excited to higher energy states in the conduction band. Therefore, the optical band gaps of doped zinc oxide films are wider than those of undoped zinc oxide films. The Burstein-Moss theory predicts that this band gap widening is proportional to $N_e^{2/3}$, where N_e is the electron density. Figure 25 shows the energy gap dependence on electron density. Only those films with a gallium concentration below 5.0 at.% are correlated with Burstein-Moss theory, since very high

gallium concentration increases impurity scattering, making the simple band gap widening theory invalid. The band gap does not linearly depend on $N_e^{2/3}$ even for films with low gallium concentrations. For films with a gallium concentration above 5.0 at.%, there is no simple correlation between the band gap and the electron density.

IV. CONCLUSIONS

Gallium doped zinc oxide films have been successfully deposited on soda lime glass substrates and silicon substrates in the temperature range 150°C to 470°C from 0.05% diethyl zinc, 0.8% water and various triethyl gallium concentrations. The film growth profiles are dramatically different for film deposited with low and high (above 0.009%) triethyl gallium concentrations. The gallium concentration in the film increases with the triethyl gallium concentration in the gas phase. For a triethyl gallium concentration of 0.0032% and a deposition temperature of 370°C, the gallium concentration in the film is around 2.5 at.%. The hydrogen concentration in the film decreases with deposition temperature. The crystalline size determined from the x-ray diffraction peak width is between 270 Å and 500 Å for undoped films and between 120 Å and 400 Å for doped films in the temperature range 260°C to 470°C. The crystallite orientation is changed by doping and only those films deposited above 430°C are highly oriented with their c-axes perpendicular to the substrate plane. Small numbers of gallium atoms introduce similar numbers of electrons in the films, but higher gallium concentrations (above 5.0 at.%) result in only about 10% doping efficiency. The electron density for films deposited at 370°C with different triethyl gallium concentrations varies between 3.7×10^{20} cm^{-3} and 9.3×10^{20}cm^{-3}. When the triethyl gallium concentration is kept at 0.0032%, the electron density increases from 0.7×10^{20} cm^{-3} for films deposited at 200°C to 10.6×10^{20} cm^{-3} for films deposited at 470°C. A higher deposition temperature leads to higher doping efficiency. The conductivity is not uniform along the gas flow direction and the peak conductivity position moves toward the reactor nozzle as the temperature increases. A film deposited at 200°C with a gallium concentration of 2.9 at.% has a conductivity of only about 1.5 Ω^{-1}cm^{-1}. When the deposition temperature is increased to 470°C, the conductivity increases to 4200 Ω^{-1}cm^{-1} for a film with a gallium concentration of 2.4 at.%. Only those films deposited above 350°C have conductivities above 1000 Ω^{-1}cm^{-1}. The electron mobility varies from 5.3 cm^2/Vs to 13.9 cm^2/Vs for films deposited at 370°C with different gallium concentrations. The mobility increases from 0.1 cm^2/Vs to 24.6 cm^2/Vs when the temperature is increased from 200°C to 470°C. Both the mobility and the conductivity increase with film thickness. The free electrons in the film reduce the film refractive index for visible light and make the film behave like a metal in the infrared range. Simple Drude theory was used to calculate the refractive index from the measured electron density and conductivity. There is some discrepancy between theoretical and measured results. The visible absorption increases with film thickness. The Figure of Merit also increases with film thickness because of the decrease of scattering frequency with film thickness. The Figure of Merit increases from 0.0005 Ω^{-1} to 1.5 Ω^{-1} when the temperature is increased from 200°C to 470°C. The band gap increases with electron density, approximately following Burstein-Moss theory for films with a gallium concentration below 5.0 at.%. Very high gallium concentration in the film complicates the band gap dependence on electron density.

References

[1]Y. Igasaki and H. Saito, J. Appl. Phys. **70**, 3613 (1991).

[2]A. Banerjee, D. Wolf, J. Yang, and S. Guha, J. Appl. Phys. **70**, 1692 (1991).

[3]J. B. Yoo, A. L. Fahrenbruch, and R. H. Bube, J. Appl. Phys. **68**, 4694 (1990).

[4]R. E. I. Schropp and A. Madan, J. Appl. Phys. **66**, 2027 (1989).

[5]Z. C. Jin, I. Hamberg, and C. G. Granqvist, J. Appl. Phys. **64**, 5117 (1988).

[6]D. R. Lide, *Handbook of Chemistry and Physics*, 71st ed. (CRC, Boca Raton, FL, 1991).

[7]R. Banerjee, S. Ray, N. Basu, A. K. Batabyal, and A. K. Barua, J. Appl. Phys. **62**, 912 (1987).

[8]A. F. Aktaruzzaman, G. L. Sharma, and L. K. Malhotra, Thin Solid Films **198**, 67 (1991).

[9]T. Minami, H. Nanto, and S. Takata, Jpn. J. Appl. Phys. **23**, L280 (1984).

[10]J. Hu and R. G. Gordon, Solar Cells **30**, 437 (1991).

[11]J. Hu and R. G. Gordon, Mater. Res. Soc. Symp. Proc. **202**, 457 (1991).

[12]W. W. Wenas, A. Yamada, M. Konagai, and K. Takahashi, Jpn. J. Appl. Phys. **30**, L441 (1991).

[13]T. Minami, K. Oohashi, and S. Takata, Thin Solid Films **193**, 721 (1990).

[14]A. Kuroyanagi, J. Appl. Phys. **66**, 5492 (1989).

[15]M. Ruth, J. Tuttle, J. Goral, and R. Noufi, J. Crystal. Growth **96**, 363 (1989).

[16]T. Minami, H. Nanto, and S, Takata, Jpn. J. Appl. Phys. **24**, L605 (1985).

[17]B. H. Choi, H. B. Im, and J. S. Song, J. Am. Ceram. Soc. **73**, 1347 (1990).

[18]B. H. Choi, H. B. Im, J. S. Song, and K. H. Yoon, Thin Solid Films **193**, 712 (1990).

[19]A. Sarkar, S. Ghosh, S. Chaudhuri, and A. K. Pal, Thin Solid Films **204**, 255 (1991).

[20]S. N. Qiu, C. X. Qiu, and I. Shih, Solar Energy Mater. **15**, 261 (1987).

[21]S. Major, A. Banerjee, and K. L. Chopra, Thin Solid Films **122**, 31 (1984).

[22]C. K. Lau, S. K. Tiku, and K. M. Lakin, J. Electrochem. Soc. **127**, 1843 (1980).

[23]M. Shimizu, T. Horii, T. Shiosaki, and A. Kawabata, Thin Solid Films **96**, 149 (1982).

[24]F. T. J. Smith, Appl. Phys. Lett. **43**, 1108 (1983).

[25]P. J. Wright, R. J. M. Griffiths, and B. Cockayne, J. Crystal Growth **66**, 26 (1984).

[26]S. Oda, H. Tokunaga, N. Kitajima, J. Hanna, I. Shimizu, and H. Kokado, Jpn. J. Appl. Phys. **24**, 1607 (1985).

[27]P. Souletie, S. Bethke, B. W. Wessels, and H. Pan, J. Crystal Growth **86**, 248 (1988).

[28]T. Maruyama and A. Nakai, Jpn. J. Appl. Phys. **28**, L346 (1989).

[29]J. Hu and R. G. Gordon, J. Appl. Phys. **71**, 880 (1992).

[30]D. A. Strickler, Ph. D. thesis, Harvard University, 1989.

[31]W. H. Press, B. P. Flannery, S. A. Teukolsky, and W. T. Vetterling, *Numerical Recipies* (Cambridge, New York, 1986).

[32]B. D. Cullity, *Elements of X-ray Diffraction*, 2nd ed. (Addison-Wesley, Reading, MA, 1978).

[33]P. Parent, H. Dexpert, G. Tourillon, and J. M. Grimal, J. Electrochem. Soc. **139**, 276 (1992).

[34]N. W. Ashcroft and N. D. Mermin, *Solid State Physics*, (Saunders College, Philadelphia, 1976).

[35]I. Hamberg and C. G. Granqvist, J. Appl. Phys. **60**, R123 (1986).

[36]J. Hu, J. W. Proscia, and R. G. Gordon, unpublished results.

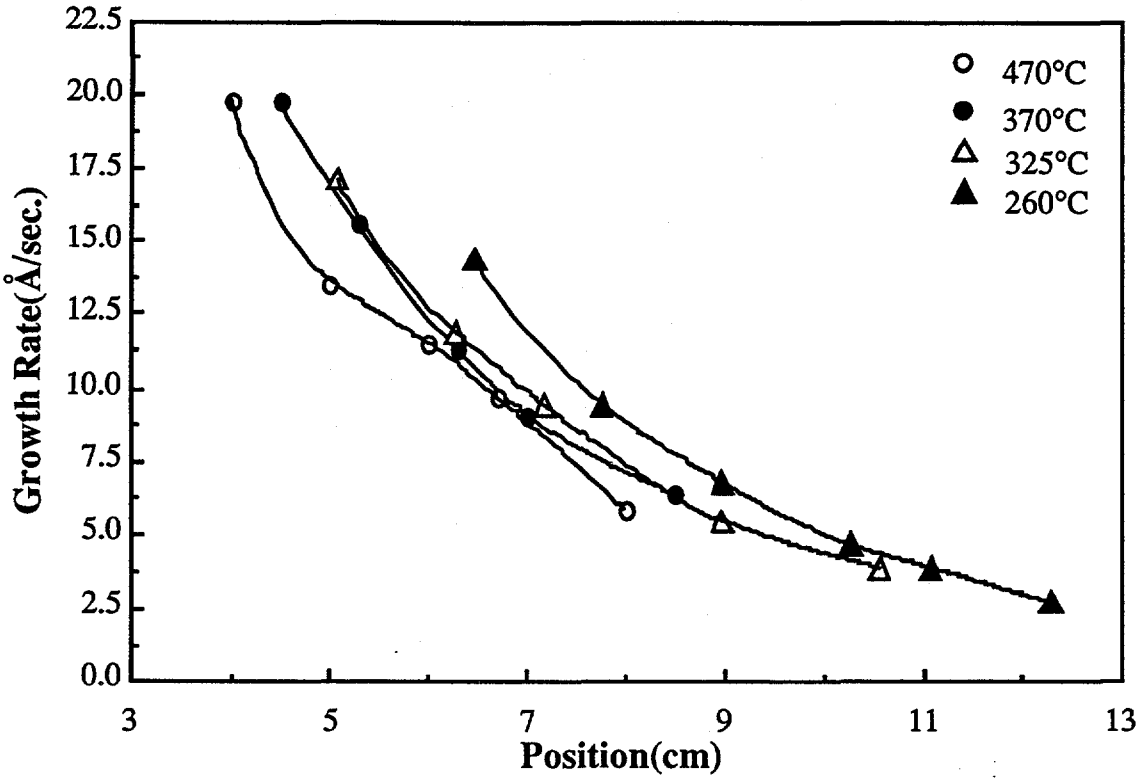

FIG. 1. Growth rate profile as a function of deposition temperature. The diethyl zinc, water, and triethyl gallium concentrations were 0.05%, 0.8% and 0.0032%, respectively.

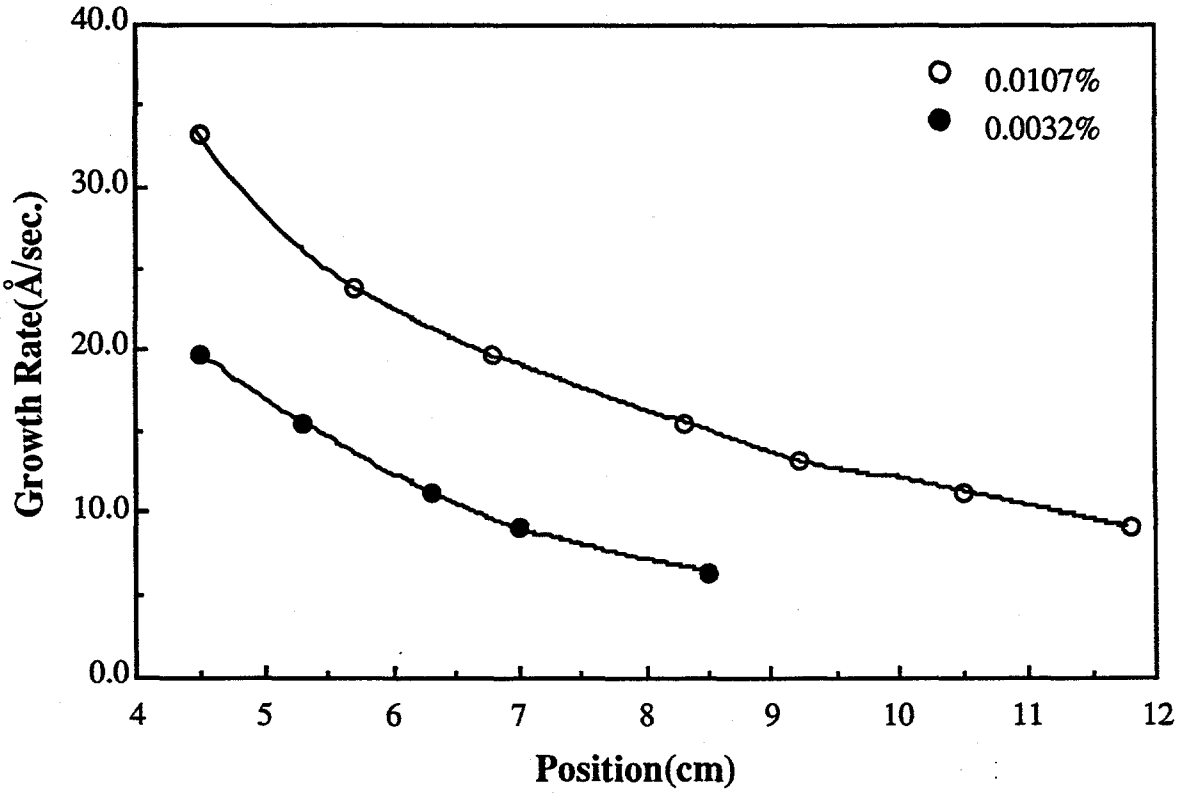

FIG. 2. Growth rate profile as a function of triethyl gallium concentration. The diethyl zinc and water concentrations were 0.05% and 0.8% and the deposition temperature was 370°C.

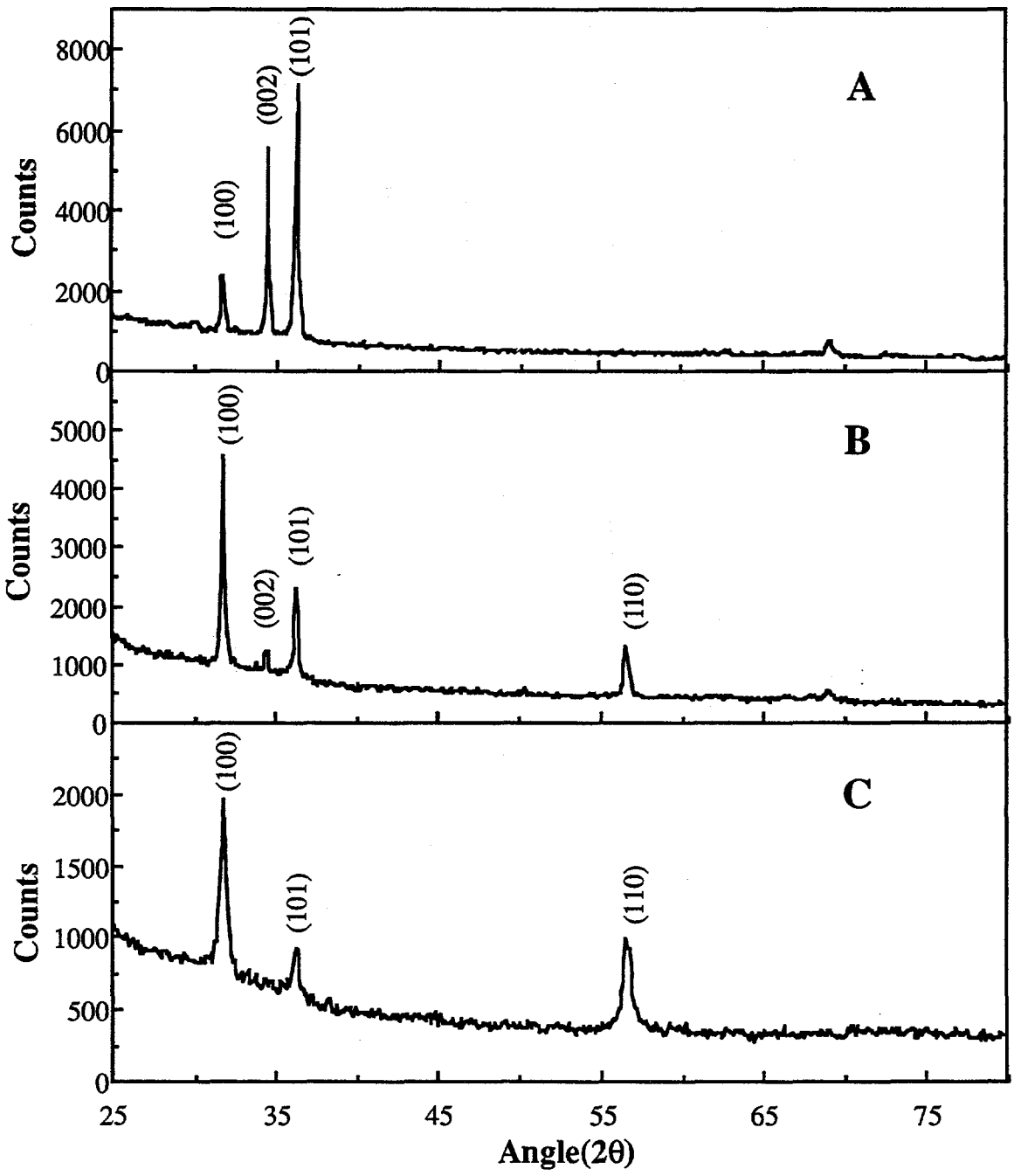

FIG. 3. X-ray diffraction spectra of zinc oxide films deposited at 370°C on soda lime glass substrates. The gallium concentrations in the films are: A, 0.0 at.%; B, 2.5 at.%; C, 7.2 at.%.

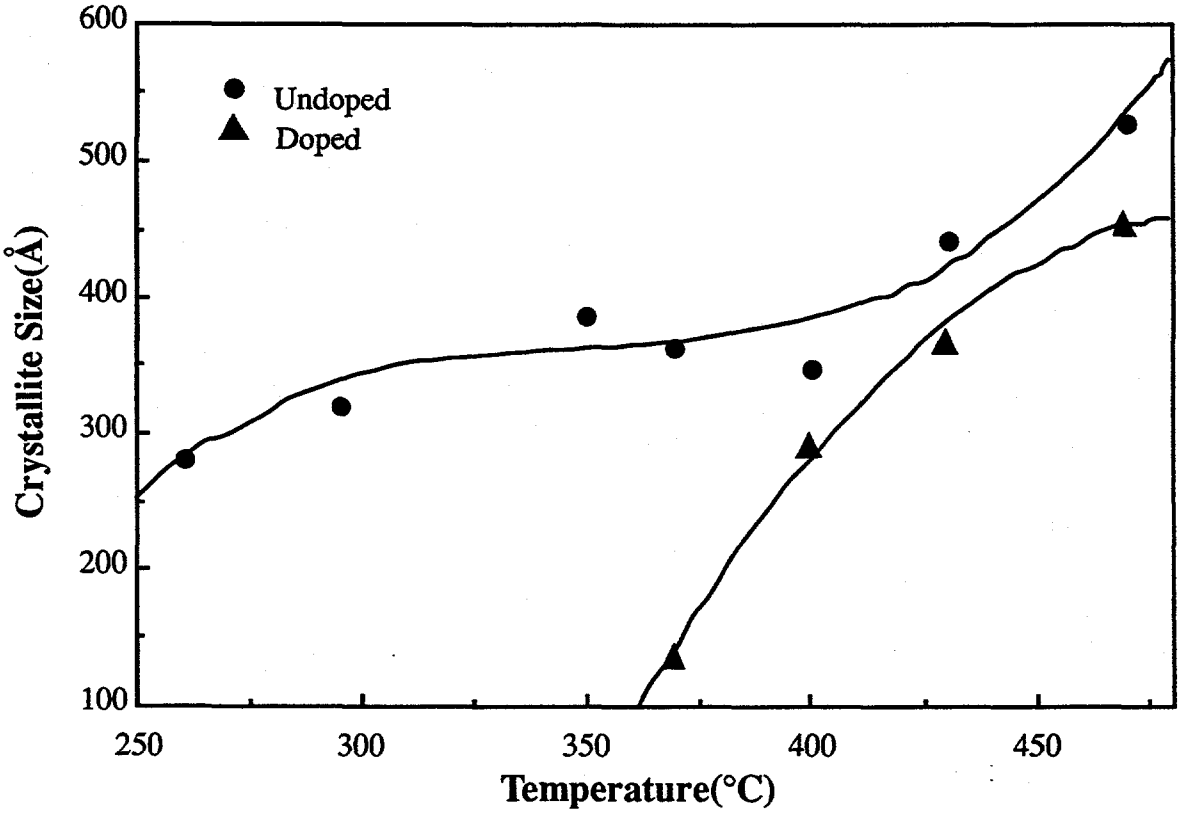

FIG. 4. Crystallite size dependence on deposition temperature. The crystallite sizes were determined from the (002) diffraction peak width. The doped films were deposited from 0.0032% triethyl gallium in the gas phase.

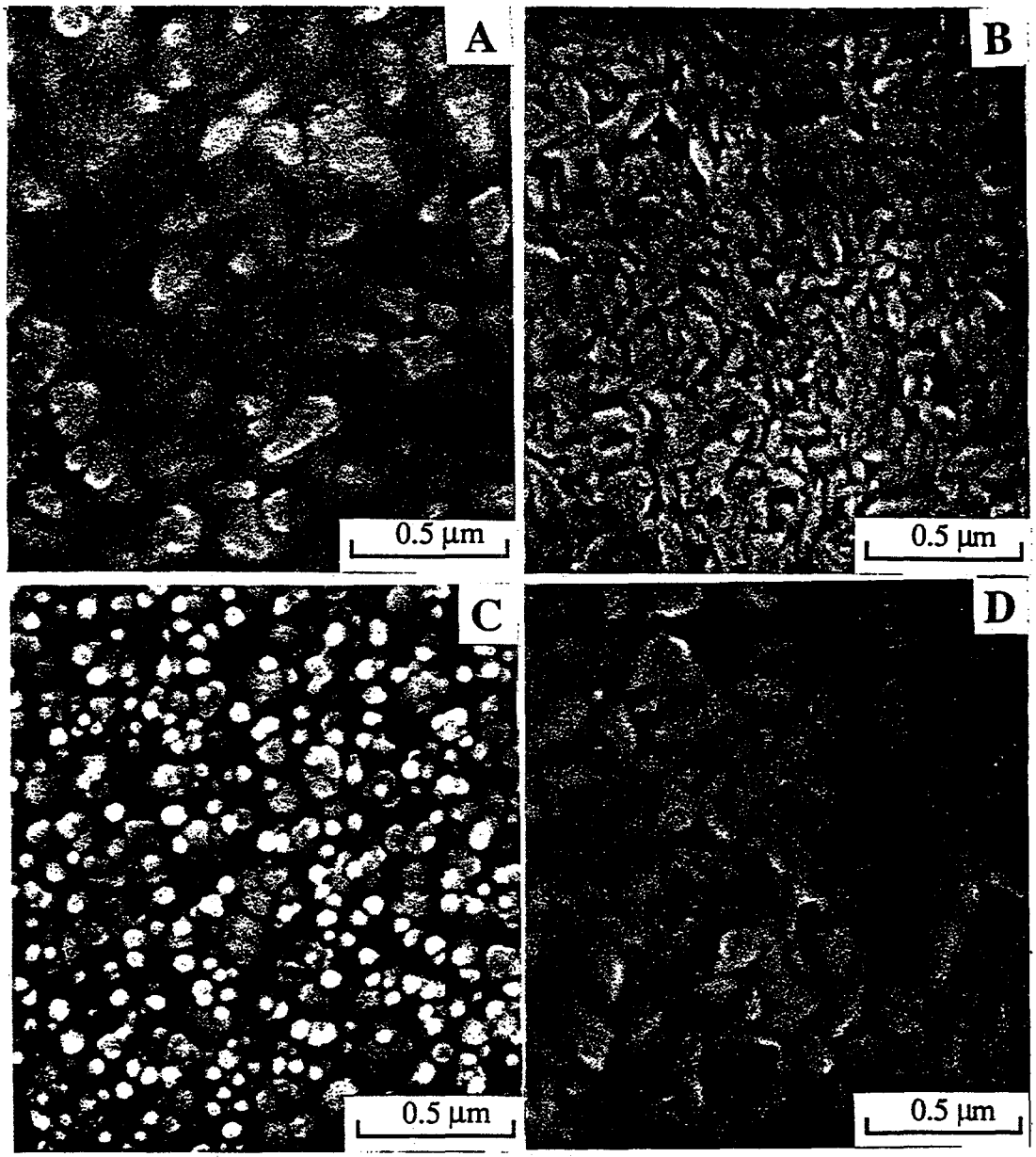

FIG. 5. Scanning electron micrographs of undoped and doped zinc oxide films deposited from 0.05% diethyl zinc and 0.8% water. Samples (a) and (b) were deposited at 350°C and (c) and (d) were deposited at 430°C. Samples (a) and (c) were undoped and (b) and (d) were doped with 0.0032% triethyl gallium in the gas phase.

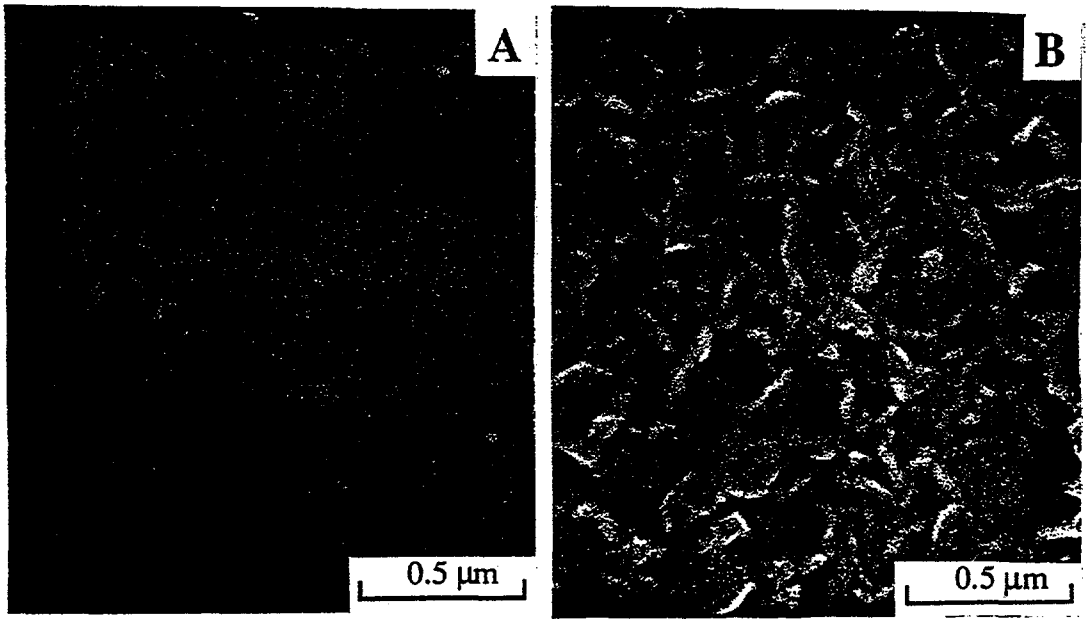

FIG. 6. Scanning electron micrographs of gallium doped zinc oxide films deposited at 370°C from 0.05% diethyl zinc, 0.8% water and 0.0032% triethyl gallium. The thicknesses of samples (a) and (b) are 0.11 μm and 1.2 μm.

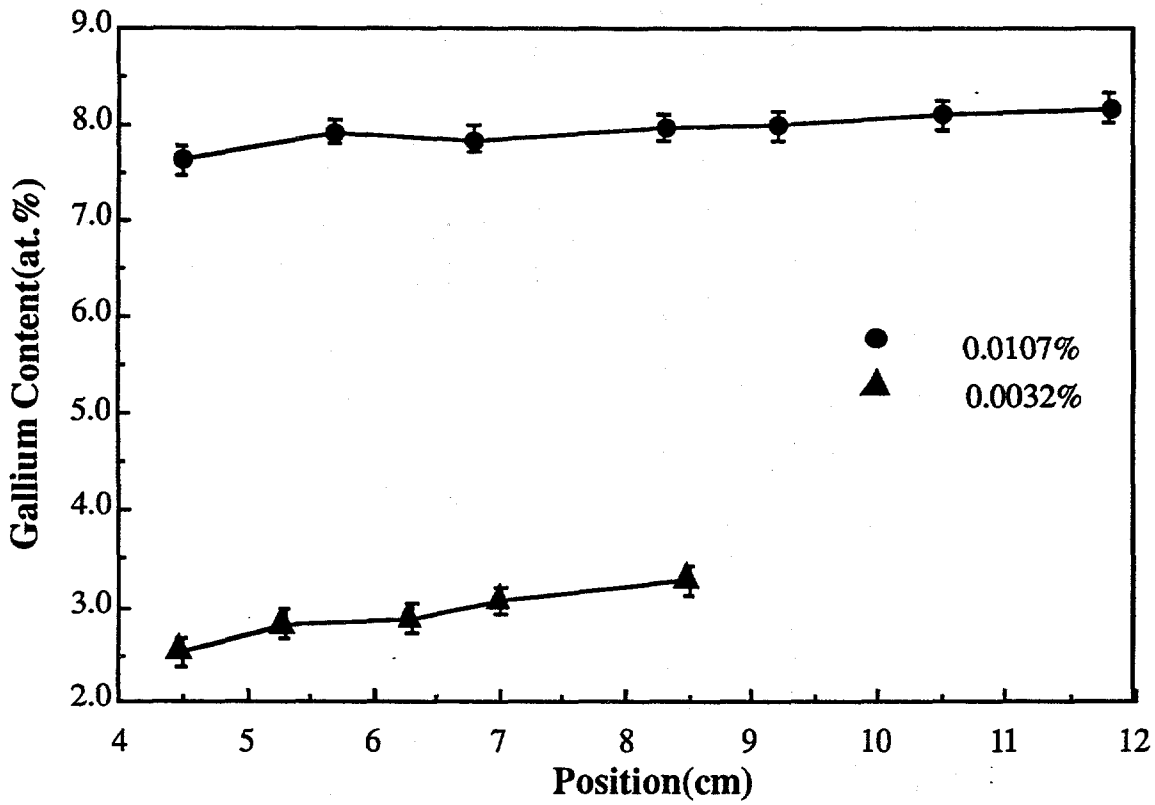

FIG. 7. Gallium concentration distribution along the gas flow direction for films deposited at 370°C from 0.0032% and 0.0107% triethyl gallium. The diethyl zinc and water concentrations were 0.05% and 0.8%, respectively.

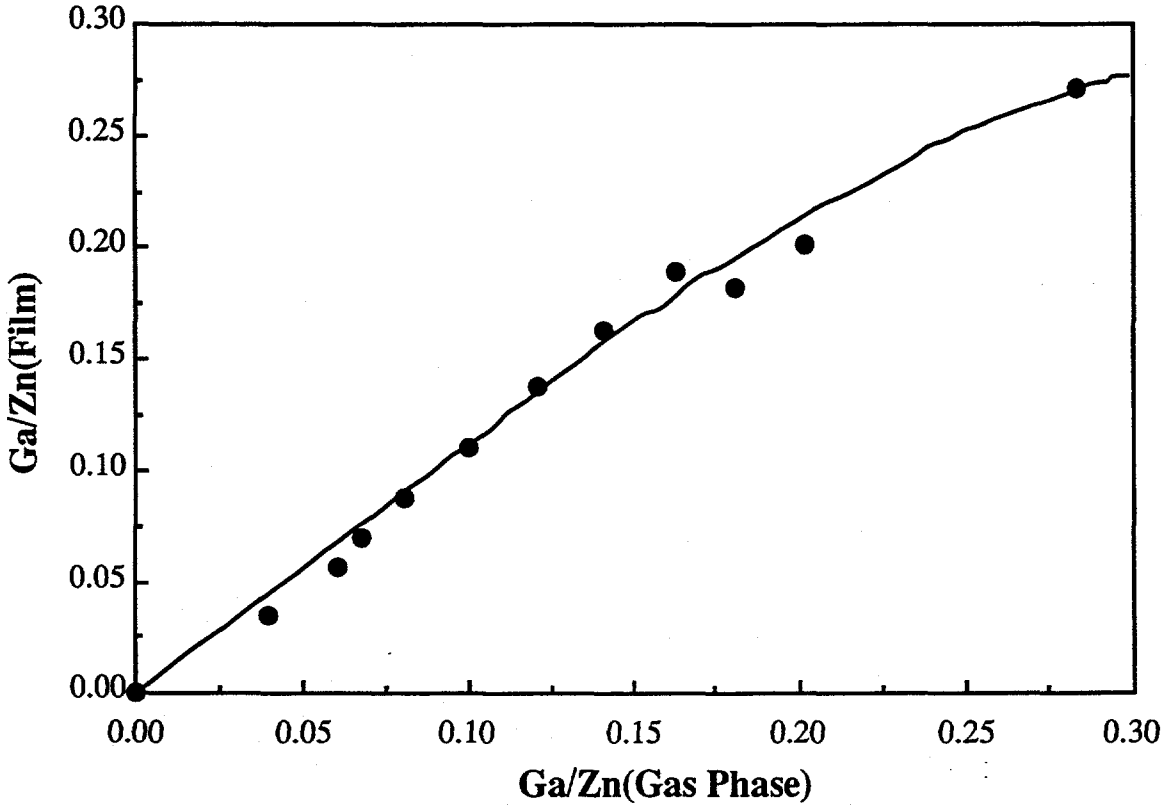

FIG. 8. Gallium to zinc ratio in the film as a function of gallium to zinc ratio in the gas phase. The films were deposited at 370°C from 0.05% diethyl zinc and 0.8% water and the samples were taken from the most conductive part on the substrates.

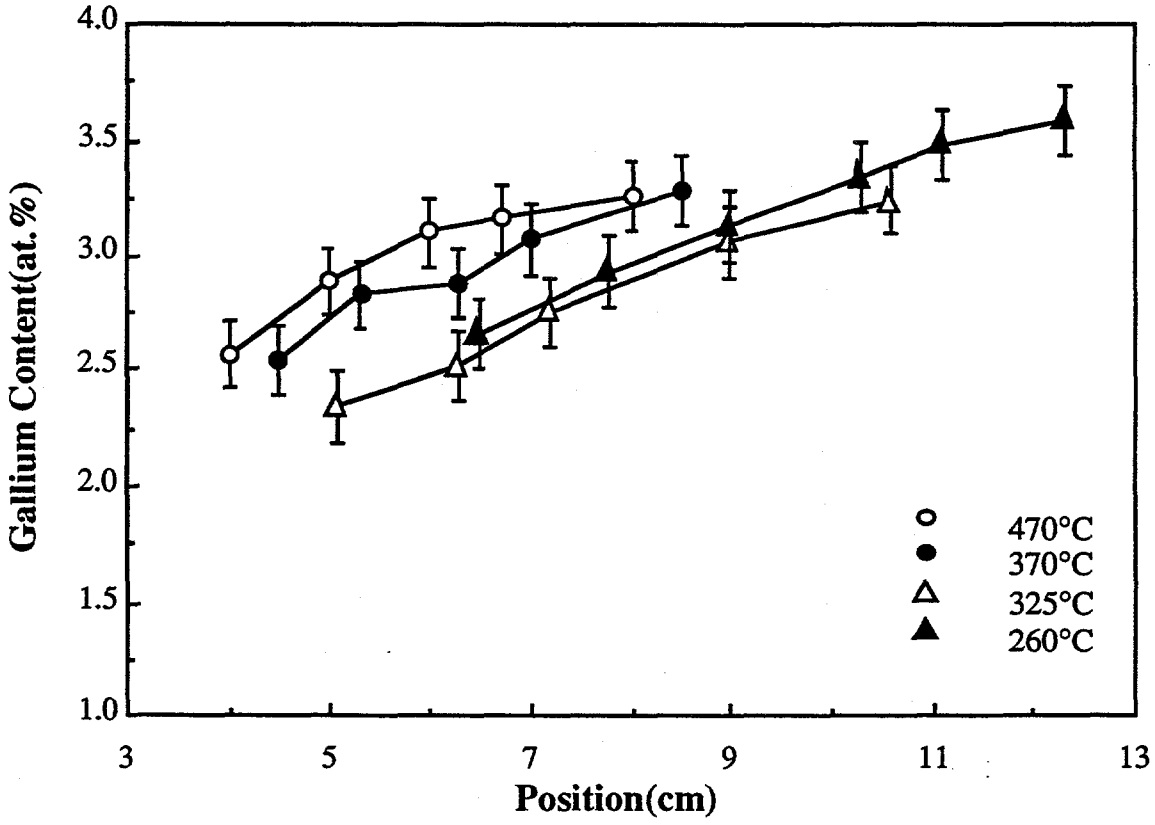

FIG. 9. Gallium concentration distribution along the gas flow direction for films deposited at different temperatures from 0.05% diethyl zinc, 0.8% water and 0.0032% triethyl gallium.

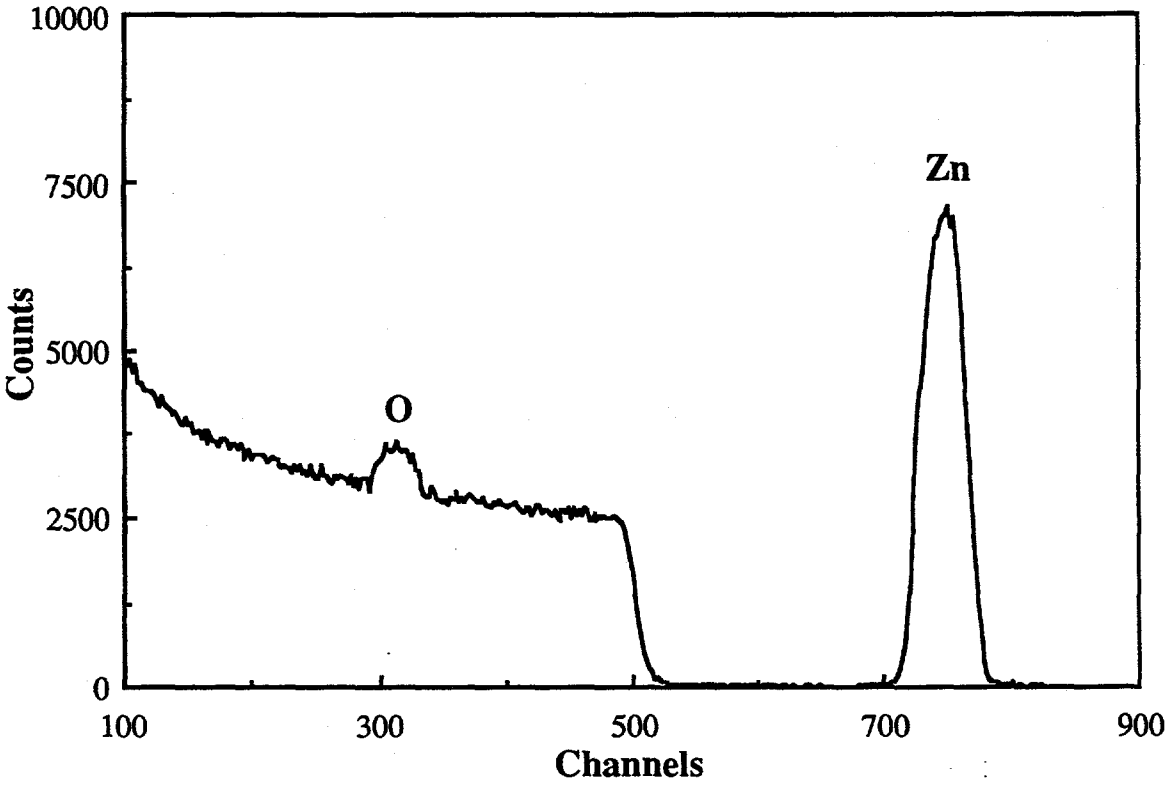

FIG. 10. RBS spectrum of gallium doped zinc oxide films deposited at 370°C on silicon substrate.

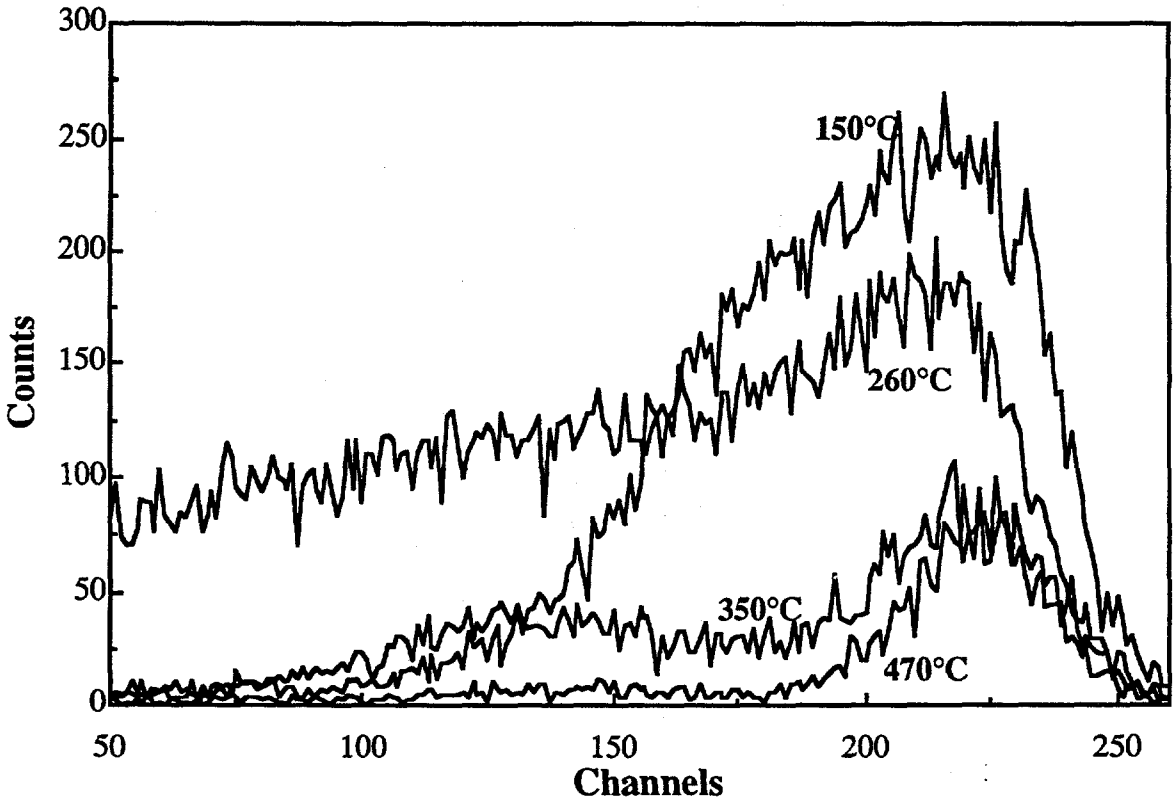

FIG. 11. FRS spectra of gallium doped zinc oxide films deposited at different temperatures on silicon substrates. The estimated hydrogen contents are: 150°C, 15.3 at.%; 260°C, 9.7 at.%; 370°C, 8.1 at.%; 470°C, 7.4 at.%. The estimated error in these values is about ±3 at.%.

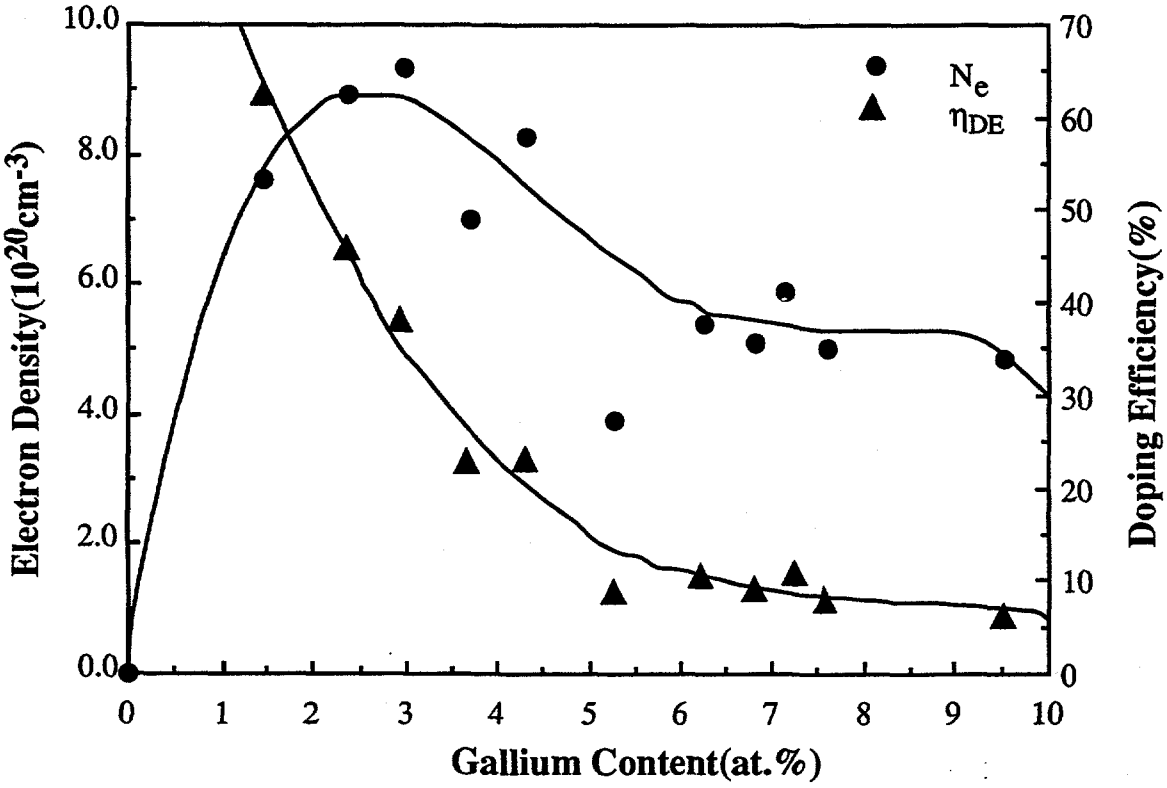

FIG. 12. Electron density N_e and doping efficiency η_{DE} dependence on gallium concentration. The films were deposited at 370°C from 0.05% diethyl zinc, 0.8% water with different triethyl gallium concentrations.

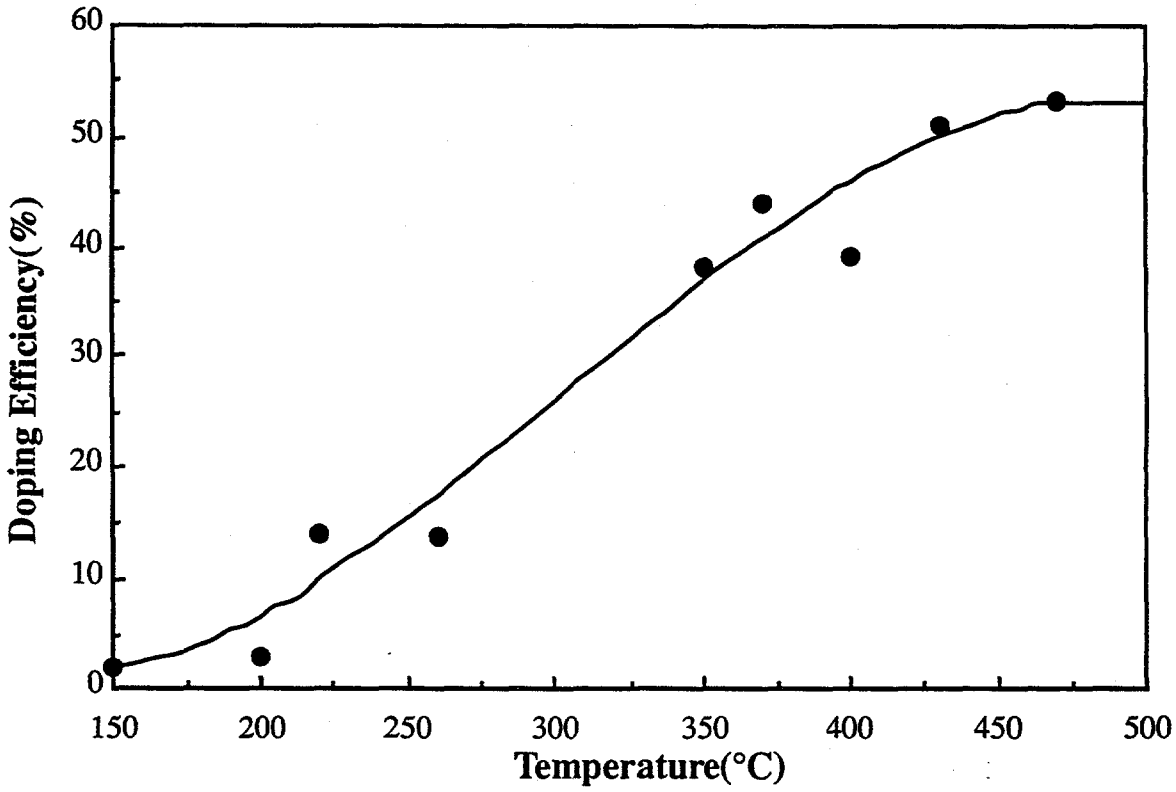

FIG. 13. Doping efficiency dependence on deposition temperature. The films were deposited from 0.05% diethyl zinc, 0.8% water and 0.0032% triethyl gallium.

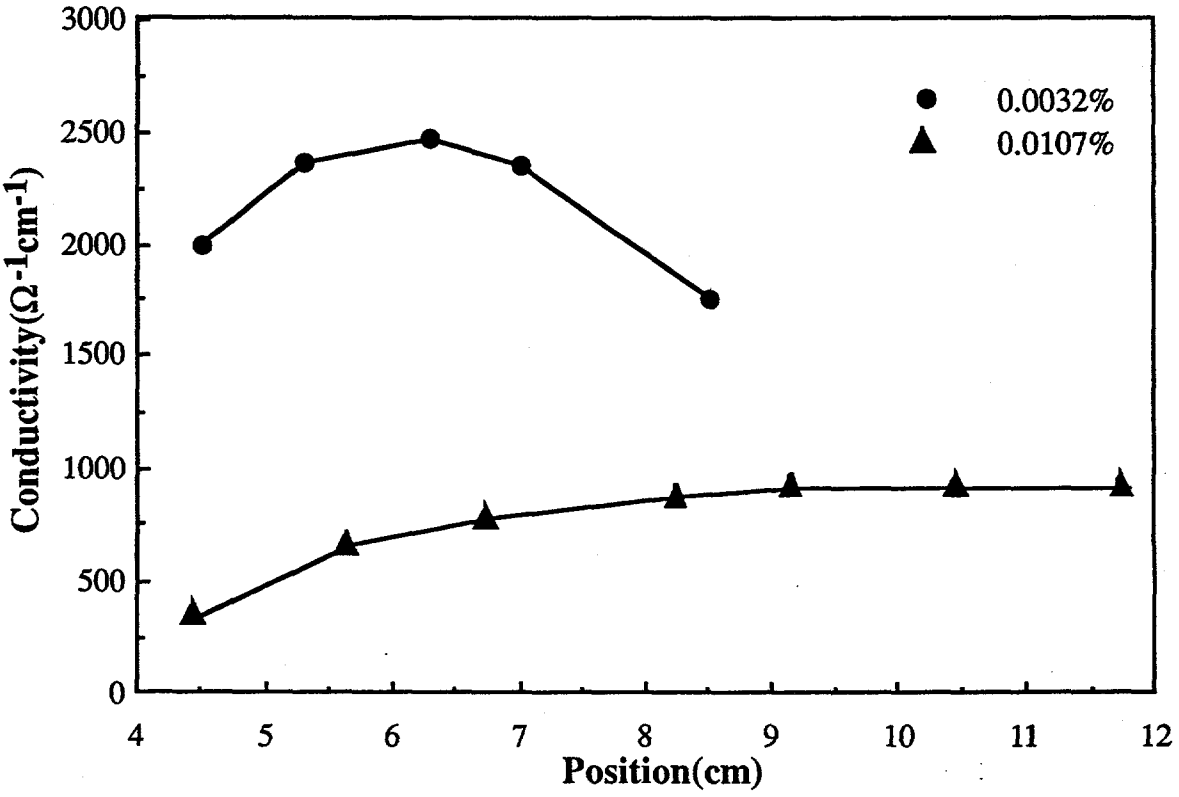

FIG. 14. Conductivity distribution along the gas flow direction for films deposited at 370°C from 0.05% diethyl zinc and 0.8% water with two different triethyl gallium concentrations.

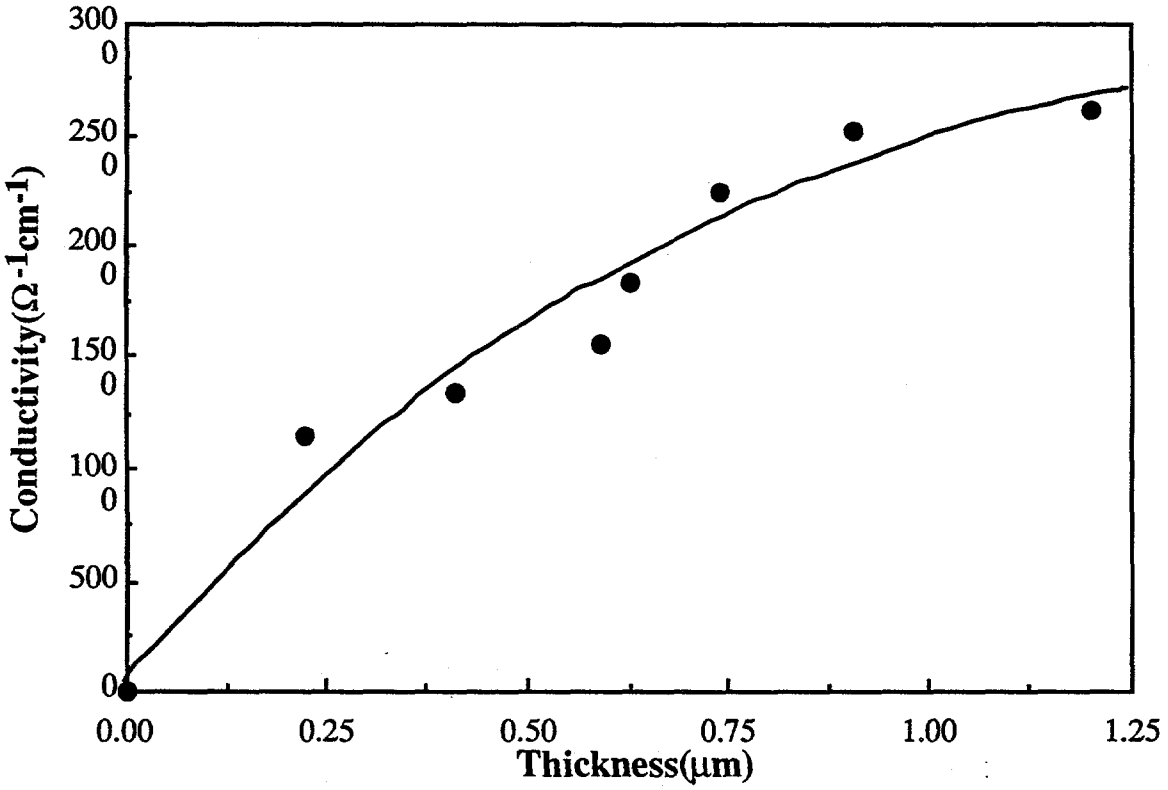

FIG. 15. Peak conductivity dependence on film thickness for films deposited at 370°C from 0.05% diethyl zinc, 0.8% water and 0.0032% triethyl gallium.

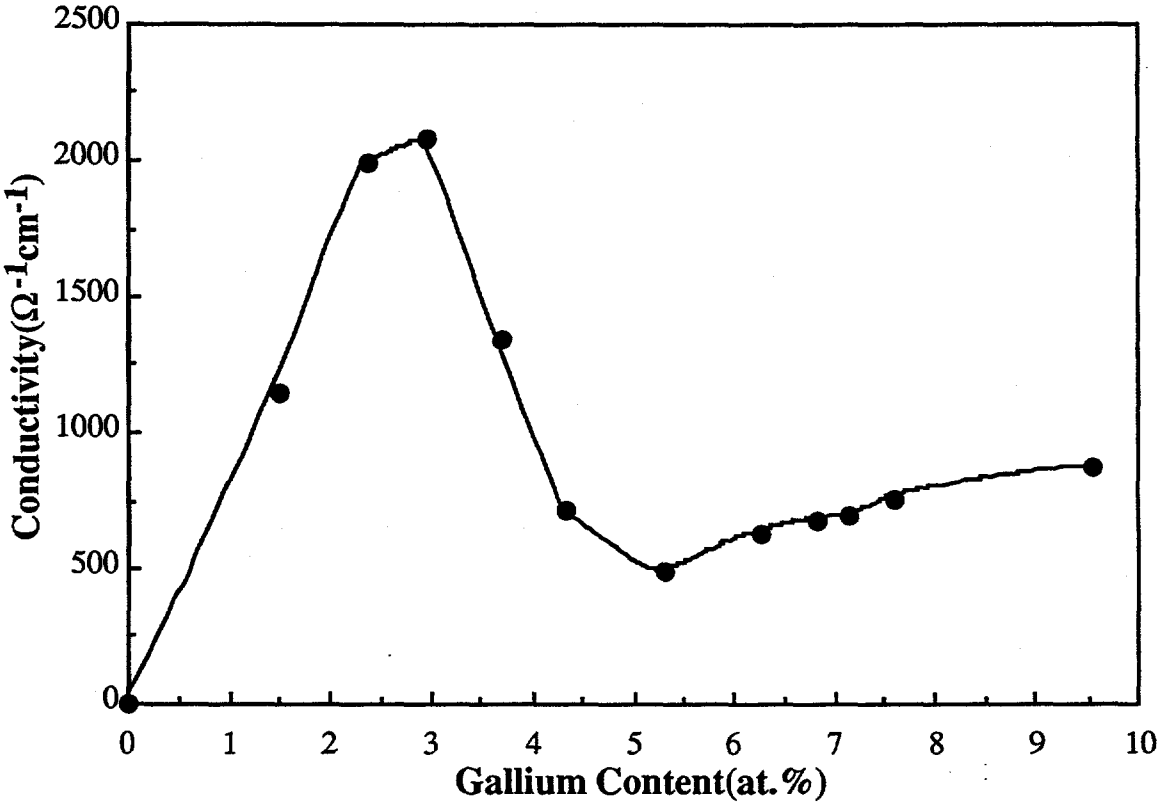

FIG. 16. Peak conductivity dependence on gallium concentration. The films are the same as those in Figure 12.

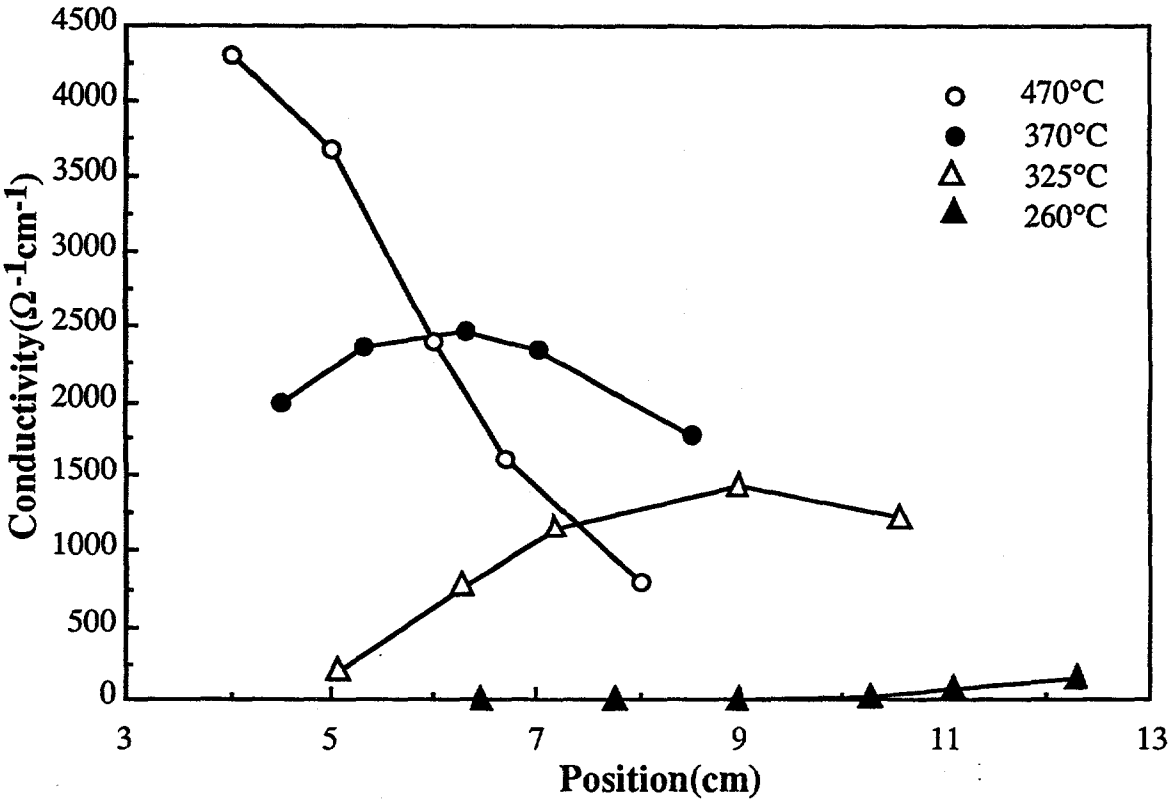

FIG. 17. Conductivity distribution along the gas flow direction for films deposited at different temperatures from 0.05% diethyl zinc, 0.8% water and 0.0032% triethyl gallium.

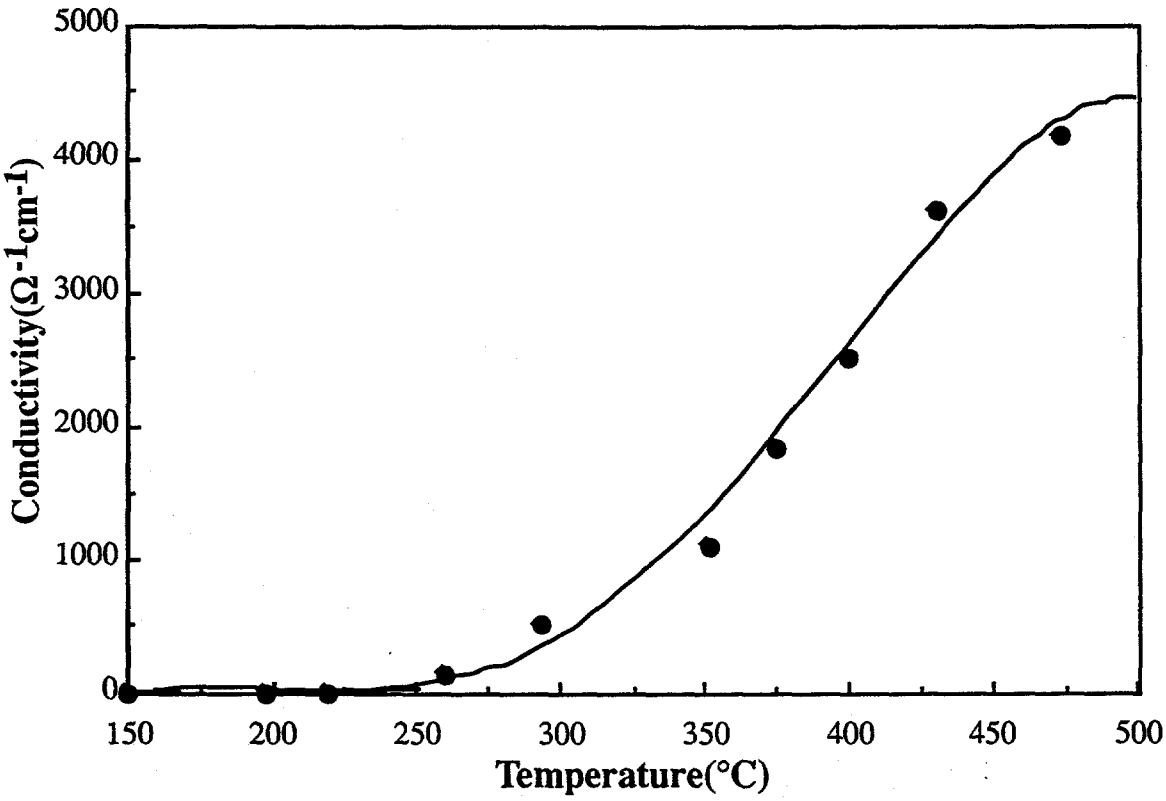

FIG. 18. Peak conductivity as a function of deposition temperature. The reactant concentrations are the same as those in Figure 17 and the film thicknesses are around 0.6 μm.

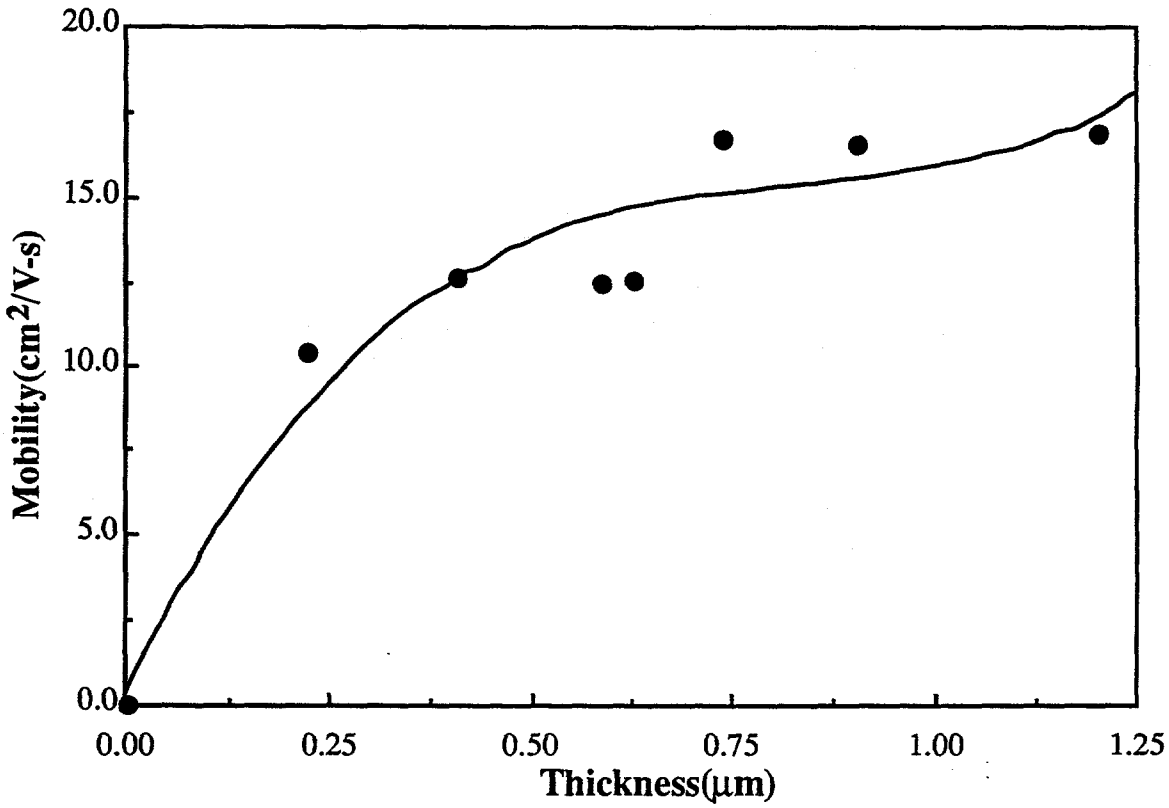

FIG. 19. Mobility dependence on film thickness. The films are the same as those in Figure 15.

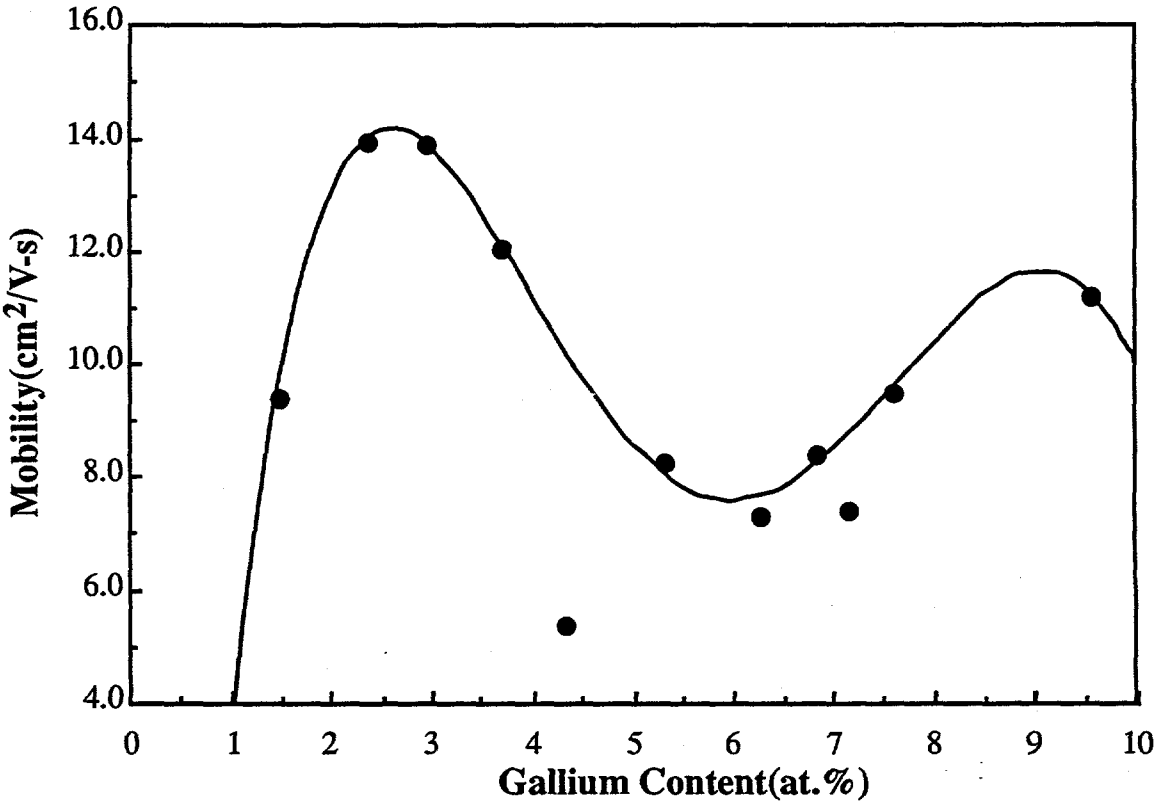

FIG. 20. Mobility dependence on gallium concentration. The films are the same as those in Figure 12.

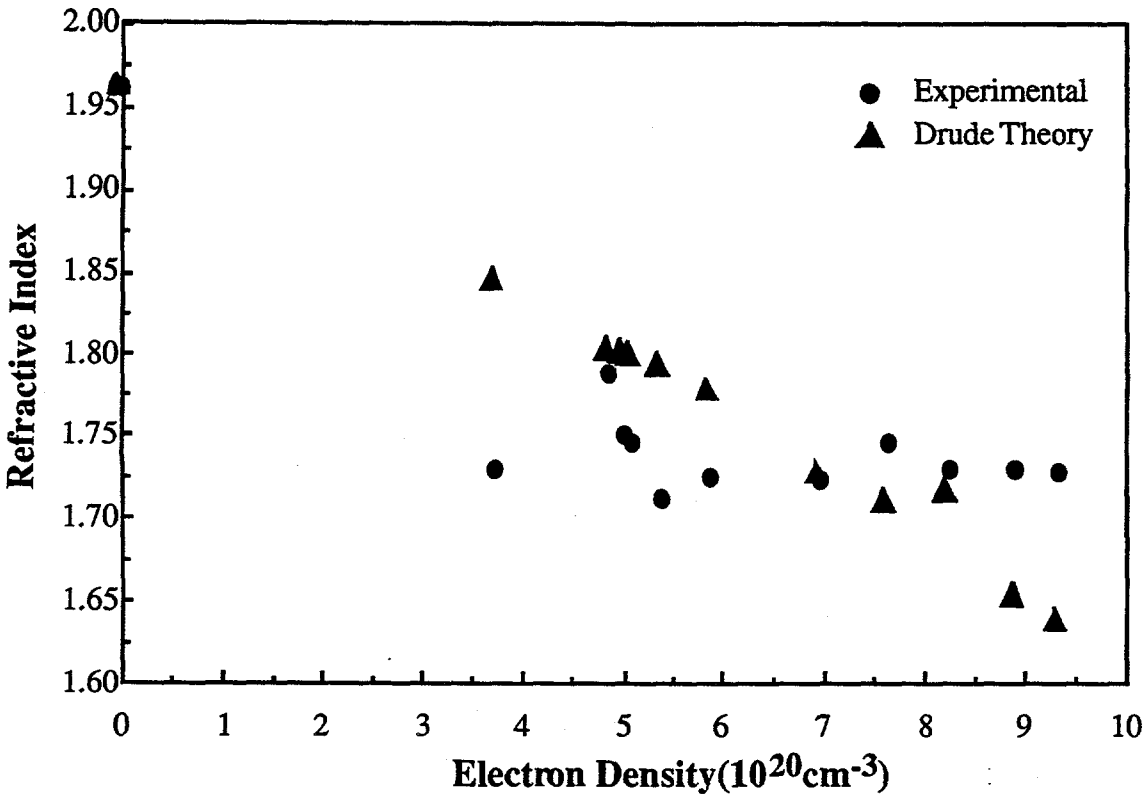

FIG. 21. Refractive index at λ = 6328 Å determined from prism coupler for film deposited at 370°C from 0.05% diethyl zinc and 0.8% water with different triethyl gallium concentrations. Also shown in the Figure is the calculated refractive index from Drude theory.

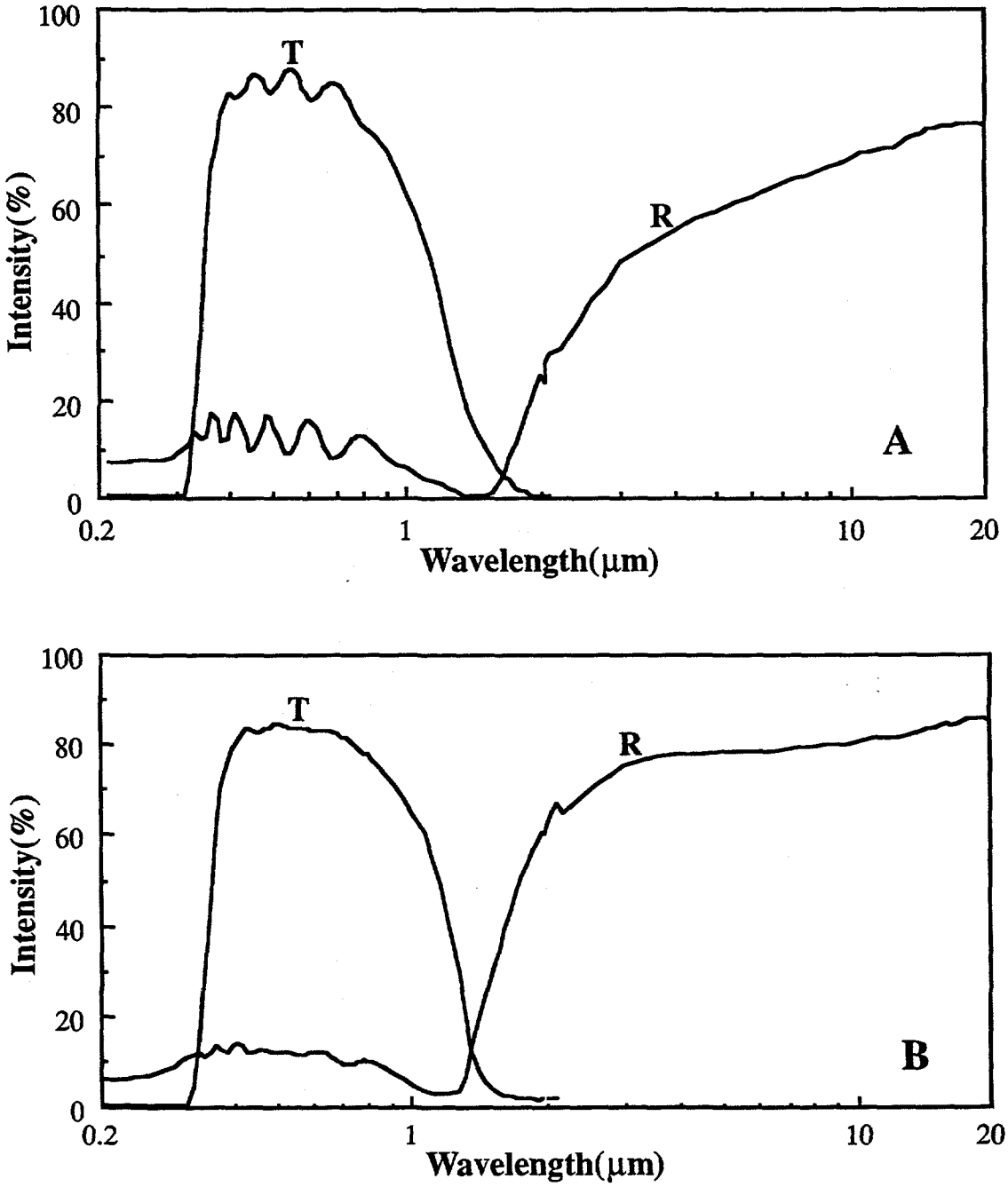

FIG. 22. Optical spectra of gallium doped zinc oxide films deposited at 370°C from 0.05% diethyl zinc, 0.8% water. The gallium concentration in (a) is 0.0107% and in (b) it is 0.0036%. The "bumps" at 2 μm in the reflectance spectra are due to the spectrometer switches (from near visible to FT-IR).

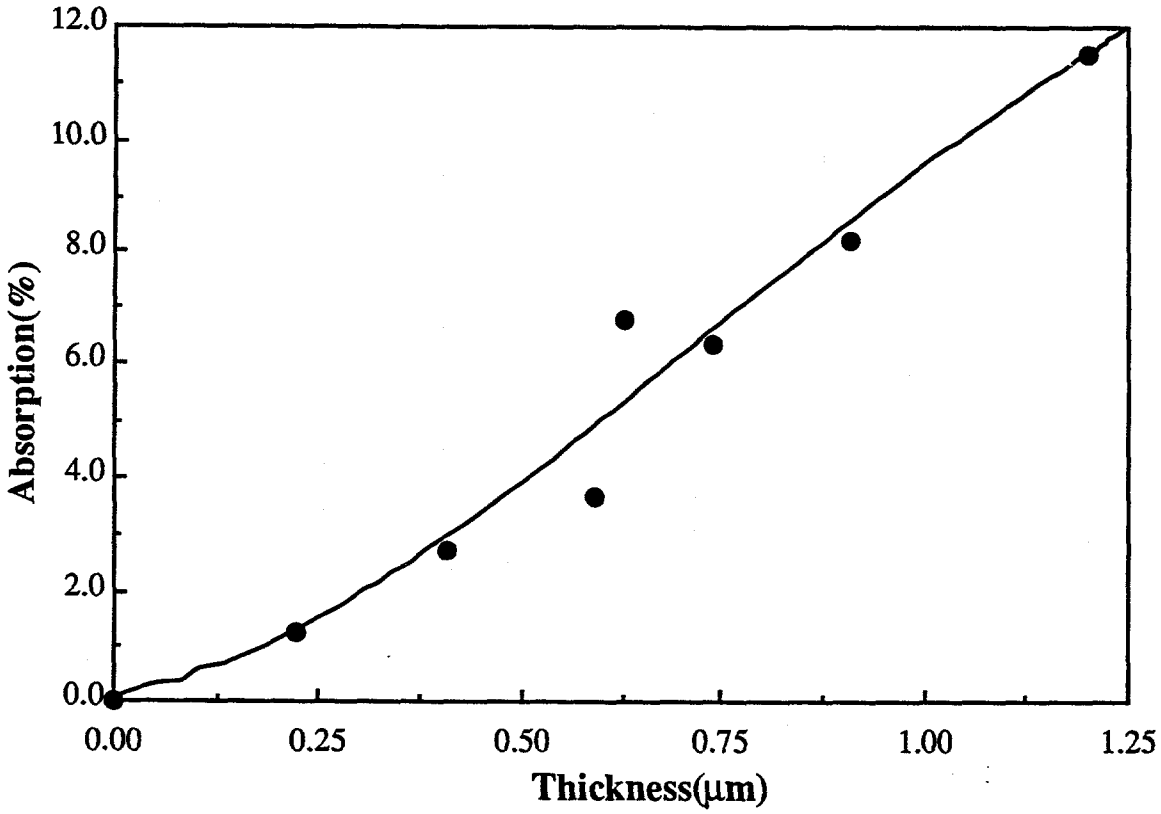

FIG. 23. Average visible absorption as a function of film thickness. The films are the same as those in Figure 15.

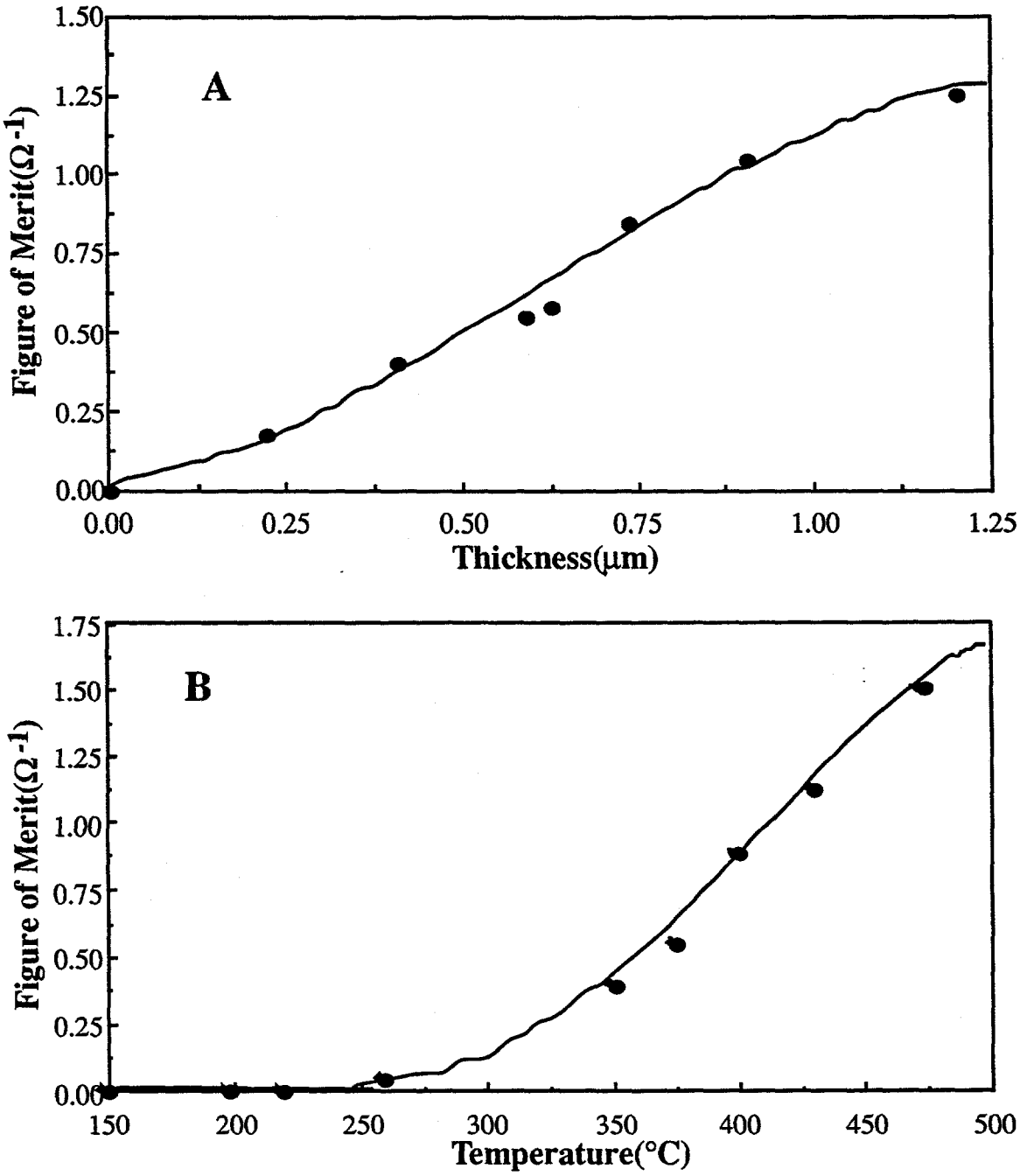

FIG. 24. (a) Figure of Merit dependence on film thickness. The films are the same as those in Figure 15. (b) Figure of Merit dependence on deposition temperature. The films are the same as those in Figure 18.

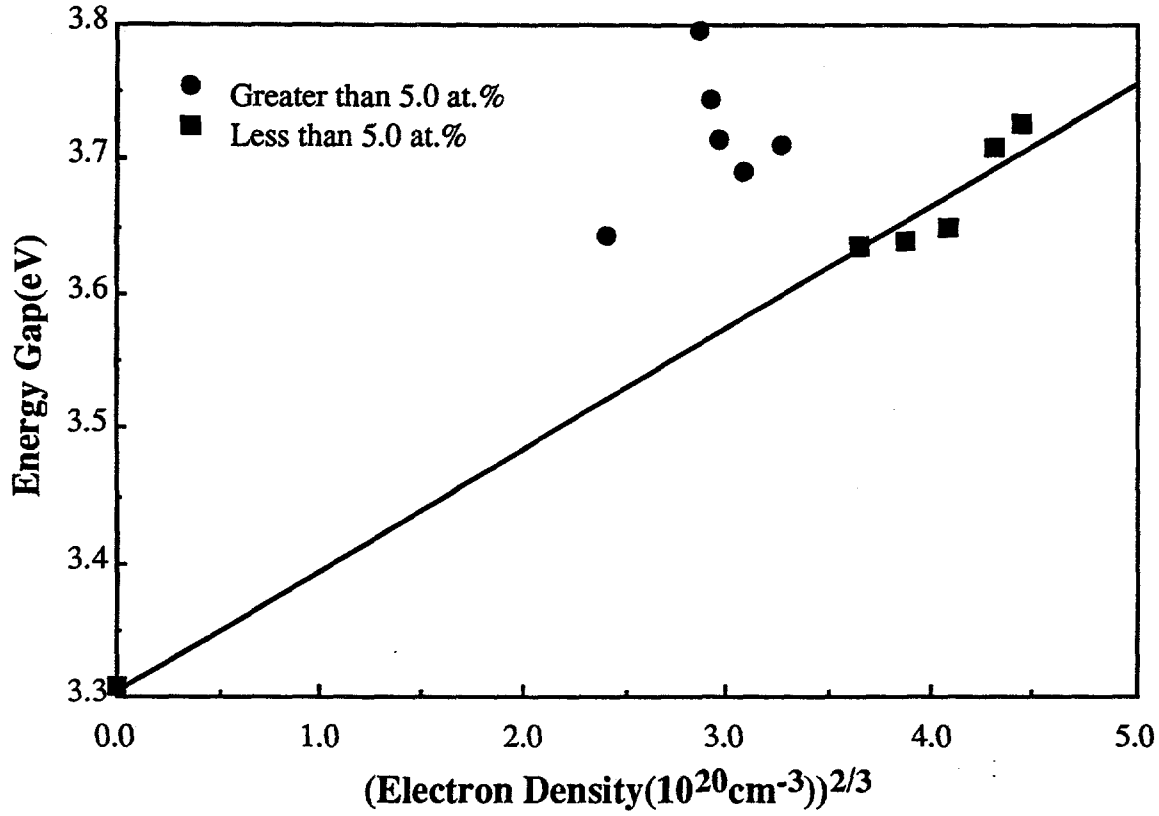

FIG. 25. Band gap dependence on electron density. The films were deposited at 370°C from 0.05% diethyl zinc, 0.8% water and various triethyl gallium concentrations. A straight line was drawn for films with gallium concentration below 5.0 at.%.

Document Control Page	1. NREL Report No. NREL/TP-411-5456	2. NTIS Accession No. DE93010009	3. Recipient's Accession No.

4. Title and Subtitle

Optimization of Transparent and Reflecting Electrodes for Amorphous Silicon Solar Cells

5. Publication Date
April 1993

6.

7. Author(s)

R. G. Gordon

8. Performing Organization Rept. No.

9. Performing Organization Name and Address

Harvard University
Department of Chemistry
Cambridge, Massachusetts 02138

10. Project/Task/Work Unit No.
PV341101

11. Contract (C) or Grant (G) No.

(C) XH-1-11032-1

(G)

12. Sponsoring Organization Name and Address
National Renewable Energy Laboratory
1617 Cole Blvd.
Golden, CO 80401-3393

13. Type of Report & Period Covered

Technical Report
1 May 1991 - 30 April 1992

14.

15. Supplementary Notes
NREL technical monitor: B. Stafford

16. Abstract (Limit: 200 words)

This report describes work to improve the performance of solar cells by improving the electrical and optical properties of their TCO layers. Boron-doped zinc-oxide films were deposited by atmospheric pressure chemical vapor deposition in a laminar-flow reactor from diethyl zinc, tert-butanol, and diborane in the temperature range between 300°C and 420°C. When the deposition temperature was above 320°C, both doped and undoped films have highly oriented crystallites with their c-axes perpendicular to the substrate plane. Films deposited from 0.07% diethyl zinc and 2.4% tert-butanol have electron densities between 3.5 x 10^{20} cm^{-3} and 5.5 x 10^{20} cm^{-3}, conductivities between 250 Ω^{-1} cm^{-1} and 2500 Ω^{-1} cm^{-1} and mobilities between 2.5 cm^2/V-s and 35.0 cm^2/V-s, depending on dopant concentration, film thickness, and deposition temperature. Optical measurements show that the maximum infrared reflectance of the doped films is close to 90%, compared to about 20% for undoped films. Film visible absorption and film conductivity were found to increase with film thickness. The ratio of conductivity to visibile absorption coefficient for doped films was between 0.1 Ω^{-1} and 1.1 Ω^{-1}. The band gap of the film changes from 3.3 eV to 3.7 eV when the film is doped with 0.012% diborane.

17. Document Analysis

a. Descriptors
amorphous silicon ; electrodes ; photovoltaics ; solar cells

b. Identifiers/Open-Ended Terms

c. UC Categories
271

18. Availability Statement
National Technical Information Service
U.S. Department of Commerce
5285 Port Royal Road
Springfield, VA 22161

19. No. of Pages
105

20. Price
A06

Form No. 0069E (6-30-87)